UNIVERSITÉ DE MONTRÉAL

INNOVATIVE VASCULAR PROSTHESES COMBINING 3D ELECTROSPUN NANOFIBER MATRICES AND BIOACTIVE COATINGS PREPARED BY PLASMA-POLYMERIZATION

HOUMAN SAVOJI

INSTITUT DE GÉNIE BIOMÉDICAL

ÉCOLE POLYTECHNIQUE DE MONTRÉAL

THÈSE PRÉSENTÉE EN VUE DE L'OBTENTION

DU DIPLÔME DE PHILOSOPHIAE DOCTOR

(GÉNIE BIOMÉDICAL)

DÉCEMBRE 2016

UNIVERSITÉ DE MONTRÉAL

ÉCOLE POLYTECHNIQUE DE MONTRÉAL

Cette thèse intitulée :

INNOVATIVE VASCULAR PROSTHESES COMBINING 3D ELECTROSPUN NANOFIBER MATRICES AND BIOACTIVE COATINGS PREPARED BY PLASMA-POLYMERIZATION

présentée par : SAVOJI Houman

en vue de l'obtention du diplôme de : Philosophiae Doctor

a été dûment acceptée par le jury d'examen constitué de :

M. JOLICOEUR Mario, Ph. D., président

M. WERTHEIMER Michael R., D.Sc.A, membre et directeur de recherche

Mme LEROUGE Sophie, Ph. D., membre et codirectrice de recherche

M. AJJI Abdellah, Ph. D., membre et codirecteur de recherche

M. THÉRASSE Éric, MD, membre

M. LAROCHE Gaétan, Ph. D., membre externe

DEDICATION

To my beloved parents.

ACKNOWLEDGEMENTS

First and foremost, I am deeply grateful to all my PhD supervisors: Prof. Michael R. Wertheimer, Prof. Sophie Lerouge and Prof. Abdellah Ajji for their continuous mentoring, inspirational guidance, encouragement, exceptional support, motivation, and providing resources in their laboratories during my PhD studies.

My kind and sincere gratitude to Prof. Wertheimer; a distinguished professor in his field, who has always been a supportive mentor for me. He has always generously been there for me whenever I needed support in the course of this research. I am honored to be his student these past few years. I have been learning from him not only through my scientific journey but also in my life. His attitude in thinking about science and technology and solving research and technical problems always inspires me as a young researcher.

My deep gratitude to Prof. Lerouge, a successful hard working and passionate researcher, for her invaluable advice, excellent guidance, continuous supports and constantly challenging me to be a better researcher. Without her great supervision and advice, I wouldn't have completed this thesis. I learned a lot from her not only in my research but also in my career path. Her broad knowledge in biomaterial and tissue engineering fields are invaluable to the success of my PhD research project and will definitely help me significantly in my future careers.

My great gratitude to Prof. Ajji, an outstanding advisor, who always encouraged and guided me during this research. His insightful suggestions, constant support and patience enabled me to complete this multidisciplinary research. This work would not have been possible without his invaluable technical and moral support.

I would like to express my gratitude to Dr. Gregory De Crescenzo for giving me the opportunity to work in his laboratory to complete the last part of this research.

I am grateful for my thesis committee members: Prof. Mario Jolicoeur, Prof. Gaétan Laroche, Prof. Éric Thérasse, for their time to read this thesis and their invaluable suggestions.

I would like to sincerely thank Dr. Marion Maire, Dr. Afra Hadjizadeh, Dr. Pauline Lequoy, Dr. Benoit Liberelle, Dr. Caroline Ceccaldi, Dr. Bachir Saoudi, Mr. Matthieu Gauthier, Mme. Suzie Poulin and Dr. Josianne Lefebvre, Mrs. Clair Cerclé, Mrs. Nicole MacDonald, Mr. Yves Leblanc for their valuable assistance, technical support and insightful suggestions during the course of this

research, to Dr. Bernard Nisol for the French translation of the Abstract, to Dr. Amir Sheikhi for the proofreading and Mr. Nicholas Laugher for the editing of the Chapters 1, 2, and 7.

I am also indebted to my amazing colleagues and friends at the Institute of Biomedical Engineering, Chemical Engineering Department and Engineering Physics Department at Ecole Polytechique Montreal, and Laboratory of Endovascular Biomaterials (LBeV), Hospital Research Center of University of Montreal (CRCHUM), and McGill University, who accompanied me along this journey, offering me practical supports and warm friendships. Many thanks to Gaël, Pradeep, Elias, Marouan, Ahmed, Angel, Juan-Carlos, Hicham, Amélie, Sepideh, Fatemeh, Yasaman, Francesco, Saoussen, Cindy, Mélusine, Jessica, Eve, Atma, Audrey, Sara, Ali, Abeer, Amin, Mandana, Ali, Alireza, Hossein, Frederic, Samantha, Charles, Vincent and many more whose names I might have forgotten to mention.

Last but not the least, I would like to give my special thanks to my beloved parents, Hourinaz Abbasi Rashti and Mohammadreza Savoji, and my supportive and kind brother, Hamed for their unconditional love and supports from overseas.

RÉSUMÉ

Malgré des efforts indéniables, l'élaboration de prothèses vasculaires (VGs) de petit diamètre (6 mm) pour le remplacement de vaisseaux occlus ou la déviation du flux sanguin (*bypass*) se heurte encore à des résultats mitigés. Parmi les principaux requis d'un greffon vasculaire synthétique de petit diamètre (SDVG) et pour l'ingénierie tissulaire de vaisseaux sanguins, citons l'hémocompatibilité et la compliance mécanique. En particulier, il est essentiel d'assurer la formation d'une monocouche continue de cellules endothéliales (ECs) à l'intérieur de la lumière, qui résiste aux contraintes de cisaillement physiologiques. Pour ce faire, une approche classique consiste à ensemencer la lumière du greffon avec des ECs, antérieurement à l'intervention. Néanmoins, une faible rétention des cellules sous flux sanguin, et la morphologie des textiles conventionnels constituent des freins à la formation de la monocouche. Les matériaux électrofilés permettent d'améliorer la conformité du greffon, et reproduisent plus fidèlement la morphologie de la matrice extracellulaire des vaisseaux sanguins ; ils présentent cependant le même problème de rétention et croissance des ECs. Dans cette recherche, il a été démontré qu'un tapis de nanofibres de PET électrofilées (ePET), organisées de façon aléatoire, et subséquemment recouvert d'une couche mince de *polymère-plasma* riche en amines primaires (L-PPE:N) permet un contrôle relativement fin des propriétés structurelles et de surface, nécessaires la formation de monocouches d'ECs confluentes sur VGs. En effet, il a été démontré que ces dépôts L-PPE:N augmentent significativement l'adhésion et la croissance d'ECs, même sous contrainte d'écoulement induite par cisaillement. La rétention cellulaire se voit aussi améliorée, mais n'est cependant pas encore idéale. En outre, les couches L-PPE:N sont également thrombogènes. Pour pallier à cela, il a été proposé de greffer du sulfate de chondroïtine (CS) sur les couches L-PPE:N; le CS est connu pour empêcher l'adhérence de plaquettes ainsi que pour favoriser l'adhésion et croissance de cellules endothéliales de la veine ombilicale humaine (HUVECs). Le greffage de CS sur L-PPE:N, lui-même déposé sur tapis électrofilés a effectivement montré une forte augmentation de la colonisation en HUVEC, et une amélioration de leur rétention (résistance au détachement).

De plus, l'alignement des ECs dans la direction du flux sanguin est connu pour renforcer la rétention des cellules dans les artères. L'approche classique pour obtenir artificiellement une monocouche de cellules alignées implique un pré-conditionnement long et coûteux de l'implant dans un bioréacteur (*in vitro*), sous flux. Ici, nous avons testé et comparé des tapis de PET

obtenus à la fois par électrofilage aléatoire et aligné : nous avons pu observer une légère augmentation de la résistance des ECs à la contrainte de cisaillement dans le cas des fibres alignées.

Nous avons également évalué et optimisé le potentiel de ces structures électrofilées pour la media des vaisseaux naturels, qui est constituée de cellules musculaires lisses vasculaires (VSMCs) et de fibres de collagène alignées circonférentiellement, essentielles à la contraction, à la dilatation et au contrôle de la pression sanguine. Nous avons ainsi fabriqué des structures de ePET aligné et avons cherché à optimiser leur compliance à l'aide de trois différentes approches d'érosion (chimique) par plasma, dans le but d'approcher au mieux les propriétés mécaniques et surfaciques des vaisseaux sanguins naturels : (i) décharges *corona* dans l'air, à pression atmosphérique (HP); (ii) plasma radio-fréquencé à basse pression (LP) et (iii) plasma micro-ondes, (ii) et (iii) étant utilisés soit avec de l'oxygène (O_2), pur ou mélangé avec Ar, ou encore avec CF_4. L'approche (iii) a notamment permis une réduction significative du module de Young après à peine 5 min. de traitement avec O_2, sans endommager les fibres. De plus, les changements observés dans la composition de surface et l'amélioration drastique de la mouillabilité/capillarité en découlant ont mené à une adhésion et une croissance accrues de cellules musculaires lisses (SMCs).

Finalement, les tapis alignés ont été modifiées avec des *couches bioactives*, basées sur les dépôts L-PPE:N décorés de CS, ce dernier servant de plus de site d'ancrage du facteur de croissance épidermique (EGF). Nous avons pu observer que ces couches (CS-EGF) promeuvent fortement l'adhésion, la croissance et la survie des VSCMs. Ceci suggère que le dépôt de couches bioactives sur tapis électrofilés constitue un excellent moyen de produire des échafaudages pour les parties luminale et médiane des SDVGs, offrant un contrôle fin sur les propriétés structurelles, mécaniques, surfaciques et biologiques nécessaires à une endothélialisation complète et stable de l'implant.

Mot clés : prothèse vasculaire; électrofilage; nanofibres; poly(ethylene terephthalate); polymérisation plasma; érosion par plasma; revêtements bioactifs; morphologie; propriétés mécaniques; chimie de surface; endothélialisation.

ABSTRACT

There have been considerable efforts in developing prosthetic small-diameter (below 6mm) vascular grafts (VGs) as an alternative to autologous grafts to bypass or replace occluded blood vessels. Primary requirements for functional synthetic small-diameter vascular grafts (SDVGs) or tissue engineered blood vessels are hemocompatibility and favorable compliance. Particularly critical is the formation of a continuous, stable monolayer of endothelial cells (ECs) on the lumen under physiological shear stress. To that purpose, seeding autologous ECs on the lumen side of the graft prior to implantation is commonly done. But its success is limited by low cell retention under flow and by the large pore size of conventional textiles that do not favor the formation of a continuous monolayer. Electrospinning enables one to enhance graft compliance and to mimic the morphology of the extracellular matrix of blood vessels, but EC growth and retention on electrospun mats still remain a problem. In this research, it was shown that random electrospun PET (ePET) nanofiber mat coated by primary-amine rich plasma polymer coating (L-PPE:N) lead to finely controlled structural and surface properties that are required for a confluent EC monolayer on VGs. EC adhesion, -growth, and -retention under shear-induced flow stress were shown to be increased by L-PPE:N coating. However, cell retention is still not ideal. Moreover, this underlying L-PPE:N substrate is thrombogenic. To tackle this problem, chondroitin sulfate (CS) was grafted on LP which is known to prevent platelet adhesion while promoting human umbilical vein endothelial cell (HUVEC) adhesion and growth. It was observed that grafting CS on L-PPE:N coated electrospun mats could significantly enhance HUVEC adhesion, growth and their resistance to detachment.

In addition, EC alignment in the direction of blood flow in the natural arteries is known to increase the cell capability to resist detachment under shear stress. This is typically achieved by a long and resource-consuming method involving *in vitro* fluid flow preconditioning in a bioreactor prior to implantation. Random and aligned electrospun PET mats were fabricated as scaffolds for the luminal layer. It was observed that EC resistance to shear stress was slightly further improved when it was directed by tuning electrospun alignment.

On the other hand, the media layer of native vessels contains vascular smooth muscle cells (VSMCs) and circumferentially-aligned collagen fibres, which are essential for contraction, dilation and blood pressure control. In this research, aligned ePET mats were fabricated as

scaffolds for the media layer, and three different plasma etching techniques were used to bring their mechanical and surface properties in line with those of natural blood vessels: (i) atmospheric pressure (“HP”) corona discharge in air; (ii) low-pressure radio-frequency plasma (“LP”) and (iii) microwave plasma asher, (ii) and (iii) in pure oxygen (O_2), or O_2 mixture with Ar or CF_4. (iii) gave substantial reduction in Young's modulus after as little as 5 min. treatment in O_2, without damage to the fibers. Changes in surface composition and drastic improvement in wettability/wicking were also observed, which resulted in promoting adhesion and growth of smooth muscle cells (SMCs). The aligned mats were then grafted with *bioactive coatings*, based on L-PPE:N coating, CS with tethered epidermal growth factor (EGF). It was found that a CS-EGF coating promoted the VSMC adhesion, growth, survival and infiltration. Our findings suggest that electrospun mats coated with bioactive coatings provides adequate scaffolds for the luminal and media side of SDVGs, with finely-controlled structural, mechanical and bioactive surface properties required for complete and stable endothelialization.

Keywords: electrospinning; nanofibers; poly(ethylene terephthalate); plasma polymerization; plasma-etching; bioactive coatings, morphology, mechanical property; surface chemistry; In vitro cell experiment; endothelialization; vascular graft

TABLE OF CONTENTS

LIST OF TABLES

LIST OF FIGURES

LIST OF SYMBOLS AND ABBREVIATIONS

1-ethyl-3-(3-dimethylaminopropyl) carbodiimide	EDC
aligned	A
atmospheric pressure plasma	HP
chondroitin sulfate	CS
coronary artery bypass graft	CABG
coronary artery disease	CAD
dichloromethane	DCM
dielectric barrier discharge	DBD
differential scanning calorimetry	DSC
electrospun PET	ePET
endothelial cell	EC
endothelial progenitor cells	EPC
enzyme-linked immunosorbent assay	ELISA
epidermal growth factor	EGF
expanded poly(tetrafluoroethylene)	ePTFE
extracellular matrix	ECM
fast fourier transform	FFT
glycoaminoglycans	GAGS

growth factor	GF
Hematoxylin-Eosin	H&E
high-voltage	HV
human umbilical vein endothelial cells	HUVECs
hyaluronic acid	HA
intimal hyperplasia	IH
left anterior descending	LAD
left internal mammary artery	LIMA
low-pressure plasma	LP
mercury intrusion porosimetry	MIP
methacrylic acid	MAA
N-hydroxysuccinimide	NHS
optical density	O.D.
percutaneous coronary intervention	PCI
phosphate buffered saline	PBS
plasma-polymerization	PP
plasma-polymerizd allylamine	PPAAm
poly(ethylene terephthalate)	PET
polycaprolactone	PCL

polycarbonate urethane	PCU
polyethylene glycol	PEG
polyurethane	PU
Low -pressure	LP
Low-pressure primary-amine rich plasma polymer coating	L-PPE:N / LP
random	R
scanning electron microscopy	SEM
small-diameter vascular grafts	SDVGs
static contact angle	SCA
trifluoro-acetic acid	TFA
trifluoromethyl) benzaldehyde	TFBA
Vascular Endothelial Growth Factor	VEGF
vascular graft	VG
vascular smooth muscle cells	VSMCs
woven PET	wPET
X-Ray photoelectron spectroscopy	XPS

CHAPTER 1 INTRODUCTION

Cardiovascular diseases are the leading cause of death worldwide [1, 2]. Small-diameter blood vessels in the body, including fine arteries of the heart and limbs, have a high prevalence of occlusion [3]. Bypass grafts from the patients' own veins or arteries are currently the only therapeutic approach when endovascular procedures (angioplasty and stenting) are not feasible or successful: A frequent major obstacle in bypass grafts is that many patients cannot provide suitable veins or arteries, due to previous surgery or antecedent vascular disease. Consequently, to address this vital demand, development of prosthetic VGs has been a rapidly growing area of research [3].

Current off-the-shelf large diameter prosthetic VGs such as expanded poly(tetrafluoroethylene) (ePTFE) or woven poly(ethylene terephthalate (PET Dacron®) have shown poor endothelialization and compliance mismatch, which lead to lack of patency when used for small diameter vessels (below 6 mm) [4]. To overcome these issues, researchers have introduced electrospun nano/micro-fiber scaffolds which possess adequate structural and mechanical properties to imitate the extracellular matrix (ECM) of the native blood vessels. These scaffolds offer great promise by possessing interconnected open structure with high porosity and surface area. Furthermore, mechanical properties of the scaffolds can be optimized to fine-tune those of native blood vessels.

While the structural and mechanical characteristics of the graft is of great importance in its performance and success, a critical design requirement for small-diameter VGs is the formation of a continuous monolayer of endothelial cells (ECs) on the lumen of the VGs which remains stable under physiological shear-flow conditions. To that purpose, seeding autologous ECs on the lumen side of the graft prior to implantation is commonly done, but its success is limited by low cell retention under flow and by the large pore size of conventional textiles that do not favor the formation of a continuous monolayer. Electrospinning enables the mimicking of the nanofibrous morphology of the ECM of blood vessels, but EC growth and retention on electrospun mats still remain a problem and present particularly severe challenges. To this aim, a suitable strategy is needed to provide the requisite strong cell-adhesion. Among the different techniques employed to improve cell adhesion and biocompatibility of polymeric scaffolds, several focus on the immobilization of bio-molecules that function as anchors for adhesion of cultured cells [5, 6]. A

particularly powerful method used to promote bio-molecule immobilization and eventually cell-adhesion is plasma-polymer deposition. Plasma-polymerization is a versatile approach for depositing polymer-like coatings with various selected functional groups (e.g., hydroxyl-, carboxyl-, or primary amine groups), which can enable further biomolecule grafting (e.g., ECM components, proteins and growth factors) and promote cell adhesion [7-9]. Therefore, this thesis aims at increasing compliance and endothelialization of VGs by combining 3D electrospun nanofiber matrices and bioactive coatings prepared by plasma-polymerization.

Chapter 2 provides an overview of the literature addressing the clinical significance of cardiovascular disease (intimal hyperplasia (IH) & atherosclerosis) in small-diameter blood vessels. A review of coronary artery disease and treatments, including bypass grafting, angioplasty, and stenting are then presented. Clinically available synthetic vascular prostheses are presented and the limitations of commercial materials SDVGs is discussed. Then, a review of electrospinning and the polymer scaffold fabrication technique; including basic concept and process parameters optimization specifically for VG development, are reviewed. The requirements of engineered SVGDs and the motivation for using electrospun scaffolds are then presented. Surface modification techniques including immobilization of bioactive coatings to promote cell-adhesion, growth, survival and *in-vitro* endothelialization are also discussed in detail. Based on the literature review, hypotheses are made and specific objectives are defined for this thesis that are presented in **Chapter 3**. The next three chapters present the three papers forming the core of the thesis. **Chapter 4** of this thesis (**Paper 1**, published in Macromolecular Bioscience [10]) deals with fabrication and characterization of morphological, physico-chemical, mechanical and biocompatibility properties of random electrospun nanofiber mats and the benefit of a plasma polymer coating. We showed that this combination led to finely controlled structural, mechanical, and surface properties that are required for confluent EC monolayer on VGs. EC-adhesion, -growth, and -retention under shear-induced flow were characterized.

Chapter 5 (**Paper 2**, published in Plasma Processes and Polymers [11]) focuses on the fabrication of the aligned scaffolds with large pore size for subsequent VSMC-seeding that possess optimal mechanical, morphological and surface-chemical properties in the media layer. The fabricated ePET nano-fibers are radially highly oriented; in order to bring their mechanical properties in line with those of natural blood vessels, a substantial reduction in Young's modulus has to be attained. Therefore, in this research, electrospinning and plasma etching are combined

to fulfill those criteria. Three different plasma-etching techniques are investigated: (i) atmospheric pressure ("HP") corona discharge in air, low-pressure (ii) radio-frequency (r.f.) discharge, and (iii) discharge in a microwave plasma asher. The best technique without visible damage to the fibers, changes in surface composition and improved wettability is chosen for further VSMC adhesion and growth experiments.

Chapter 6 (**Paper 3**, published in Biomacromolecules [12]) aims to use biomolecules' immobilization to further improve the cell adhesion, growth, survival and retention on the electrospun PET scaffolds for the luminal and media layers. As previously shown in our team, grafting bioactive coatings including chondroitin sulfate on nitrogen-rich plasma coating prevents platelet adhesion while promoting HUVEC adhesion and growth on the flat surfaces [13]. We therefore hypothesize that these bioactive coatings on electrospun PET mats can enhance HUVEC adhesion, growth, and their resistance to detachment. In addition, EC alignment in the direction of blood flow in the natural arteries is known to increase the cells capability to resist detachment under shear stress. This is typically achieved by a long and resource consuming method involving *in vitro* fluid flow preconditioning in a bioreactor prior to implantation. But, a recent study has shown an improvement in EC retention by tuning the topography (e.g., orientation) of electrospun fibers [14]. Therefore, we also investigate EC resistance to shear stress by tuning electrospun alignment and immobilization of bioactive coatings.

In **Chapter 7**, the general discussion, including the recommendations and limitations are presented, followed by the conclusion.

CHAPTER 2 LITERATURE REVIEW

2.1 Clinical Significance of Intimal Hyperplasia & Atherosclerosis

Cardiovascular diseases (CVDs) are the leading cause of death worldwide [1]. An estimated 85.6 million American adults (>1 in 3) have more than one type of CVD. Of these, 43.7 million are estimated to be ≥60 years of age. Small-diameter vessels (below 6 mm) in the body, including fine arteries of the heart and limbs have high prevalence of occlusion. This is caused by intimal hyperplasia (IH), which usually precedes atherosclerosis and eventually leads to distal tissue ischemia such as infarction in the case of coronary disease [15], as shown in **Figure 2.1**. There can be significant variability in which size of arteries and locations are affected in individual patients, although atherosclerosis is often a systemic disease. IH gradually happens by formation of the multi-layer of the cells on the elastic membrane of the arterial wall and expressing α-smooth-muscle actin [16]. The pathology of small-vessels disease (e.g., coronary) comprises a number of distinct features such as IH, appearance of foam cells/macrophages and cholesterol buildup, platelet aggregation and thrombogenesis, inflammation, etc. These features often overlap and enhance each other. IH usually refers to the cellular morphogenesis caused by a cell proliferation/differentiation process [17].

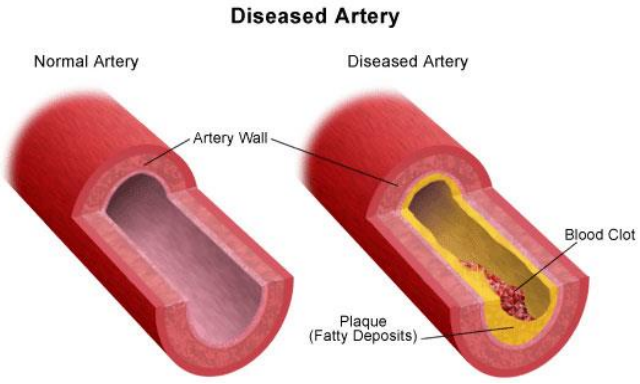

Figure 2.1 Schematic of atherosclerosis disease

from: https://stanfordhealthcare.org

2.2 Current Therapies and Limitations

Treatment options for coronary artery disease (CAD) depend on various factors, including severity and extent of the disease, type of symptoms such as chest pain and shortness of breath, overall heart function, other medical conditions such as diabetes, peripheral artery disease, and prior stroke or heart attack. Drug therapy has been used for decades to combat IH and atherosclerosis. Overall, it has not been satisfactory. Therefore, several approaches have been proposed to treat CAD, including angioplasty, stenting and bypass grafting.

2.2.1 Balloon Angioplasty

Angioplasty-also known as percutaneous coronary intervention (PCI)- is a minimally invasive procedure with a low risk of complication. Angioplasty may especially be recommended if the chest discomforts (angina) due to reduced blood flow have not responded to medication and lifestyle changes. During the procedure shown in **Figure 2.2**, a catheter containing a small balloon on its tip is inserted at the site of the blockage and is expanded to widen the narrowed artery by compressing or flattening the atherosclerotic plaque.

2.2.2 Stenting

Most of the time, to keep the artery open and reduce the risk of renewed narrowing, a small metal coil (stent) is implanted in the clogged artery, as illustrated in **Figure 2.2**. Stenting, like angioplasty, is a minimally invasive procedure. Even with stenting, it is still possible for the coronary artery to narrow again. With bare-metal stents, such restenosis occurs in as many as 15% to 30% of patients depending on the type of stent. This percentage is much lower in patients who receive drug-eluting stents [18]. If restenosis occurs, patients may require another balloon angioplasty, stent procedure, or bypass surgery. Although stents have proven to be a safe and effective treatment, their use may, on rare occasions, result in what is known as stent thrombosis which may cause a heart attack.

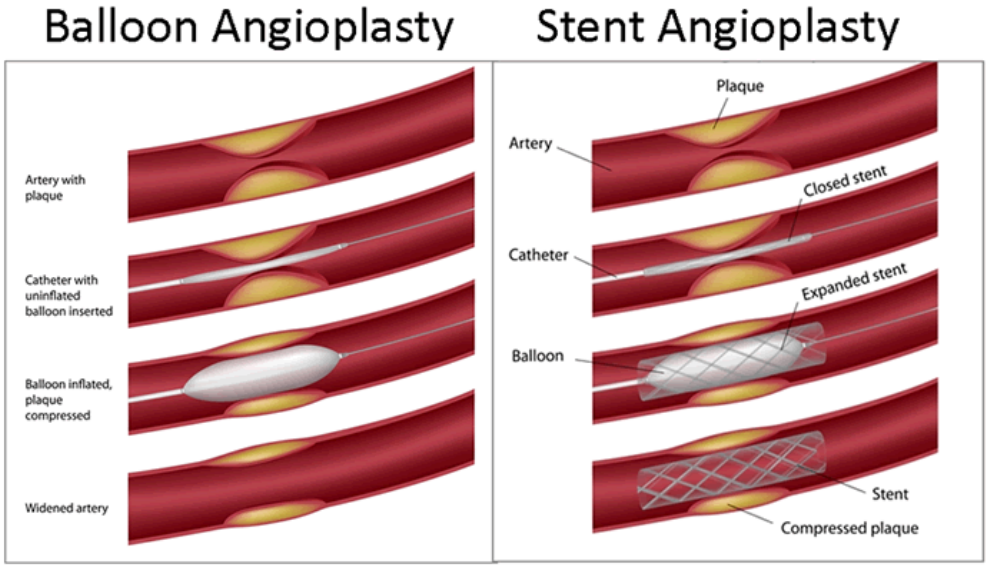

Figure 2.2 Schematic of balloon angioplasty and stenting

from: http://www.keyword-suggestions.com

2.2.3 Coronary Artery Bypass Graft (CABG)

Bypass grafts from the patients' own veins or arteries constitute another therapeutic approach if interventional procedures (balloon angioplasty and stenting, used in cases of less than 70% occlusion [19]) are not feasible or successful. In CABG (**Figure 2.3**), which is performed in cases with a greater degree of occlusion, autologous veins or arteries from the patient are grafted to bypass partially or completely occluded coronary artery, thereby improving myocardial oxygenated blood supply and preventing infarction.

Different autologous vessels may be employed to establish cardiac revascularization. The use of arterial grafts for replacing the left anterior descending (LAD, a coronary artery) was established before [20], the left internal mammary artery (LIMA) being the vessel of first choice for this procedure. IMAs are usually patent for many years postoperatively (10-year patency >90%) [21, 22] because of the fact that <4% of IMAs develop atherosclerosis, and only 1% have atherosclerotic stenoses of hemodynamic significance [23].

Reversed saphenous vein grafts (SVGs) are commonly used in patients undergoing CABG. Their disadvantage is a declining patency with time: 10% to 25% of them occlude within 1 year of

CABG [24]; an additional 1% to 2% occlude each year during the 1 to 5 years after surgery; and 4% to 5% occlude each year between 6 and 10 years postoperatively. Therefore, 10 years after CABG, 50% to 60% of SVGs are patent, only half of which have no angiographic evidence of atherosclerosis [25].

In general, autologous graft shows great promise in CABG procedure since it has the natural architecture. It is also a living, non-thrombogenic endothelium, is biocompatible, and has encouraging surgical handling characteristics. SVs have shown structural and functional changes leading to thrombosis, calcification and premature occlusion of the graft, while an autologous artery is more robust and longer-lasting.

A recent trial comparing CABG and PCI, reviewed the records of nearly 190,000 patients 65 years or older with multi-vessels disease. 86,244 underwent CABG and 103,549 underwent PCI. The median follow-up period was 2.67 years. At 1 year, there was no significant difference in mortality between the groups (6.24% CABG versus 6.55% PCI; risk ratio, 0.95). At 4 years, there was lower mortality with CABG than with PCI (16.4% versus 20.8%; risk ratio, 0.79) [26].

A major obstacle in bypass grafts is that many patients (5-30%) cannot provide veins or arteries suitable for grafting, due to previous surgery or antecedent vascular disease. Consequently, considering the mentioned limitations for the above VG alternatives and to address this vital demand, the development of prosthetic VGs has been a rapidly growing area of research [27].

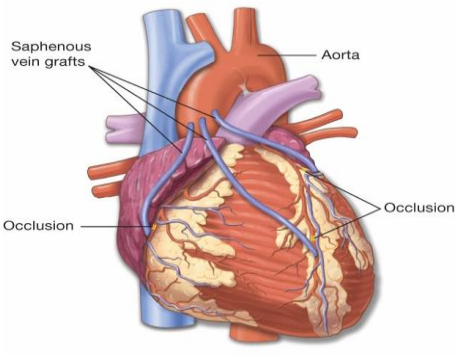

Figure 2.3 Schematic of the commonly used saphenous vein and internal mammary artery graft for CABG; from: http://biology-forums.com

2.3 Clinically Available Synthetic Vascular Prostheses

There have been growing investigations to find alternate sources to mimic the structural and mechanical performance of native blood vessels, due to the high demand for bypass graft operations. Prosthetic materials that are currently used clinically are woven or knitted poly(ethylene terephthalate) (PET, Dacron®), expanded poly(tetrafluoroethylene) (ePTFE, Teflon®) as VGs for arteries with an inner diameter of more than 6 mm [28]. These materials have been validated as successful grafts for large-diameter arteries in which high flow and low resistance leads to low rates of thrombosis and excellent rates of long-term patency. However, in the long term, several complications may happen for *smaller* size, depending on the diameter, including thrombosis and IH. Therefore, the graft success rate (high patency in the long run) is highly dependent on internal diameter, and it falls steadily as the diameter becomes smaller [29].

The mechanisms involved in the development of IH have been largely established. In humans IH develops as early as 6 weeks after grafting and leads to narrowing of the vessel lumen. Generally, in the case of large grafts, the occlusion mechanism is well-stablished in the literature. They trigger immune responses initiated first by plasma protein, followed by platelet adhesion, and the migration of ECs and SMCs [30]. These initially cause static aggregation of lipid and blood factors (thrombosis), surrounded by ECM and followed by a continuous excessive SMC in-growth and plasma protein deposits in the chronic phase, which is covered by a fibrous cap (IH).

ePTFE exhibits a 5-year patency rate of 91 to 95% when implanted as an aortic graft [31]. Similar to Teflon®, Dacron® also shows low patency rate of 56% in young patients with premature atherosclerosis over 10 years [32].

2.4 Challenges of Prosthetic Grafts as Small-Diameter VGs (SDVGs)

Small-diameter blood vessels experience low blood flow and high shear compared to medium and large diameter ones. This makes the synthetic SDVGs (< 6 mm i.d.) more prone to thrombus formation and IH. This phenomenon is more acute in SDVGs for the coronary, renal, and carotid arteries: especially after increased contact time of blood components with grafts, and the increased activation of blood coagulation, this would result in high rates of thrombosis and low

patency in SDVGs [33]. So far, a primary reason for the failure of SDVGs made from synthetic materials has been their thrombogenic characteristics, but clinical observation also comes up with possible evidence that the patency rates of small grafts are improved by matching the elastic properties (compliance) of the graft to that of natural artery. Although there is still controversy that 'elastic mismatch' *per se* is the cause of IH, it is generally accepted that mechanical factors are important in its genesis. These include disturbed flow at the anastomosis, leading to fluctuations in shear stress at the endothelium, injury due to suturing and stress concentration at the anastomosis [34].

For example, Hehrlein et al. [35] compared the patency of ePTFE (3-5 mm i.d.) and SV grafts and concluded that 86% of SV grafts, while only 59% of ePTFE grafts were patent after 1-year follow-up. Dacron SDVGs (3-4 mm i.d.) have not shown encouraging performance, as evidenced by low medium-term patency rates [35].

Researchers have been investigating strategies to minimize thrombosis in small grafts, and to ensure appropriate mechanical (compliance) properties similar to those of natural blood vessels. While many different approaches can be used to tackle the current issues for SDVGs, two are most commonly used: (1) endothelialization; and (2) tuning the mechanical (compliance) properties of the grafts [36].

2.5 Importance of VG Endothelialization

Figure 2.4 presents the structure of native blood vessels: The inner layer named *intima*, is composed of a monolayer of endothelial cells, ECs. The endothelium is a continuous semi-permeable, non- thrombogenic protective barrier in the blood vessel wall, which controls blood flow and vessel tone, platelet activation, adhesion and aggregation, leukocyte adhesion and SMC migration and proliferation [37].

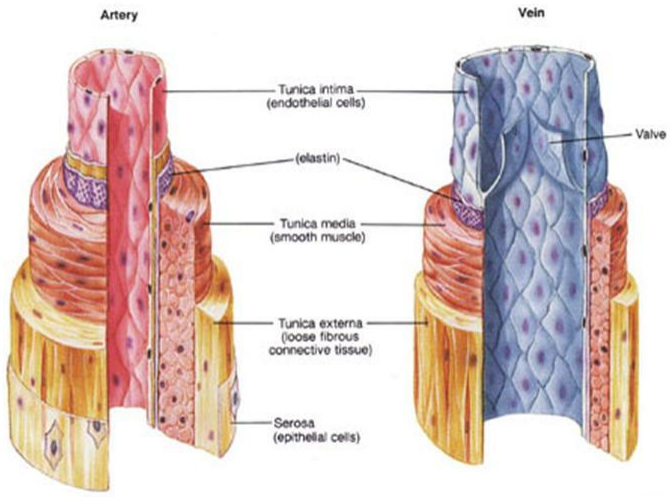

Figure 2.4 Structure of native blood vessels [38].

Unfortunately, it has been shown that VGs do not spontaneously endothelialize *in situ*/*in vivo* due to low initial EC attachment, spreading and growth.

The EC monolayer formed on synthetic VGs was observed to be less than 10% of physiological levels, compared with EC of native vessels [39]. ECs possess limited capacity for regeneration. After about 70 cell cycles, ECs can no divide and therefore, currently available VGs implanted into humans manifest limited EC ingrowth, typically not extending beyond 1-2 cm of the anastomoses [36].

This can also be explained by poor cell-adhesive properties as well as the structure and morphology of the grafts.. Therefore, graft patency is very limited for SDVGs below 6 mm, due to resulting thrombosis: Adhesion and agglomeration of platelets occur on the impaired endothelialized grafts, which is the main reason for thrombosis. Thus, it is necessary to accelerate EC attachment and proliferation on the internal surface, especially under blood flow conditions, to establish good long-term patency [40].

A promising method to improve the anti-thrombogenic properties of VGs is to seed ECs or capture endothelial progenitor cells (EPC) so as to form a complete monolayer on the lumen of VGs [41, 42]. Seeding of ECs provides an interface between the blood flow and the underlying VG, one that improves resistance of VGs to thrombosis and IH. Two approaches can be proposed: 1) *in vitro* pre-seeding prior to implantation; 2) promoting *in vivo* endothelialization

EC monolayer formation by *in-vitro* cell seeding comprises EC-adhesion to the graft surface, which takes place over a period of weeks; preferably within a shorter time, EC-growth or -proliferation leads to confluent EC layer formation [43]. Several studies showed that *in vitro* endothelialization of grafts prior to implantation decreases thrombogenic complications and improves long-term patency [42]. These techniques and their limitations are described in more details in the next section.

2.5.1 EC Seeding and Maturation Techniques

Three main techniques have been employed by researchers for seeding and maturation of the grafts: (1) a single-stage procedure, (2) a two-stage procedure, and (3) pre-conditioning in a bioreactor.

In (1), developed by Herring et al. [44], the ECs are harvested and then immediately seeded on grafts. In order to assure a successful outcome, the harvested cell density should be high. In subsequent randomized clinical trials, EC-seeded ePTFE resulted in increased patency rates of arterial bypass grafts up to 9 year follow-up [45]. A major obstacle for single-stage seeding is the weak adhesion and possible detachment (70%) of ECs from the lumen when exposed to shear force and cyclic strain due to blood circulation a few minutes or hours after exposure to pulsatile flow [46].

In (2), ECs are extracted from the patient's vein, artery, subcutaneous fat, or blood as progenitor cells. They are then cultured for a prolonged period in order to increase the number of cells, before seeding on the lumen, where they proliferate until confluency for 2-4 weeks in static culture before implantation [47]. In a clinical study, seeding of 4mm precoated Gore-Tex coronary with fibrin glue, including 5 ng/mL Human Basic Fibroblast Growth Factor (hbFGF), showed a 90% graft patency rate after 52 weeks post-implantation [48]. However, this procedure is time-consuming and labor-intensive, has the risk of contamination and infection within the cell culture medium, and risk of inefficient proliferation of the cells with time [40]. These render it impractical in emergency situations in clinical settings. Moreover, the EC-adhesion and -resistance to flow-induced shear are impaired once the bare or unmodified graft is implanted *in-vivo*, leading to probable cell-detachment [14].

To promote EC attachment and high retention rate under physiological condition, shear stress preconditioning has been used for decades [49]. In this procedure, cells are gradually subjected to low shear stress in a bioreactor in order to mature the EC layer. This stategy has shown significant impact on EC cell retention after *in-vivo* implantation [49]. In all cases, however, limited cell retention can be at least partly explained by inertness of these biomaterials, which justifies the use of bioactive coatings as a possible solution. In addition, the graft morphology has a large impact on the formation of a confluent EC monolayer. In that sense, small pores on the woven/non-woven structure of grafts facilitate ECs to form an adherent monolayer on the top surface and ensures satisfactory endothelialization.

2.6 Importance of Mechanical (Compliance) Properties

Most commercial VGs (Dacron® and Teflon®) suffer from unsatisfactory mechanical properties including low compliance, and high stiffness or rigidity [27]. To simplify a complicated physical phenomenon in a clinical setting, the "compliance" of a tube has been defined to express a change of diameter with changing pressure. In general, it has been found that as compliance mismatch increases, graft patency decreases [50]. Compliance mismatch prevents a synthetic graft from stretching at the surgically-made connection between it and the native blood vessel - the so-called "anastomosis region". This causes the frequency of the pulsatile blood flow to be dampened, leading to an increase in the flow velocity, a concomitant increase in wave reflection and energy loss. The extent to which the pulse amplitude is dampened depends upon the length of the rigid portion [51], its lack of elasticity causing turbulence and shear stress, which in turn produce inconsistent blood flow profiles and damage to ECs. On the other hand, reduced shear stress can cause flow stagnation in affected areas, increasing the interaction between platelets and the vessel wall, and accumulation of chemokine factors. This promotes thrombosis and severe IH, hence eventual occlusion of the graft [50].

To prevent this scenario from occurring, a VG should closely match the compliance of the adjacent native blood vessel. Beside matching compliance, VGs should also have sufficient tensile stiffness to withstand forces related to vessel contraction and physiological blood pressure [52]. Therefore, the fabrication of synthetic VGs with mechanical properties similar to those of native blood vessels remains a challenge, and it has become a fast-growing area of research.

2.7 The Limitations of Commercial Materials as SDVGs

To develop "ideal" SDVGs with good patency rates, it is crucial to design a structure that mimics the native blood vessel ECM, and that matches its mechanical compliance (see above). Another key factor, also described earlier, is thrombo-resistance of the surface, which can be obtained via a complete, stable monolayer of ECs. Woven or knitted Dacron® (PET) fabrics with differing degrees of porosity have been tested as SDVGs in some animal studies. Woven grafts are typically much less porous than knit ones, but all exhibit higher stiffness than native small blood vessels. To improve their bioactivity, different coatings have been investigated, for example gelatin, collagen, heparin, fibrin, and growth factors [53, 54]. The outcomes of those studies showed no significant reduction in thrombus formation, and impaired *in-vivo* endothelialization even with functional coatings [55, 56]. Expanded PTFE (ePTFE) with pore sizes between ca. 30µm and 100µm were developed by paste extrusion, followed by solvent evaporation, biaxial stretching and high-temperature sintering, but ePTFE is also less compliant than natural arteries and veins [50]. Despite its mechanical mismatch, ePTFE has gained some acceptance for peripheral vessel bypass, particularly for the femoropopliteal artery. Indeed, there have been debates about the superiority of ePTFE over Dacron®, and this controversy still persists. Bio-functionalization of ePTFE grafts has been attempted in order to improve their patency, for example fibrin / growth factor combinations [57, 58], but surprisingly no improvement was found in the animal models studied. As such, no solid conclusions could be drawn.

To overcome compliance mismatch of the above-described conventional materials, a less stiff, more elastic material has been sought, for example polyurethane (PU) [59, 60]. Polyester-based PU (PEU) grafts such as Estane® were used in an animal study, but with discouraging results due to its instability by hydrolysis or to enzymatic attack, or both [61]. Mitrathane®, a polyether PU (PEEU) graft is more stable under both acidic and alkaline conditions, but this graft is prone to the enzymatic stress cracking after implantation [62].

Vascugraft® polycarbonate urethane (PCU), using a spray technique to resolve the instability of PEU and PEEU, produces microporous fibers with inter-connected pores. However, this graft also showed disappointing clinical results in a 15-patient study caused by early occlusion [63].

Therefore, there still exists an unmet need of a material to mimic the structural and mechanical performance of native blood vessels. The 3D network of blood vessels ECM has a fibrous structure [64]; woven and knitted Dacron and ePTFE are far from that fibrillar morphology, therefore they are inadequate to form an endothelial monolayer (**Figure 2.5**).

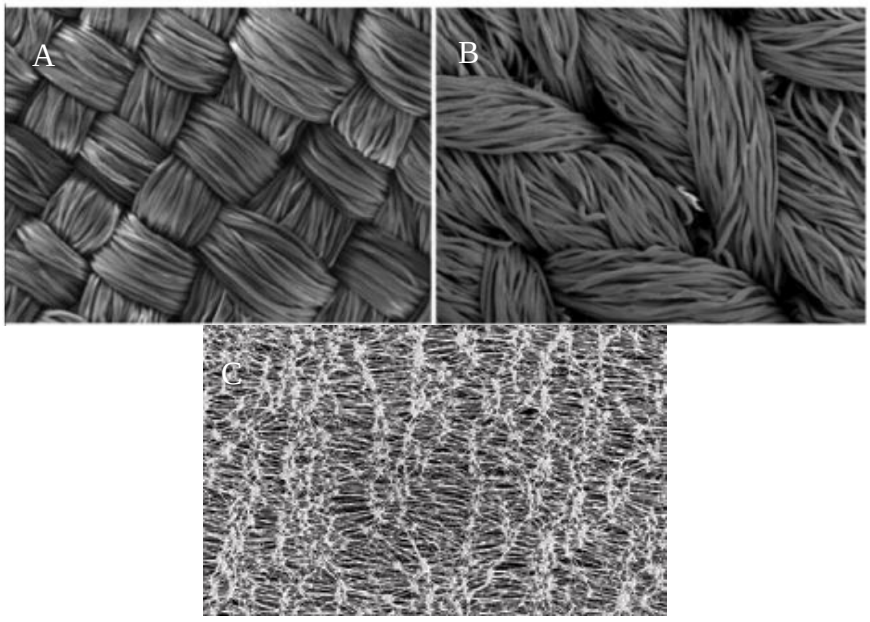

Figure 2.5 Morphological structure of woven (A); knitted (B) PET;

ePTFE grafts (C) from [65].

There have been a growing number of studies to design VGs with hierarchical structures having more 'biomimetic' topography and mechanical interactions of the native ECM. To this aim, scaffolds based on different techniques have been considered, generally by electrospinning, self-assembly, and phase separation [66, 67]. In the following, we shall focus on electrospinning.

2.8 Electrospinning

2.8.1 Principle

Electrospinning, a versatile technique for fabricating nano/micro fibers, has great potential for developing a microenvironment that mimics natural ECM [68, 69]. It is simpler and more efficient than other competing techniques like self-assembly or phase separation, being able to

produce a highly porous (>70% porosity) network of continuous ultrafine fibers ranging from nanometer to micrometer diameters. The first patent about electrospinning had already described an apparatus for producing polymer filaments that took advantage of electrostatic repulsions between surface charges [70]. In the early 1990s, that since-forgotten technology was reintroduced to fabricate thin fibers of various organic polymer [71]. By applying an electric field, polymer solution or melt is drawn from a spinneret to a collector. A high voltage is required to overcome surface tension. A so-called "Taylor cone" is formed, in which the narrow jet is accelerated towards the grounded or oppositely-charged collecting target, while the solvent evaporates [67]. For producing VGs, a rapidly-rotating cylindrical mandrel can be used as the target / collector, to produce a tubular scaffold. At low rotational speed, fibers organize randomly, while at high speed the fibers will align near-perpendicularly to the axis of rotation [72]. **Figure 2.6** shows a schematic of the electrospinning process, and a SEM micrograph of electrospun nanofibers. Different fiber morphologies such as beaded-, ribbon-, porous fibers and core-shells, can also be fabricated [67]. A broad range of polymers and co-polymers with sufficiently high molecular weights can be employed, yielding fiber diameters ranging from several nanometers to micrometers. Electrospun nanofiber mats form non-woven, random or aligned sheets or arrays [73].

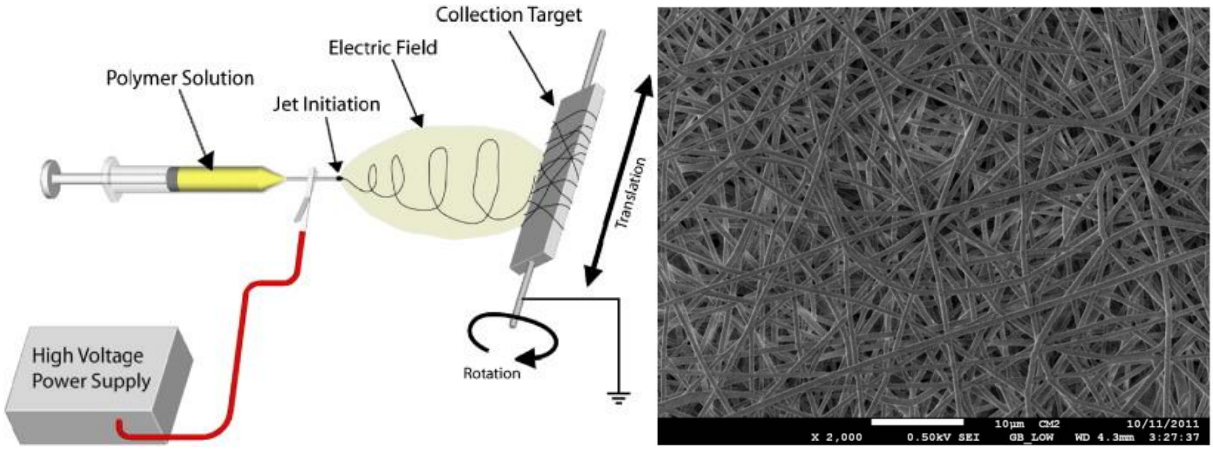

Figure 2.6 a) Schematic diagram of the electrospinning process;

from http://www.people.vcu.edu/~glbowlin;

b) SEM images of PET electrospun nanofibers

The fibers' properties depend on many parameters like processing conditions, polymer solution, and ambient conditions. Solution characteristics include the molecular weight of the polymer, its concentration, its viscosity and surface tension, charge density, conductivity, and dielectric constant. Process variables include flow-rate, applied voltage, distance between needle-tip and collector, and the collector composition and geometry. Ambient conditions include temperature, humidity, and pressure [73]. Good understanding of these variables allows one to reproducibly fabricate defect-free nanofibers with controllable morphology.

2.8.1.1 Effect of Electrospinning Parameters on Structure and Morphology

As just mentioned, structure and morphology of electrospun fibers are determined by a synergetic interaction between those various sets of parameters [74]. For example, viscosity influences fiber diameter. It can initiate bead-like shape, and influences jet trajectory [75]. There is an optimal viscosity for obtaining continuous fibers, and a higher viscosity produces larger diameters and pore sizes [75]. A minimum solution concentration is required to form a bead-free fiber; below a critical concentration, a mixture of beads and fibers results [75].

Solution conductivity, another key player, mainly depends on polymer type and solvent. Increased electrical conductivity results in a reduced nano-fiber diameter [76]. Molecular weight of the polymer plays an important role in electrical and rheological properties [77], with high values producing larger fiber diameters and pore sizes, while lower ones favor bead formation rather than smooth fibers [78]. Polymer jet velocity is obviously influenced by flow rate. Tuning the latter governs the solvent evaporation time, hence the formation of smooth, uniform fibers [79].

Applied voltage plays an important role in stability of the Taylor cone. For example, increased voltage results in higher jet velocity and reduced fiber diameter, which eventually leads to beaded fibers [75]. Distance between needle-tip and collector changes fiber diameter and morphology of the final mat. A minimum distance is required to allow fibers to properly dry before depositing on the collector, but increasing distance reduces the fiber diameter and eventually leads to bead formation [75].

Ambient conditions also influence fiber diameter and morphology. For example, as temperature increases, solution viscosity decreases, resulting in smaller fiber diameters and pore sizes, while high humidity forms circular pores on the fibers [80].

2.8.1.2 Effect of Electrospinning Parameters on Mechanical Properties

Recent studies have shown strong correlation between mechanical properties of a VG and IH. The reader is reminded that compliance, the measure of VG diameter change with pressure, is one of the key factors to success or failure [50]. Despite high burst pressures and suture retention strengths, compliance values of PET and ePTFE are much below native vessel values [81]. As a result, the compliant natural artery will expand and contract to maintain constant wall shear stress, whereas a stiff synthetic graft resists those changes in diameter. As also explained earlier, this compliance mismatch perturbs blood flow, results in zones of recirculation, flow separation, and low wall shear stress at the endothelium [34] that, along with cell-biological factors, stimulate IH [29]. Therefore, a VG that closely matches native artery compliance can greatly improve long-term clinical success.

Native blood vessels consist of alternating layers of elastin and collagen, which provide both high burst pressure and high compliance (respectively 1680 ± 307 mmHg and 4.4 ±0.8%/mmHg 10^{-4} for the saphenous vein) [50, 82]. Reproducing these in synthetic VGs is very challenging, given that they are often inversely related. The hierarchical structure of alternating elastin / collagen in arteries provides for a low tensile modulus with high elastic recovery, accompanied by strong strain hardening response at higher strains [83]. A synthetic material that can mimic this stress-strain behavior will obviously better match the required compliance properties and thereby reduce danger of IH. For example, electrospun fiber diameter and alignment, both of which can readily be “tuned”, are known to influence mechanical properties [84-86].

Electrospun nanofiber mats exhibit unusual, and unique mechanical properties compared with macroscopic film structures [87]. **Figure 2.7** shows that the stress-strain curve of an electrospun mat does not manifest “necking”, contrary to an injection-molded bulk polymer sample [86, 88].

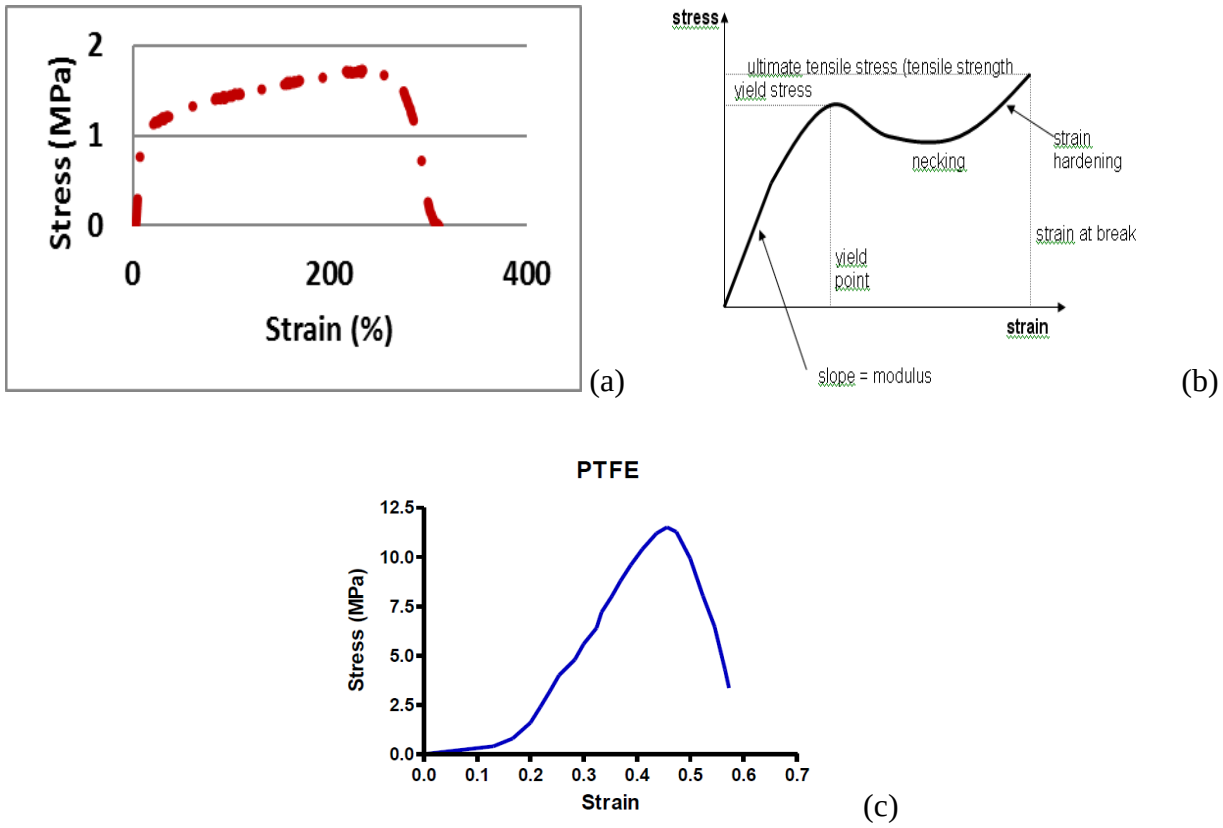

Figure 2.7 Typical stress-strain curve of the electrospun mats (a), the bulk polymer sample (b) and ePTFE VGs (c).

(a): authors' result on random ePET mat; (b) from (http://www.hardiepolymers.com); (c): from [89].

In electrospun fibers, crystallinity and molecular orientation play important roles in determining the physical and mechanical properties of resulting mats [90]. For example, the amorphous fraction influences strength and elastic modulus of fibers, while the crystalline phase imparts dimensional stability. Therefore, both phases combine to govern the overall mechanical properties of fibers [86], while the tensile properties of mats also depend on the properties of individual fibers, as well as their mutual interactions and arrangements within the mats. Therefore, those properties are not easily explained [87]. For example, deformation of a single fiber depends on its diameter: below a critical value, tensile strength is observed to increase exponentially, while large fibers show bulk-like properties [86]. This can be explained by gradual ordering of the macromolecular chains and increased crystallinity [90].

Other key factors which affect mechanical properties are the degree of fiber alignment within the mat, their entanglement, and interface properties where there is fiber-fiber contact. Tensile properties of random electrospun mats are generally lower than those of aligned ones, due to the fact that during tensile testing only fibers oriented along the loading direction are solicited, while perpendicularly oriented ones experience little if any force [91]. In the non-linear region of a typical stress-strain curve, fibers tend to align in the loading direction until they become highly oriented (ultimate tensile strength), eventually breaking at several locations (elongation at break).

2.8.1.3 Effect of Electrospinning Parameters on Cell Adhesion, Growth and Infiltration

Morphology and topography can regulate cell-adhesion, spreading, orientation, proliferation and infiltration through the phenomenon of contact guidance. The effect of fiber diameter on cellular activity has been extensively studied [92-94], but the results are not conclusive due to synergetic effects of porosity, pore size and fiber diameter. For example, Chen et al. [95] investigated fiber diameter (0.1-1.6 μm) in highly porous (pore size > 50 μm) electrospun polycaprolactone (PCL) scaffolds, observing initial surface proliferation and subsequent depth penetration of cells with increasing culture time. They concluded that fiber diameter < 1 μm improved cell-proliferation due to higher surface area and protein adsorption that promoted cell-adhesion. This was confirmed by Whited et al. [14], using random and aligned electrospun PCL/collagen fibers of different diameters (100 nm, 300 nm and 1200 nm). HUVEC-adhesion and growth were seen to be greater on sub-μm random and aligned scaffolds (100 nm, 300 nm) compared with the 1200 nm one.

Lowery et al. [92] observed that peak pore diameter related linearly with fiber diameter by a factor of 3.44 (R^2 = 0.97). This demonstrates that randomly aligned electrospun fibers of 1 μm diameter create a fabric having a peak pore diameter of 3.44 μm, smaller than the average rounded cell diameter of 5–20 μm. Other studies implanted VGs in animal models with fiber diameter less than 1 μm and confirmed that these VGs inhibit cellular penetration [96-98].

2.8.1.3.1 *Effect of Fiber Orientation*

The effect of topography and orientation on cell morphology and alignment has been controversial in the literature. Whited et al. [14] investigated electrospun random, semi-aligned and fully-aligned polycaprolactone (PCL)/collagen fibers with different diameters (100 nm, 300

nm and 1200 nm). They concluded that the fiber orientation had a significant influence on HUVEC orientation at 1200 nm, but no significant influence for smaller diameters. Gaharwar et al. [99] observed that anisotropic mats of electrospun fibers promote EC proliferation and led to highly organized endothelial constructs. Further, the metabolic activity of HUVECs seeded on aligned PGS-PCL scaffolds was higher than on random ones [99]. On the other hand, HUVECs seeded on random hexyl methacrylate (HMA)/methyl methacrylate (MMA)/ methacrylic acid (MAA) scaffolds with small pore size exhibited a significantly higher growth compared with aligned ones [100].

2.8.1.3.2 *Effect of Porosity and Pore size*

The “ideal” VG scaffold should have adequate porosity and pore size to fulfill the requirements of each particular layer [101]. For example, small pore size enables adherence and localization of ECs on the topmost surface and formation of the confluent monolayer, while large pore size allows VSMCs to migrate into the wall [10, 11, 102].

Research indicates that electrospun fiber mats behave differently from more rigid porous materials. For example, in a rat model it was shown that cells could penetrate into electrospun PGA mats with fiber diameters as low as 0.22 μm and pores of only 1.5 μm, much smaller than the assumed minimum of 10 μm. This was explained by the ability of cells to push aside individual fibers [103]. Ju et al. [104] demonstrated that fiber diameters < 1.0 μm inhibited infiltration of SMCs. De Valence et al. [96] investigated bilayered PCL mats featuring a less porous (fiber diameters 0.83 μm) and a more porous layer (diameters of 2.21 μm); after implantation, they noted reduced infiltration when the adventitial layer was less porous, but neither case affected the rate of endothelialization [96, 105].

Thus, there is an apparent paradox that fibers with < 1 μm diameter and lower porosity inhibit cellular infiltration. To address this, methods for producing increased pore size but without increasing fiber diameter have been investigated, based on bi-layers, salt leaching, sacrificial fibers, air-flow impedance, and cryogenic spinning [106-108].

2.8.2 Advantages of Electrospinning for VG

Electrospinning is a very promising technique for VG since it can be used to create nano/micro-fibrous scaffolds that mimic the structure and mechanical properties of natural blood vessels [109].

Nano/micro-fibrous constructs can assure mechanical strength, cell-attachment, and reservoirs of biomolecules just like natural fibrous components of the ECM. They can also allow seeded cells to bridge voids, attach at multiple sites and control cellular functions, such as phenotype, ECM deposition, and infiltration into pores [92]. Other desired features for engineered VGs include high porosity for infiltration and tissue in-growth, high surface-to-volume ratio, tunable mechanical properties, capability of surface modification, and ability to load drugs or genes [110].

A nano/micro-fibrous scaffold is often very strong: Electrospinning enables one to tune strength and elasticity through different fabrication parameters, including fiber alignment, crystallinity, porosity, thickness, and others. However, mechanical properties tend to be material-dependent. Although numerous studies have attempted to increase compliance of electrospun scaffolds, it is still an ongoing challenge to meet the compliance of the natural blood vessels in order to achieve optimal therapeutic value [111].

Most important for *in vivo* application, an electrospun VG should possess anti-thrombogenic properties, for the reasons explained earlier. Next, it should facilitate infiltration of cells to achieve adequate new tissue formation. Analyzing and understanding reported *in vivo* studies enables one to understand benefits and challenges of electrospun VGs, and sheds light on design criteria.

AVflo™ (Nicast) was the first commercially available large-diameter electrospun PU vascular access graft for hemodialysis [112]. Nanovessel IV™ (Nanofiber Solutions) is a synthetic nano-fibrous veterinary blood vessel for enhancing vein and artery formation. Although electrospun nanofibers have great potential to replace occluded blood vessels in humans, limited studies have been performed on animal models. Furthermore, they do not apply to clinical trials in humans since they did not sufficiently address mechanical performance under dynamic conditions, or regulatory issues like sterility, stability, and quality control [113].

2.9 Surface Modification of Nanofiber Scaffolds to Improve Bio-functionality

2.9.1 Rationale

As described before, the patency rates of VGs depend upon their ability to inhibit thrombosis and IH: inadequate endothelialization is presently the most important limitation. *In situ* and*in vitro* endothelialization show promise to enhance patency rates after implantation. Strategies for minimizing thrombosis include thrombo-resistant scaffold materials, anti-coagulant or anti-platelet drug eluting polymers, chemical modification of the luminal surface, and expediting development of a confluent endothelial layer.

In all cases, understanding cell interactions with scaffolds is key for choosing the best strategy towards endothelium formation on VGs. Cells interact via integrin receptors on their membranes with their corresponding ligands on ECM such as collagen, fibronectin, vitronectin, laminin, etc. [114, 115]. The same mechanism is applicable on biomaterials surfaces *in vitro*: After initial contact with cell culture medium or body fluid, proteins adsorb on the biomaterial surface, mediating its interaction with living cells.

The interaction of adsorbed proteins with adhesion receptors, such as integrin on inflammatory cells, plays a crucial role in the recognition of biomaterials [116]. The presence of adsorbed proteins (albumin, fibrinogen, fibronectin, vitronectin, γ-globulin, and others) modulates host inflammatory cell interactions and adhesion, and they are thus linked to subsequent inflammatory and wound-healing responses. Natural polymers generally induce cell-ECM interactions, but they do not possess satisfactory mechanical properties. In contrast, most synthetic polymers used as biomaterials and scaffolds, despite being mechanically strong and chemically stable, generally possess chemically and biologically inert hydrophobic surfaces (low surface energy), leading to inadequate cell attachment, -spreading and -proliferation [117]. Thus, surface modification has been widely studied [118-120], including physico-chemical methods (surface roughness, -energy, and/or chemical composition), or by immobilizing bioactive molecules.

Thus, surface modification can be categorized into: i) physical patterning / modification [121], inducing specific topographical features to physically control cell behavior; ii) chemical

treatments, which introduce functional groups that improve cell affinity through enhanced wettability; and iii) bio-functionalization with bioactive molecules like ECM proteins [Collagen (Types I to XXVIII), fibronectin and gelatin], peptides [Arg–Gly–Asp (RGD)], glycoaminoglycans (GAGS), and growth factors, through physical adsorption or chemical immobilization [122-124]. Candidates for these include irradiation by γ-rays [125], electron beams [126], lasers [127], ultraviolet photons (UV) [128], and plasma treatment [129], but also wet-chemical treatments with NaOH [130], hydrogen peroxide (H_2O_2) [131], or graft polymerization [132]. Wet chemistry is the one most frequently encountered in the literature [6]. For example, in the case of PET, OH^- hydrolyses the ester groups and breaks the polymer chain, forming carboxylic acid and hydroxyl groups at the end of the two new chains. It was shown to increase surface roughness of PET fibers, cell adhesion and -proliferation [133]. Another technique, to introduce amine functional groups on PET surfaces and to thereby promote cell affinity, is aminolysis [134]. However, although wet chemistry is easy, it is also harsh and causes undesirable loss of mechanical properties and irregular surface etching. Furthermore, it tends to entrain problems of toxicity and environmental impact [117]. In contrast, a particularly powerful dry technique is non-thermal plasma treatment, which can produce unique surface properties, such as chemical cues and/or roughness without changing favorable bulk properties of the substrate; examples of resulting surface-near functionalities are primary amines, carboxylic or hydroxyl groups, among others, all known to promote cell adhesion and/or to enable immobilization of biomolecules [135]. Due to these advantages, plasma surface modification demonstrates great potential and will therefore be reviewed next.

2.9.2 Surface Modification by Plasma

2.9.2.1 Basic Concepts

Plasma, the “4th state of matter”, can occur when there exists a source of energy that exceeds the ionization potential of gas molecules. The resulting dissociation and ionization of a neutral gas leads to an equal number of negative and positive charges: electrically quasi-neutral, plasma is a highly reactive multi-component system containing charged particles (electrons, negative and positive ions), excited atoms and molecules, reactive atoms and radicals, and UV photons [136]. Thermal plasmas, in thermodynamic equilibrium, have gas temperatures of several thousand

degrees. They are so destructive that they cannot be employed for surface modification of heat-sensitive materials such as polymers [136]. On the other hand, “cold” (non-equilibrium) plasmas have low gas temperature, but high-temperature electrons: temperature of the gas, that of neutrals and ions, is approximately room temperature. Therefore, non-destructive, it can be utilized for surface modification of heat-sensitive materials like polymers. In this research, we always refer to cold plasmas [136].

In order to generate plasma, energy for ionization must be continuously supplied by an external source, such electrical energy [136]. The most common and convenient source is alternating current (AC), which can be applied at low (line) frequency of 60 Hz, audio frequency (for example, 20 kHz), radio- (13.56 MHz) or microwave frequency (2.45 GHz).

2.9.2.2 Plasma Processes

The surface of a polymer in contact with plasma undergoes reactions with highly reactive species that include ions, atoms and molecular free radicals. Breakage of covalent bonds at the polymer surface and reaction with above-named species changes the polymer’s surface properties while the bulk remains unaffected. Several parameters dictate the type of the reactions that take place, including the gas (composition, and flow rate), power, time of exposure, among others. Process types can include etching, surface functionalization, and deposition of a plasma-generated coating [137].

2.9.2.2.1 *Surface Functionalization*

In this process, hydrogen atoms or chain fragments on the polymer are removed by the plasma and replaced by oxygen- or nitrogen-bearing radicals, leading to the formation of polar hydrophilic groups such as hydroxyl, carbonyl, carboxyl, primary amine groups, etc. on the surface [138]. Therefore, selection of the reagent gas for example oxygen, air, ammonia, is important in determining the type(s) of functional groups [139]. Surface functionalization is mostly aimed to increase the surface energy (wettability). However, this property is not permanent because such surfaces tend to undergo so-called “hydrophobic recovery” [140]. Plasma modification of 3D fibrous structures occurs because the plasma species penetrate readily

inside the porous structures, but most characterization techniques only permit access to the outside surface [141]. Many studies have investigated cell interactions with plasma-modified fibrous structures or fabrics after immobilization of various bioactive molecules including proteins such as gelatin, collagen, laminin, fibronectin, etc. [142-147]. For instance, electrospun nanofibers composed of biodegradable polymers such as PGA, PLLA, or PLGA were modified using oxygen and acrylic acid plasma treatment to promote fibroblast adhesion and proliferation, without significant change in mechanical properties [148-150]. Air or argon plasma treatment has also been extensively used to incorporate carboxylic acid groups on the electrospun nanofibers, leading to enhanced cellular activity [151, 152].

2.9.2.2.2 *Grafting*

Free radicals on a polymer surface can react with a monomer, to initiate polymerization on the surface. This may take place in the plasma chamber by directly introducing the monomer, or by post-reaction of the monomer with reactive groups (**Figure 2.8**) [7]. Unlike plasma modification, grafting tends to be permanent. Surface graft polymerization not only can improve hydrophilicity, but also can introduce functional groups for subsequent covalent immobilization of biomolecules to promote cell adhesion, proliferation, and differentiation [153]. For example, graft polymerization of hydrophilic methacrylic acid (MAA) monomer was initiated on hydrophobic porous PU scaffolds, resulting in improved endothelialization [154]. In another example, gelatin was covalently attached on PMAA-grafted PET nano-fibrous scaffolds using water-soluble carbodiimide chemistry, leading to significant increase in EC-adhesion and growth [155].

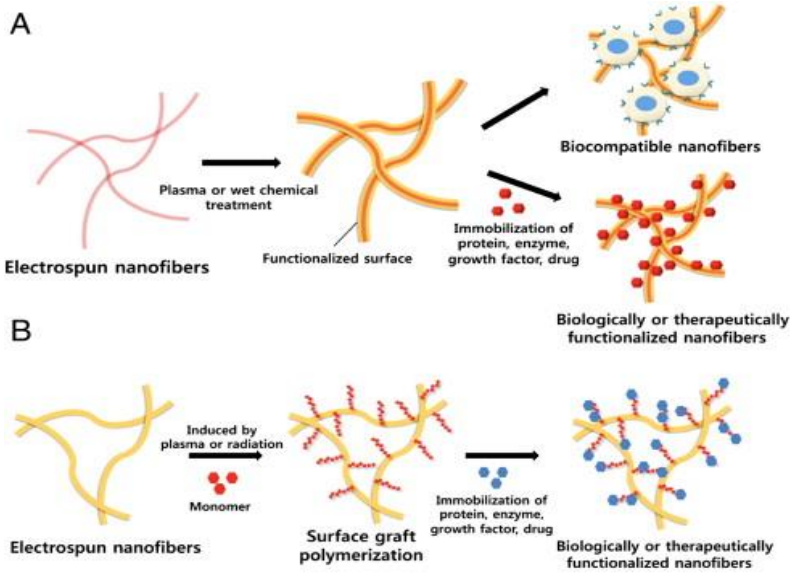

Figure 2.8 Surface modification techniques of electrospun nanofibers: (A) Plasma treatment or wet chemical method; (B) Surface graft polymerization from [156].

2.9.2.2.3 *Etching*

Physical sputtering occurs when energetic ions bombard the topmost layer of a polymer surface [157]. To improve the efficiency of *physical* etching by non-reactive (inert) gases such as argon or helium, oxygen and/or fluorine-containing gases such as SF_6 and CF_4 can be introduced so as to add more rapid *chemical* etching, whereby the polymer bulk again remains unchanged. Unlike wet-chemical etching, plasma etching is a controllable and selective *dry* process [158].

2.9.2.2.4 *Plasma-Induced Deposition of Polymer-Like Coatings (Plasma Polymerization)*

In this laboratory, plasma-assisted deposition is done in a capacitively-coupled parallel-plate radio-frequency (r.f.) plasma reactor (**Figure 2.9**), utilizing precursor gases or vapors at low pressure (usually <20 Pa) that fragment under electron-bombardment and undergo plasma-polymerization via free radical reactions. When the process gas consists wholly or in part of an organic compound, for example a hydrocarbon, the resulting free radical fragments give rise to a "plasma polymerization" process, the plasma polymer film being deposited on any solid substrate surface placed within the plasma chamber, including the chamber walls. Even methane, ethane

and others which have no unsaturated bonds can form plasma polymers, contrary to conventional polymerization. Due to the complex fragmentation and recombination processes, the resulting films' structures are unlike conventional polymers. The structures of plasma polymers can even be varied by including "co-monomers", for example by introducing oxygen, nitrogen, ammonia, SO_2, or other heteroatom-containing gases into the process gas, thereby introducing functional groups such as hydroxyl, carboxyl, carbonyl, amine-, etc. Therefore, plasma polymerization is an important method to modify inert surfaces like PTFE, PE, PET or others for biomedical applications. It must again be underlined that the substrate's physical (e.g., mechanical) properties are not appreciably influenced by this very thin coating [159]. Numerous articles and reviews in the literature have demonstrated the great interest in amine- ($–NH_2$) containing organic surfaces for biotechnological applications, either to directly foster cell adhesion or to immobilize biomolecules [118, 160]. It is particularly clear that nitrogen-(N)-containing groups are excellent, most specifically the primary amine ($–NH_2$) functionality, among others [161, 162].

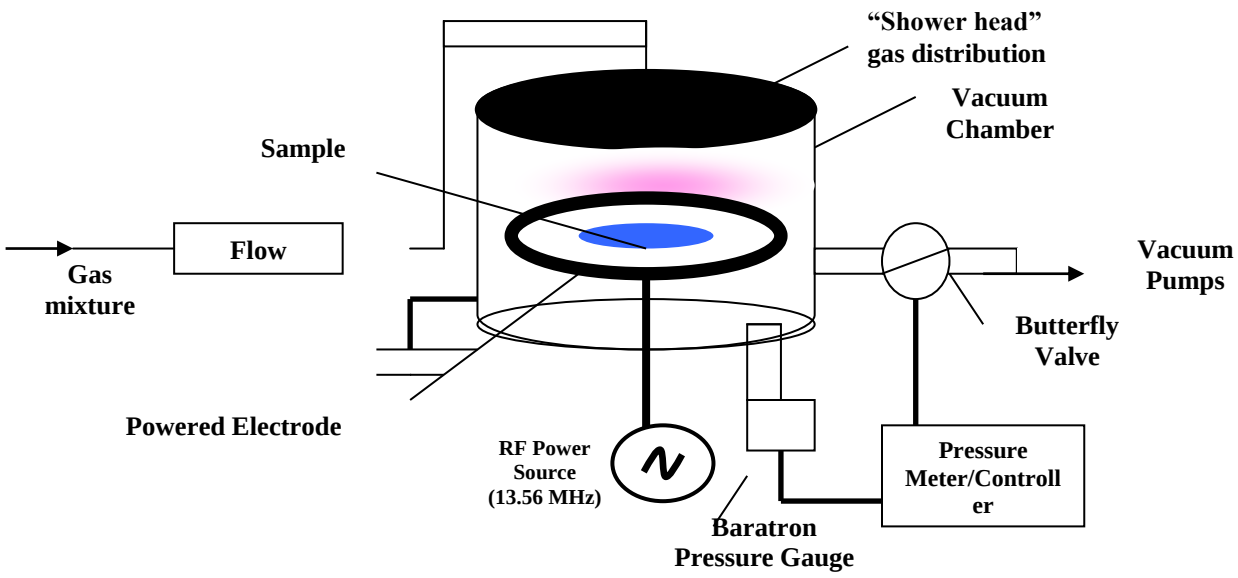

Figure 2.9 A schematic diagram of a capacitively coupled plasma reactor [160].

2.9.3 Previous Related Plasma Polymerization Work in This Laboratory

In previous collaborations, the teams developed low-pressure plasma-polymerized ethylene doped with nitrogen (L-PPE:N / LP) coatings, which were deposited on PET and PTFE surfaces to improve EC attachment and resistance to shear flow [163]. The results showed that cell adhesion and adhesion rate, spreading, focal adhesion, and resistance to flow-induced shear were improved, compared with bare and gelatin-coated PET and PTFE. Therefore, L-PPE:N appears to be a promising candidate for improving the endothelialization of VGs [163]. In other similar studies of our group, we showed similar performance for VSMCs, fibroblasts and mesenchymal stem cells (MSC), namely to adhere and proliferate on L-PPE:N-coated surfaces [164, 165]. Moreover, L-PPE:N has several other advantages over plasma-induced grafting pre-treatment, for example different nitrogen- ([N]) and primary amine ([–NH_2]) concentrations [162, 164]. In contrast to coatings made from pre-adsorbed proteins, plasma polymer is firmly adherent on substrates. One drawback is slow partial conversion of primary amines to amides, due to oxidation by atmospheric oxygen [166]. Finally L-PPE:N can be used to immobilize selected biomolecules through reactions with their carboxylic acid groups.

2.9.4 Plasma Polymerized Coating for Electrospun Mats

Plasma polymerized coating on electrospun nano-fiber mats has been discussed in several recent studies, for example plasma-polymerizd allylamine (PPAAm) was used to coat the fiber surfaces of electrospun non-woven poly(L-lactide-co-D,L-lactide). *In vitro* cell experiments using human osteoblasts confirmed improved cell spreading on the positively-charged, amino group-containing PPAAm surfaces already after 1 h of incubation, and the rapid formation of filopodia along and between the electrospun polylactide fibers [167].

In another recently published study, plasma-polymerizd oxygen-functionalized hydrocarbon coatings were applied on synthetic fibrous PCL substrates. The authors showed that these scaffolds were suitable for *in vitro* development of muscle tissue, especially for cellular alignment and myotube formation [168]. Allylamine was plasma-polymerized on electrospun PLGA mats, resulting in highly hydrophilic substrates containing amine groups. To further

improve bioactivity, heparan sulfate was immobilized on the plasma-polymer and it was shown to support embryonic stem cell culture and differentiation [169].

2.10 Bioactive Coatings for VGs

In this section, we will summarize the different strategies employed by the researchers in order to tackle the issues of IH and thrombosis in SDVGs, and prolong the graft patency.

First, coatings have been developed to decrease risks of thrombosis in VG using various anticoagulants (heparin), antiplatelet factors (glycoprotein inhibitors), and antiproliferating agents (rapamycin) [170]. However, it is now generally recognized that the efficacy of this approach is limited in time, and that the best non-thrombogenic surface is a complete monolayer of ECs. Therefore, bioactive coatings have been created to foster either *in vitro* or *in situ* pre-endothelialization. Since *in vitro* endothelialization is time-consuming and costly, *in situ* endothelialization has been recently experimented extensively to find highly desirable and fast methods [171]. *In vivo* circulating ECs could potentially be captured onto a functionalized graft for *in situ* endothelialization [172]. Unlike *in vitro* endothelialization, *in situ* endothelialization includes some advantages such as fast availably upon demand, simpler surgical procedures and more stable endothelium formation *in vivo.* However, the challenge is to develop a coating which captures and homes ECs.

2.10.1Bioactive Coatings for *in-vitro* or *in-situ* Endothelialization

The main challenge in endothelialization is to find a more specific and selective biomolecule to capture cells. Once it is selected, the bioactive molecule can be immobilized on the biomaterial's surface via physical adsorption or chemical conjugation [173]. To resist the shear stress of the blood flow *in vivo*, chemical conjugation has shown the greater promise by establishing an anchor-like binding mechanism leading to longer stability and controllability of the biomolecules. Usually, functional groups including primary amines ($-NH_2$), carboxyl (-COOH), hydroxyl (-OH) or thiol (-SH) groups induced on the surface of the biomaterials using the previously described methods, can be used as a binding site for the bioactive molecules [54, 173].

Biomolecule immobilization demonstrated great promise due to more durability and stability resulting in enhanced and continuous cell response [174]. Moreover, in the case of GFs, lower quantities of immobilized GFs are required to stimulate cellular function when compared to diffusible form where large amounts are required by a sustainable source (either medium renewal *in vitro* or controlled release). Covalent immobilization provides long term availability and strong attachment leading to an irreversible and durable binding of functional groups [175].

Due to the promising anti-platelet adhesion property of GAGs, several groups including our team, have explored the use of GAG molecules to modify the surfaces of cardiovascular devices. To prevent platelet adhesion, chondroitin sulfate (CS) and hyaluronic acid (HA) are used for the luminal surface coating of VGs [176-179]. Because GAG coating provides a low adhesion layer mimicking the EC surface, further studies are needed to verify the biological function *in vivo*. GAGs are also key intermediaries of growth factor binding, and they have been shown to influence the bio-activities of different GFs through interaction via their glycosaminoglycan moieties as well as their core proteins [180, 181]. GAGs immobilization strategies have included physisorption, electrostatic deposition, and covalent bonding to surfaces [182, 183]. For example, cross-linked collagen surfaces have been used for the covalent immobilization of heparin to improve blood compatibility, but the use of highly thrombogenic materials such as collagen for VGs may be problematic [4,10].

Our team has been working on bioactive coatings combining L-PPE:N / LP coatings, CS and GF immobilization (e.g. Epidermal Growth Factor (EGF) and Vascular Endothelial Growth Factor (VEGF)) to promote ECs and VSMC adhesion, growth, and survival, as well as vascular repair around vascular implants [13, 184-187].

CS, a glycosaminoglycan naturally encountered in blood vessels, has demonstrated anti-apoptotic properties in rat and human VSMC as well as in fibroblasts [184, 188-190].

Similar to *in vitro* endothelialization, non-selective cell adhesive proteins or peptide motifs such as collagen [191], fibronectin [192], gelatin [171] and RGD peptides [193] have been used to recruit EPCs from blood circulation. However, these bioactive coatings are not selective for ECs and other circulating cells, because platelets, leukocytes and SMCs can also be captured and homed on the lumen, leading to IH. For example, in a clinical study, gelatin-coated grafts resulted in significant inflammation [194], rendering this technique undesirable.

Several growth factors and biomolecules have been studied as promising candidates for promoting cellular activities of ECs and ECPs. Growth factors (GFs) are naturally occurring components that can influence cellular activity in the body in soluble form, or they can be ECM-incorporated stimulators for the cells. Therefore, there have been many attempts to incorporate GFs into scaffolds in order to take advantage of their intrinsic regenerative properties through sustained release or surface immobilization on different constructs [195, 196].

VEGF with very high EC specificity and without mitogenicity for other cell types, is a secreted protein ligand that activates transmembrane receptors on ECs. The activation of VEGF receptors (VEGFR-1(flt-1) and VEGFR-2(KDR/flk-1)) provokes different cell signaling pathways leading to EC survival, proliferation and vascular organization [197]. Covalently immobilized VEGF was shown to improve endothelialization by increasing EC adhesion, proliferation and migration *in vitro* [198]. It also has potential to promote EPC differentiation to the endothelial lineage under shear-induced flow [199], but burst release of VEGF from a device surface or secreted from monocytes may lead to tumor development [200].

EGF, a 6-kDa mitogenic polypeptide, has been shown to possess anti-apoptotic properties and to enhance VSMC growth. Our team has recently developed bioactive coatings for vascular implants, ones that combine CS and covalently immobilized EGF, to favor vascular cell growth and resistance to apoptosis [184, 189].

Heparin, an anti-coagulant, has also been widely employed in VG engineering. Its effect in promoting EC-adhesion, -proliferation and -growth has been observed *in-vitro* and *in-vivo* [201, 202].

Selective cell-capturing biomolecules including antibodies, peptides and aptamers could target specific surface molecules of ECs. To take advantage of their capabilities, scaffolds could be functionalized with these biomolecules for *in-situ* endothelialization.

Cell-specific binding peptides including YIGSR and REDV, more specific to ECs, are respectively derived from laminin and fibronectin. Some studies have investigated their potential for promoting cellular activity of ECs compared to SMCs, and for preventing platelet adhesion [203-206].

The key factor influencing bioactivity of immobilized biomolecules includes its final conformation on biomaterials, whereby the active side of the biomolecule should be easily

accessible by the receptors of cells [207, 208]. A spacer can be incorporated onto the short peptide motifs to make them more readily accessible. On the other hand, to further enhance bioactivity and binding affinity of antibodies, and considering their “Y” configuration, tuning their spatial orientation is a critical factor in surface engineering [209]. Several studies have noted that oriented antibodies, as opposed to random ones, orienting significantly increased the capture efficiency [207]. Generally, random orientation involves primary amine groups, which are distributed throughout the antibodies. However, in order to orient them on a biomaterial surface, various site-selective techniques using specific moieties on the antibodies have been proposed [210, 211].

Other strategies to maintain GF bioactivity are to employ ECM binding tags that can be genetically fused to the GF, or pairs of high affinity peptides with variable stabilities in which one is bound to the substrate of interest while the other is fused to a GF by genetic engineering [212]. Our team has investigated the bioactivity of random covalent and oriented tethered EGF for VSMC survival. The results demonstrated that random covalent EGF immobilization are not an optimal strategy to take the full advantage of protein bioactivity due to inappropriate conformation and/or epitope inactivation, thus inhibiting optimal communications with cells [213]. An innovative oriented immobilization strategy for GFs based on two high-affinity peptides including Ecoil and Kcoil with high specificity that bind to each other to form stable coiled-coil structures, was developed [214]. Ecoil-tagged EGF (Ecoil-EGF) was produced in human embryonic kidney (HEK) 293 cells and its bioactivity was confirmed on human epidermoid carcinoma (A-431) and human corneal epithelial (HCE-2) cell lines [215]. Therefore, the bioactivity and protein surface density of EGF on the film-like scaffolds are significantly promoted by utilizing oriented EGF immobilization strategy, where all immobilized EGF molecules are attached via a tag added to a specific EGF region in order to allow immobilization without epitope inactivation [185].

In a very recent study in our group [186], the synergetic effect of co-immobilized EGF and VEGF on the CS-grafted film-like scaffolds on *in vitro* cellular activity was investigated. CS layer has shown to promote cell adhesion but reduces nonspecific adsorption of plasma proteins [13]. In *in vivo* environment, GFs show collective or complementary effects on wound healing or angiogenesis. There is an unmet need of research to illuminate the potential synergies existing between GF that could be utilized to promote VGs bioactivity. The results showed the feasibility

of the controlled combination of EGF and VEGF with pro-survival properties for ECs and VSMCs compared to each GF captured alone, demonstrating a collaborative effect of these GFs [186].

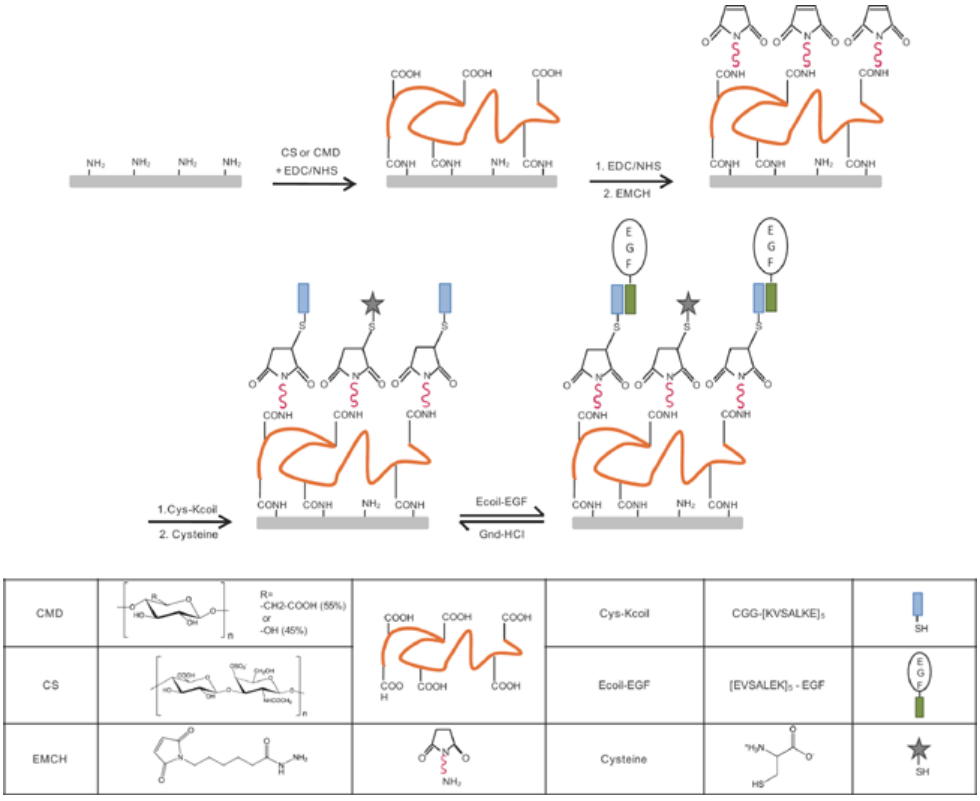

Figure 2.10 Schematic illustration of the grafting steps for the oriented EGF immobilization on CS and CMD. The grafting of CS or CMD layers on aminated surfaces was followed by the chemical grafting of cysteine-tagged Kcoil peptides using EMCH as heterobifunctional linker. Remaining EMCH thiol-reactive groups were deactivated using cysteine molecules. Ecoil-tagged EGF proteins were captured on the surface via the reversible E/K coiled–coil interaction [185].

One of the challenges which the bioactive immobilized biomaterials face in the *in vivo* environment is the issue with non-specific protein adsorption. For example, once a biomaterial is implanted inside the body, proteins in the blood such as fibrinogen is adsorbed on its surface leading to mask the bioactive coatings. There are few studies addressing this issue by utilizing an anti-fouling PEG layer, with the longer PEG chain length which showed to reduce fibrinogen adsorption [13]. Our team has also investigated utilizing star PEG grafting and CS to create

nonfouling and nonthrombogenic surfaces. The outcome of these studies showed that CS is as effective as PEG in reducing fibrinogen adsorption (~90% reduction) and nonthrombogenicity. Furthermore, CS significantly promoted HUVEC adhesion and growth compared to PEG-grafted and bare scaffolds [13, 216]. In another study [217], Anti-CD34 Ab, randomly immobilized onto the PEG layer, as expected, resulted in a slight increase in fibrinogen adsorption. However, platelet adhesion was somehow similar and EPC adhesion was greater than the control scaffold before antibody immobilization.

CHAPTER 3 HYPOTHESES & OBJECTIVES

As seen in the literature review, conventional prosthetic VGs (ePTFE, PET) have proven unsatisfactory for small-diameter vessels (below 6 mm) due to poor endothelialization and compliance mismatch, which lead to thrombogenesis and consequently the lack of patency. In this thesis, we hypothesize that combination of electrospinning and surface modifications can provide adequate scaffolds for luminal and media layers of SDVGs. Bioactive coatings are particularly interesting since they can be applied to any kind of surface (versatile approach).

The specific hypotheses of this thesis are:

Hypothesis 1: Electrospinning of PET can create nanofibrous structures that are more compliant and favor the formation of an EC monolayer compared to conventional woven PET or ePTFE structures;

Hypothesis 2: Plasma coating can improve the biological properties (EC attachment and growth) of electrospun mats;

Hypothesis 3: Plasma etching techniques can help optimize the compliance of the structure without damage to the fibers;

Hypothesis 4: Bioactive coating made of CS and GFs can further optimize the biofunctionality of the structure to promote envisaged cell adhesion, growth, survival and infiltration.

The general objective of this thesis is: 1) to create scaffolds for subsequent cell-seeding in the luminal and media layers, by fine tuning properties of 3D electrospun scaffolds by plasma-assisted coating and/or etching accompanied by bioactive coatings (e.g. CS and/or oriented tethered EEGF) for VG applications; and 2) to evaluate these in regards to their morphology, physico-chemical, mechanical properties, as well as their ability to favor cell adhesion, growth, survival and resistance to shear.

The rationale and specific objectives of the three papers are described below:

Paper 1

3D nanofibrous mats are excellent candidates as scaffolds that provide mechanical compliance, morphology and surface area that mimic those of natural blood vessels. Electrospun PET appears to be an excellent candidate for small-diameter grafts in regards to mechanical properties, stability, biocompatibility, and low cost, but foremost due to the fact that PET VGs have already been FDA-approved and clinically used for a few decades. However, the synthetic polymers are generally chemically quite inert; this doesn't favor endothelialization and could also lead to thrombus formation. Plasma-polymerization of thin coating on the inner surface is an interesting method to promote biomolecules immobilization via carbodiimide chemistry and eventually to enhance directly EC adhesion and growth

Therefore, we hypothesized that 3D electrospun nanofiber mats combined with nitrogen-rich plasma-polymerized coating can provide scaffolds that are morphologically suitable, mechanically compliant and biocompatible for optimum EC-adhesion, -growth, and -shear resistance properties.

The specific objectives of the first paper were thus to create 3D electrospun random nano-fibrous PET scaffolds for the luminal side of VG, to combine them with optimized nitrogen-rich L-PPE:N (or LP) coatings, and to evaluate these in regards to their composition, morphology, mechanical properties, as well as their ability to favor HUVEC adhesion, growth, and resistance to flow-induced shear.

Paper 2

In this paper, we focused on the medial layer of VG. Aligned electrospun fibrous scaffolds have been investigated to mimic circumferentially aligned orientation similar to that in the media layer in natural vessels. Yet, it was shown that tensile properties, including Young's modulus, of random and aligned ePET mats are higher than those of natural arteries. Therefore, we hypothesized that etching techniques can help optimize the mechanical properties of electrospun mats in order to provide scaffolds that are morphologically suitable for VSMC infiltration and guidance, and mechanically compliant for VG application.

The specific objective of the second paper was thus to compare the effect of various low- and high (atmospheric-) pressure plasma-etching on mechanical, morphological, chemical, and biocompatibility properties of aligned ePET mat scaffolds, specifically destined for the media layer of VG.

Paper 3

In our first objective of this research, we showed that random electrospun nanofiber mats coated by primary-amine rich plasma polymer coating (LP) lead to finely controlled structural and surface properties that are required for confluent EC monolayer on VGs. EC adhesion, -growth, and -retention under shear-induced flow stress were shown to be increased by L-PPE:N coating. However, cell retention is still not ideal. Moreover, this underlying L-PPE:N-coated substrate is thrombogenic. Our team recently demonstrated that grafting CS on LP plasma coating prevents platelet adhesion while promoting HUVEC adhesion and growth.

We therefore hypothesized that grafting CS on LP coated electrospun mats can enhance HUVEC adhesion, growth and their resistance to detachment.

In addition, EC alignment in the direction of blood flow in the natural arteries is known to increase the cell capability to resist detachment under shear stress. This is typically achieved by a long and resource-consuming method involving *in vitro* fluid flow preconditioning in a bioreactor prior to implantation. Our second hypothesis was therefore that EC resistance to shear stress may be further improved if they can be directed by tuning electrospun alignment.

Furthermore, bioactive coatings comprising CS-grafted surfaces with EGF in an oriented manner have shown by our team to enhance VSMC adhesion, growth and survival on the film-like structure.

Therefore, we hypothesized that bioactive coatings (LP+CS+oriented tethered EGF) with aligned mats having larger pore-size for the media layer can favor VSMC adhesion, growth, survival and infiltration.

The objective of this study is thus to immobilize CS on plasma-coated random (R) and aligned (A) electrospun nanofiber mats and to evaluate their bioactivity and ability to favour EC adhesion, growth and resistance to shear-induced flow. In addition, it is also to investigate

simultaneous VSMC survival and infiltration and circumferential alignment under the guidance of grafts with circumferentially oriented fibers. **The specific objectives of the third paper were thus to:**

1- **investigate electrospun mats with *bioactive coatings* that improve cell behavior, said coatings being based on LP coating and CS, with or without EGF.**
2- **investigate the effect of immobilized CS on random or aligned mats with small pores on HUVEC adhesion and growth under flow for the lumen side of the VGs.**
3- **investigate the effect of a CS-EGF coating on aligned scaffolds with large pores in regards to increased VSMC survival and infiltration into the pores.**

CHAPTER 4 ARTICLE 1: ELECTROSPUN NANOFIBER SCAFFOLDS AND PLASMA POLYMERIZATION: A PROMISING COMBINATION TOWARDS COMPLETE, STABLE ENDOTHELIAL LINING FOR VASCULAR GRAFTS

Houman Savoji, Afra Hadjizadeh, Marion Maire, Abdellah Ajji, Michael R. Wertheimer*, Sophie Lerouge*

_____

Houman Savoji, Prof. Abdellah Ajji, Prof. Michael R. Wertheimer

Institute of Biomedical Engineering, École Polytechnique de Montréal, Montreal, QC, H3C 3A7, Canada

Prof. Afra Hadjizadeh, Prof. Abdellah Ajji

Department of Chemical Engineering, École Polytechnique de Montréal, Montreal, QC, H3C 3A7, Canada

Houman Savoji, Dr. Marion Maire, Prof. Sophie Lerouge

Laboratory of Endovascular Biomaterials (LBeV), Research Centre, Centre Hospitalier de l'Université de Montréal (CRCHUM), Montreal, QC, Canada

Prof. Michael R. Wertheimer

Department of Engineering Physics, École Polytechnique de Montréal, Montreal, QC, H3C 3A7, Canada, E-mail: michel.wertheimer@polymtl.ca

Prof. Sophie Lerouge

Department of Mechanical Engineering, École de technologie supérieure, Montreal, QC, H3C 1K3, Canada, E-mail: Sophie.lerouge@etsmtl.ca

This article has been published in "*Macromolecular Bioscience 2014, 14, 1084–1095* " *[10]*.

Abstract

In the quest to reduce risk of thrombosis in vascular grafts, it is essential to provide a surface with morphological and mechanical properties close to those of the extracellular matrix beneath the luminal endothelium, and to favor the growth of a confluent, stable monolayer of endothelial cells. This is accomplished here by combining electrospun poly(ethylene terephthalate) (PET) mats with an amine-rich thin plasma-polymerized coating, designated “L-PPE:N”. Its deposition does not modify the open, highly porous mats and leads only to small changes in mechanical properties. L-PPE:N significantly improves the adhesion and growth of human umbilical vein endothelial cells (HUVEC) and their resistance to flow-induced shear stress. These properties favor the formation of desired confluent HUVEC monolayers on the topmost surface, unlike conventional vascular grafts (ePTFE or woven PET), where cells migrate inside the material. This combination is therefore highly advantageous for the pre-endothelialization of the luminal side of small-diameter vascular prostheses.

Keywords: electrospinning, plasma polymerization, mechanical property, surface chemistry, endothelialization.

4.1 Introduction

Cardiovascular diseases are the leading cause of premature death worldwide, occlusion of blood vessels being a major problem [218]. Autologous grafts from patients' own veins or arteries can provide a solution when angioplasty or stenting are not feasible, but not when treatment is impeded by previous surgery or antecedent vascular disease. In such circumstances, synthetic vascular grafts constitute the only option [219]. Current commercial grafts are made from synthetic polymers, expanded poly(tetrafluoroethylene) (ePTFE) or Dacron® [woven poly(ethylene terephthalate), PET], but they are used clinically only as large-diameter vessels, > 6 mm [219] since their patency rate is poor as smaller-diameter vessels. This is mainly due to inadequate endothelialization and to mechanical compliance mismatch, which lead to occlusion on account of thrombosis and intimal hyperplasia [220]. Therefore, synthetic scaffolds are required that simulate the mechanical and 3D nano-fibrous morphological properties of the extracellular matrix (ECM) beneath endothelial cells (ECs) [221]. Electrospinning is the ideal technique for producing such micro-/nano-fibrous interconnected network scaffolds of high porosity and large surface area; hence it is an excellent candidate for producing vascular graft scaffolds. Fabrication parameters such as polymer solution and processing conditions can be fine-tuned for particular applications [111].

In recent years, several prototypes of electrospun prosthetic vascular grafts have been reported [222, 223] for tissue engineering purposes, including ones comprising biodegradable polymers, with variable degradation rates, ranging from weeks to years [224-228]. However, their mechanical properties are still not ideal. Moreover, biodegradable scaffolds face some important challenges such as the difficulty to predict and match the degradation rate with vascular tissue growth, and possible cytotoxic degradation products [229, 230]. In addition, the stability of the endothelium may be impaired on a biodegradable scaffold. Therefore, there exists a need for permanent scaffolds with appropriate physical and biological properties. Electrospun PET appears to be an excellent candidate for small-diameter grafts in regards to mechanical properties, stability, biocompatibility and low cost, but foremost due to the fact that PET vascular grafts have already been FDA-approved and clinically used for a few decades [231, 232]. Several researchers, including some of us [231-235], recently reported studies of electrospun PET mats with controllable characteristics such as fiber diameters, -orientations and mechanical properties,

achieved by varying process parameters. However, literature data suggest that achieving good coverage of ECs on such PET scaffolds may be problematic [219]. The reason is the polymer's surface inertness: EC adhesion, growth and resistance to flow-induced shear stress has proven to be limited on PET [232, 236]. This might be overcome by a suitable treatment to increase surface roughness, surface energy, or by grafting bioactive molecules. Candidates for these include dry processes such as irradiation by γ-rays [237], electron beams [238], lasers [239], ultraviolet photons (UV) [240], and plasma treatment [241], but also wet-chemical treatments with NaOH [130], hydrogen peroxide (H_2O_2) [131], or graft polymerization [132]. Wet chemistry is the one most frequently encountered in the literature [242-244]; for example, NaOH was shown to increase surface roughness, hence cell adhesion and –proliferation [133]. However, wet-chemical treatments also tend to entrain problems of toxicity and environmental impact [245].

A particularly powerful alternative technique, developed among others by members of this team [162], is the deposition of a plasma-polymerized (PP) coating containing suitable functional groups; examples are primary amines ($–NH_2$), or carboxylic groups, known to promote cell adhesion and/or to enable immobilization of biomolecules [7, 162]. Thanks to the high density and stability of functional groups they can incorporate, PP coatings are more effective than mere plasma-induced grafting of surface-near groups [7]. Oxygen-containing PP coatings on fibrous PCL substrates were reported to be suitable for *in vitro* muscle tissue development, especially for cellular alignment and myotube formation [168]. Numerous articles have also demonstrated the particular effectiveness of nitrogen-, particularly of amine-containing PP coatings [7, 160, 168]. For example, N-rich plasma-polymerized ethylene (L-PPE:N) coatings deposited on PET and PTFE films showed that EC adhesion rate, spreading, focal adhesion, and resistance to flow-induced shear were greatly improved, compared with bare and gelatin-coated PET and PTFE [246]. In other words, L-PPE:N appears to be a particularly promising candidate for the endothelialization of vascular grafts [246].

Therefore, the objective of this study has been to combine optimized nitrogen-rich L-PPE:N coatings with electrospun random nano-fibrous PET scaffolds, and to evaluate these in regards to their composition, morphology, mechanical properties, as well as their ability to favor HUVEC adhesion, growth and resistance to flow-induced shear.

4.2 Experimental Section

4.2.1 Fabrication of PET Nano-Fibre Scaffolds

4.2.1.1 Electrospinning

PET scaffolds (ePET) were fabricated by electrospinning; since the details have been described earlier [231], we repeat only the essential aspects here. Briefly, 9 % wt/vol polymer solution was prepared by dissolving PET pellets (DuPont selar PT 7086, intrinsic viscosity of 1) in 1:1 mixture of analytical grade dichloromethane (CH_2Cl_2) / trifluoro-acetic acid (TFA) (both from Sigma Aldrich), and gently stirring for 24 h. Two (2) ml of polymer solution was electrospun at a rate of 0.5 ml/h for 4 hrs with the aid of a syringe pump, in an enclosure with controlled ambient humidity (*RH*: 8-25%) and temperature (20-25 °C). The power supply provided a constant voltage of 15-17 kV between the tip of the grounded spinneret needle (size 22G) and the rotating collector. The latter, a drum rotating at 1.6 m/s (the diameter, 20 cm, and speed differed from those in ref. [231]), was placed at a distance of 15 cm from the needle tip. The actual nano-fibre mat was collected on an aluminum foil wrapped around the metal drum. Electrospun mats were first dried in ambient air for ca. 3 days, then cut into pieces and carefully peeled from the aluminum foil for subsequent experiments. The pieces of scaffolds were stored in a desiccator until further use.

4.2.1.2 Plasma-Polymerization

Here, too, we merely present the essentials, because details have been described earlier [160, 247]. L-PPE:N coatings were deposited on the surface of nano-fibre mats in a low-pressure (“L”) capacitively coupled radio-frequency (r.f., 13.56 MHz) glow discharge plasma reactor, using ethylene (C_2H_4) / ammonia (NH_3) gas mixtures (C_2H_4: 99.5%; NH_3: 99.99%; Air Liquide Canada Ltd., Montreal, QC). The coatings were deposited at 600 milliTorr (80 Pa) pressure in the cylindrical aluminum/steel reactor chamber, flows of the high-purity feed gases being controlled using electronic flow meter/controllers (Vacuum General Inc., San Diego, CA), and admitted into the chamber via a shower-head gas distributor of 10 cm diameter. The flow rates of C_2H_4 “monomer” and of NH_3, $F_{C_2H_4}$ and F_{NH_3}, were kept constant at 20 standard cubic centimeters per minute (sccm) and 15 sccm, respectively, resulting in a mixture ratio $R = F_{NH_3}/ F_{C_2H_4} = 0.75$. The

deposition was performed under mild plasma conditions (power, P = 10 W, negative d.c. bias voltage, V_B = - 40 V) for a duration of 15 min. These conditions were previously shown to yield a thin layer, ~100 nm, of L-PPE:N on a glass microscope slide [247], with adequate nitrogen and amine concentrations, [N] and [NH_2], and minimal solubility in cell-culture media [247, 248].

As will be shown later, commercial woven PET samples ("wPET", Dacron®, Medtronic Vascular, Santa Rosa, CA), both bare and L-PPE:N-coated, were also investigated as control materials, mainly in regard to their cell-biological characteristics.

4.2.2 Materials Characterization

4.2.2.1 Scanning Electron Microscopy (SEM)

Selected samples were examined by field-emission scanning electron-microscopy (FE-SEM) using a JEOL model JSM-7600 TFE instrument (JEOL Ltd., Tokyo, Japan) at a voltage of 0.5 kV and a working distance of 4 mm, at different magnifications. Nano-fiber mat surfaces were sputter-coated under vacuum with a thin layer of gold in a dedicated coater for 20 seconds, and were then mounted on a suitable sample holder using double-sided tape. The diameters of 100 randomly-selected fibers (at least two experiments with triplicate samples of both pristine and L-PPE:N-coated mats) were examined by SEM; Dacron® samples were also examined, both coated and uncoated. Micrographs were analyzed using image analysis software (NIH Image software).

4.2.2.2 Mercury Intrusion Porosimetry (MIP)

Porosity and pore size of nano-fiber mats were determined using an AutoPore IV 9500 instrument (Micromeritics Instrument Corporation, U.S.A.) with a 15-ml penetrometer. The mats were cut into 1.5×3 cm^2 rectangles and weighed. A sample was then placed into the cup of the penetrometer, which was closed by tightening the cap. The penetrometer and sample was transferred into the pressure chamber of the porosimeter for measurement to take place. Working pressures were in the range 0.015-220 MPa. The determination of porosity is based on the relationship between the applied pressure and the pore diameter into which mercury intrudes, according to the Washburn equation [249]:

$$D = (-4\gamma cos\theta)/P_L \quad (1)$$

where P_L is the pressure of the liquid, D is the pore diameter, γ is the surface tension of mercury (484 mNm^{-1}), and θ is the contact angle, taken to be 140° between mercury and the pore wall at ambient temperature [249]. The measured intrusion was corrected for expansion of the penetrometer. The experiment was performed on four nominally identical samples of both bare and L-PPE:N-coated mats.

4.2.2.3 Mat Thickness

The mats' thicknesses were measured using a digital gauge (Film Master, Qualitest, designed for film thickness measurements with better than 10 μm resolution). To minimize possible error resulting from compression of the mats during measurements, they were sandwiched between two rigid PET films.

4.2.2.4 Tensile Testing (Dry and Wet)

Tensile properties of the mats were evaluated using a uniaxial tensile testing machine (Instron, ElectroPuls™ E3000). Samples were prepared by cutting mats into 0.5 cm x 2 cm strips; a given sample was then inserted into the Instron's jaws, the distance between the upper and the lower jaw being set at 1.5 cm. The tensile test was performed using a 250 N load cell, at a speed of 10 mm/min. Young's modulus, yield strength, yield strain, tensile strength and elongation at break were calculated manually using Stress-Strain curves. Samples were tested in the "dry" state (in ambient air) or in the "wet" state. In the latter case, to better mimic physiological conditions in the body, samples were first immersed in phosphate buffered saline (PBS) solution at 37 °C for 24 h, then cleared from excess liquid using tissue paper and immediately tested as described above. Experiments were repeated three times; at least 12 samples were used in each experiment to test reproducibility.

4.2.2.5 Surface-Chemical (XPS) Analyses

X-Ray photoelectron spectroscopy (XPS) analyses were performed in a VG ESCALAB 3MkII instrument, using non-monochromatic Mg Kα radiation [160, 247, 248]. The size of the analyzed area was about 1 mm^2, and the sampling depth was in the 1-5 nm range on account of the fibers' geometries. Spectra were acquired at 0° emission angles (normal to the mat surface), and charging was corrected by referencing all peaks to the carbon (C1s) peak at binding energy, BE = 285.0 eV. The X-ray source was operated at 15 kV, 20 mA. Quantification of data was performed using Avantage v4.12 software (Thermo Electron Corporation) by integrating the area under a specific peak after a Shirley-type background subtraction, and using sensitivity factors from the Wagner table.

For the case of L-PPE:N-coated mats, the near-surface-concentrations of primary amine groups, [NH_2], were determined using the highly-selective derivatization reaction of 4-(trifluoromethyl) benzaldehyde (TFBA, 98%, Aldrich) vapor with NH_2 groups [250]. By this reaction TFBA is covalently linked via imine bonds, whereby [NH_2] values could readily be deduced from the fluorine concentrations, [F], at the surface, determined by XPS, as described in detail in earlier work from these laboratories [160, 247, 248]. The reader is referred to those articles for any additional information required. Data acquired by XPS survey spectra of both derivatized and pristine samples were combined to calculate [N], [NH_2], and other quantities of interest.

4.2.2.6 Chemical Aging after Immersion, and Depth Analysis

Possible changes in [N] and [NH_2] of L-PPE:N-coated mats after water immersion were measured by XPS, as also reported earlier by Ruiz et al. [247]. After immersion in Milli-Q water for 1, 3 and 7 days after deposition of L-PPE:N, XPS measurements were performed on dried samples with and without derivatization, to study possible chemical "ageing" effects, mostly changes in [NH_2]. To assess possible chemical composition gradients across the thickness of a mat, a 2-layer sample of similar thickness was prepared by electrospinning 1 ml of PET solution for 2 h, followed by overnight drying; then, a second layer was electrospun for 2 h on top of the former, after which the composite sample was coated with L-PPE:N from one side. XPS analyses were performed on the top, bottom and mid-plane locations of this special composite sample by the same procedure as that described above.

4.2.3 Biological Testing

4.2.3.1 Cell Culture and Seeding

HUVECs (Cell Applications Inc., 200p-05n, lot 2729) were cultured in 1% gelatin-coated flasks, in complete medium EGM-2 bullet Kit (Lonza, CC-3162), and used at passage # 3-5. Samples were cut into 1×1 cm^2 squares, placed into 24-well polystyrene culture plates, four samples of each: bare and L-PPE:N-coated electrospun mats; bare and L-PPE:N-coated woven PET (Dacron®, Medtronic Vascular, Santa Rosa, CA) and sterilized in 500 µL of 70% ethanol for 5 min, followed by a rinse with sterile water. Samples were dried overnight under a laminar hood. The next day, cloning glass cylinders (0.8 cm inner diameter; 1 cm height) were placed on the samples to prevent their movement after cell seeding, and to prevent cell adhesion outside the sample. HUVECs were detached with 0.05% trypsin/EDTA (Invitrogen, 25300-054), counted and diluted to obtain a cell suspension of 100,000 cells/ml. 200 µL of this solution (20,000 cells) was added to each well. As control, cells were also cultured directly on polystyrene culture plates coated with 1% gelatin (hereafter "PCP"). After a 4h adhesion period, cloning cylinders and medium were removed, wells were rinsed with PBS to remove non-adherent cells, and 500 µL of complete medium was added to each well. The plates were incubated for 1, 7, 14 and 21 days, the culture medium being changed every 2 days.

4.2.3.2 Cell Adhesion and Growth

4.2.3.2.1 *AlamarBlue Assay*

Cell adhesion and growth was assessed using AlamarBlue reduction assay (Cedarlane, 30025-1(BT)), during which cell metabolic activity reduces resazurin dye (blue) to resorufin (pink). At days 1, 7, 14 and 21, culture medium was removed and 500 µL of complete medium plus 50 µL of AlamarBlue were added to each well and incubated for 4 h at 37 °C, 5% CO_2. After 4 h, 150-µL aliquots were pipetted into 96-well plates (Corning) in triplicate, and the plates were examined at excitation/emission wavelengths of 560/590 nm in a fluorescence plate reader (BioTek, Synergy 4). The experiment was repeated three times to assure reproducibility. To confirm these data, the density and homogeneity of cells on the mats were directly observed after

staining cells by crystal violet solution (0.075% w/v in a 3% v/v acetic acid solution) for 15 min, rinsed 3 times with Milli-Q water and air-dried prior to capture by microscopy (not shown here).

4.2.3.2.2 *Immunofluorescence Analysis ("Live / Dead" Assay)*

To estimate cell survival and distribution on or inside the various mats, HUVEC grown for 1, 7 and 21 days were stained by calcein-AM (2 µM) and ethidium homodimer-1 (5.5 µM) (Invitrogen) in serum-free medium for 45 min at 37 ºC in the dark, before rinsing with D-PBS. The polyanionic dye, calcein, produces intense uniform green fluorescence in living cells (excitation/emission, 495 /515 nm). Ethidium homodimer-1 (EthD-1) enters cells with damaged membranes and produces a bright red fluorescence upon binding to nucleic acids in dead cells. The samples were transferred onto microscope slides and green (live) or red (dead) cells were imaged with Olympus FV10-MSASW software under a Laser Confocal Scanning Microscope (Olympus multiphoton FV-1000 MER, Olympus, Canada). Both planar and Z-stack images (images of planes at various depths within the sample) were taken.

4.2.3.2.3 *Scanning Electron Microscopy (SEM)*

To visualize cell morphology on controls and modified scaffolds, some samples with cells grown for 7 and 21 days were fixed at room temperature for 1 hr with 3% glutaraldehyde (diluted in PBS), before rinsing twice with PBS. Thereafter, they were dehydrated in successive ethanol solutions of different concentrations (30, 50, 70, 95 and twice 100%; 10 min each). Samples were air-dried under a hood overnight, then mounted and gold- coated (Coater: Emitech, K550X) for 2 min for SEM (Hitachi, S-3600N).

4.2.3.3 Cell Resistance to Laminar Shear Stress

To study the HUVECs' resistance to shear when on mats, the following procedure was used: Samples from the two types of electrospun mats (L-PPE:N coated and uncoated) were cut (10 mm x 22.5 mm), placed in 6-well polystyrene culture plates, sterilized in 2 ml of ethanol (70%, in MilliQ water) for 5 min, and then left to dry under the hood overnight. Next, perforated press-to-seal silicone isolators (5 mm x 20 mm x 2.5 mm; Cat. S5560, Sigma-Aldrich, Canada) were

placed on the mats to constrain cell seeding. Mats were then seeded with HUVECs (250 μL in complete medium, passage # 3-5, 10^6 cells/mat), which were left to adhere during 48 hrs to obtain a confluent monolayer of cells. Following this, the cell-populated mats were subjected to laminar flow-induced shear stress for one hour in a parallel-flow chamber (Glycotech, C 31-001, Gaithersburg MD, USA). This setup consists of a peristaltic pump to produce laminar flow; a coiled heat exchanger to maintain the medium's temperature; and the actual flow chamber, comprising a stack on the gasket (5 mm x 20 mm x 0.25 mm), assembled as specified by the manufacturer. The pump was run at 6 mL min^{-1}, to obtain a shear stress of ca. 15 dynes cm^{-2} (similar to an actual physiological value [251, 252]) in the flow chamber, and maintained for 1 hr. Since cell detachment generally occurs during the first 30-45 min, the 1 hr duration was felt to suffice in order to assess the cells' adhesion strength [246, 253]. The numbers of cells retained on the mats after shear stress tests were compared with those on similar surfaces that had not been tested, by measuring the cells' metabolic activity by AlamarBlue assay (Cedarlane, 30025-1(BT)). The morphology and distribution of the cells was also inspected by SEM (Hitachi, S-3600N) after sample preparation, as described above.

4.2.4 Statistical Analysis

All data are expressed as means ± SD. Statistical analysis was carried out using ANOVA with Bonferroni-Holm's post hoc analysis, or by independent t-test when comparing 2 groups only (pristine vs L-PPE:N-coated). Values of p lower than 0.05 were considered significant for all tests.

4.3 Results and Discussion

4.3.1 Physical Properties of Pristine and of L-PPE:N-Coated Mat Samples

4.3.1.1 Scanning Electron Microscopy (SEM)

Figure 4.1 shows a SEM micrograph of a typical electrospun ("ePET") mat after L-PPE:N deposition, thin enough not to lead to perceptible differences between bare and plasma-coated samples (bare and coated Dacron® samples are not shown here). The micrograph clearly

illustrates the randomly interconnected web structure of the electrospun PET nano-fibers, which display smooth surfaces devoid of “beads” (spherical defects). This confirms favorable processing conditions. Nano-fiber diameters could readily be obtained from micrographs like **Figure 4.1**, and values were found to be in the range from 200 to 800 nm, see **Figure 4.2**. Mean values of 551 ± 91 nm and 567 ± 111 nm were found for untreated and plasma-coated mats, respectively, with a mean increase of only 16 nm (n = 200, p = 0.2868). This is much less than the nominal ~100 nm deposit thickness expected, based on values measured on flat surfaces. While the large variability in fiber diameters (see **Figure 4.2**) may obscure variations due to coating, several other factors explain why electrospun mats have thinner coatings than flat substrates. First, the high porosity of the mat greatly increases the surface area to be coated and, second, fibers deep within the mats are less readily accessible to the plasma’s active precursor species.

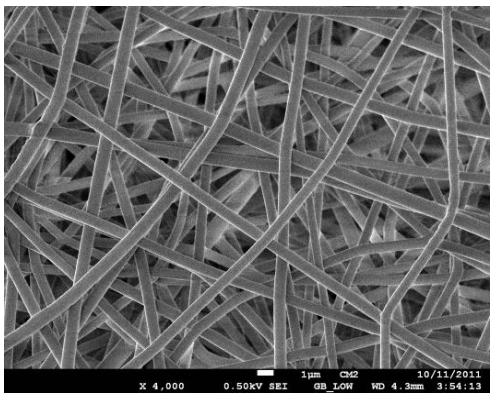

Figure 4.1 SEM micrograph of a plasma-coated electrospun PET nano-fiber mat; no distinction was possible between pristine (bare) and plasma-coated materials (scale bar: 1 µm).

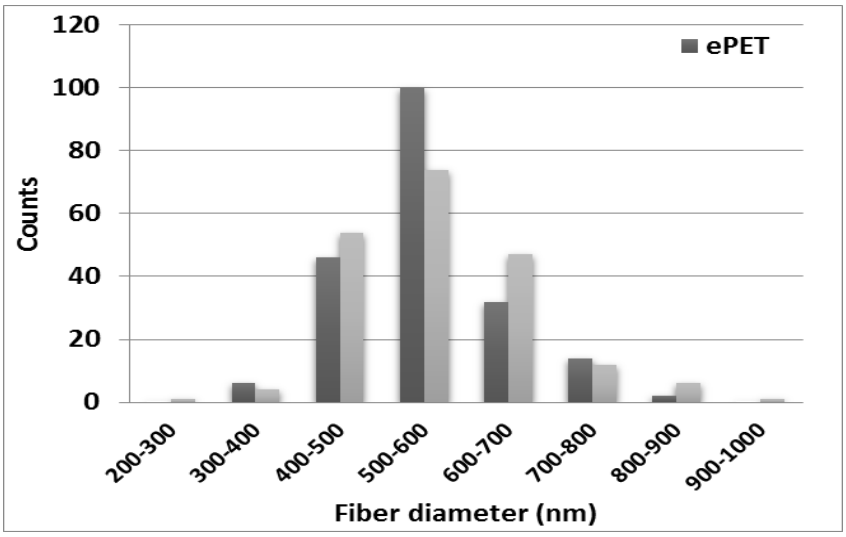

Figure 4.2 Distributions of fiber diameters, as-prepared (ePET); after deposition of L-PPE:N (ePET-LPPE:N).

The results of mat thickness measurements show significant variation from the center to the edges (50-90 μm). Therefore, samples for later experiments, for example tensile tests, SEM, biological tests, and others, were taken exclusively from the central portions.

4.3.1.2 Mercury Intrusion Porosimetry (MIP)

Mercury intrusion porosimetry results are shown in **Figure 4.3** and **Table 4.1**. Properties such as porosity, pore dimension and volume directly influence successful use of a given scaffold. The overall porosity of the present mats, 87%, is highly desirable for the intended application, vascular grafts, by readily permitting the transport of nutrients, metabolic wastes and gases [46]. Moreover, as seen later in this text, the pore size is low enough to avoid EC intrusion into the scaffold. As expected, the porosity did not change significantly after plasma coating, also in agreement with SEM analysis (**Figure 4.1**). On the other hand, the total intrusion volume and average pore diameter (4V/A) tend to be slightly decreased after plasma-coating (**Table 4.1**), although the number of samples investigated was too small for statistical analysis.

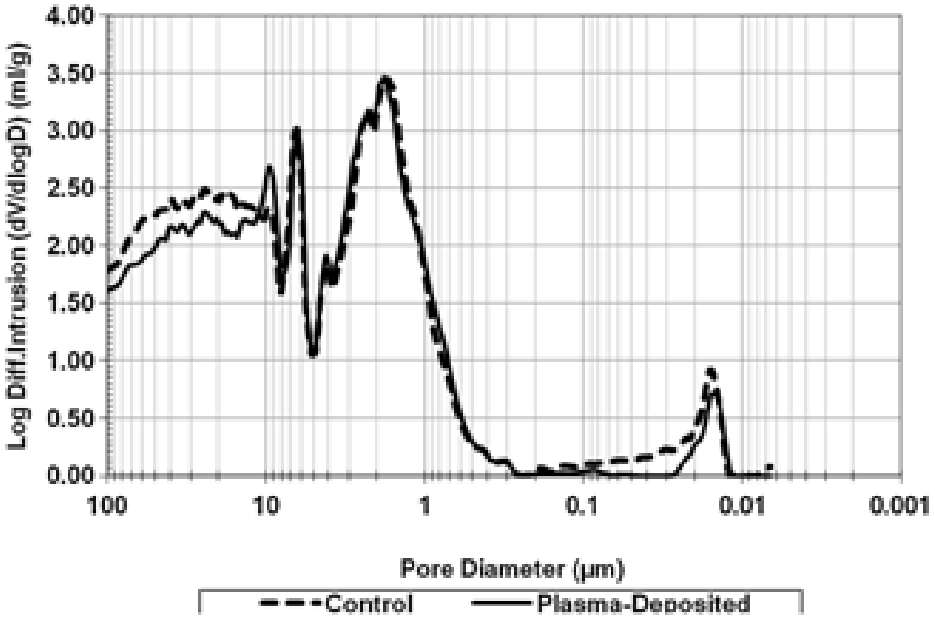

Figure 4.3 Pore-size distributions of pristine (bare) and L-PPE:N coated electrospun PET nanofiber mats (n=4).

Table 4.1 Porosity and pore properties of electrospun mats, bare and L-PPE:N-coated (n=4).

Sample	Intrusion (ml/g sample)	Porosity (%)	Average Pore Diameter (4V/A) (µm)
Bare mat	5.3±0.4	87±1	3.2±0.5
Coated mat	4.7±0.4	86±1	2.5±0.9

4.3.1.3 Mechanical Properties

The tensile properties of pristine (bare) and plasma-coated mats were measured in the length direction of the 0.5 cm x 2 cm sample strips. Knowledge of stress-strain behavior of nano-fiber mats facilitates understanding their performance under dynamic stress encountered in use. Tensile properties under dry and wet conditions are summarized in **Table 4.2**, while **Figure 4.4** shows a typical stress-strain plot; bare and L-PPE:N-coated mats led to nearly indistinguishable curves. The PET mats were seen to exhibit elastic (linear) behavior up to about 1 MPa, followed

by further deformation and rupture at about 250% of elongation. In the presence of the L-PPE:N coating, the ultimate tensile stress was found to be slightly increased while maximal strain was reduced ($p < 0.05$). Young's moduli of the coated mats were also somewhat higher (34 ± 7 vs 20 ± 6 Mpa; $p < 0.05$), confirming that coated electrospun mats are slightly stiffer, indicative of an eventual graft's overall mildly reduced compliance. This may be due to the fact that L-PPE:N tends to "glue" nano-fibers together, thereby impeding their ready displacement under applied load. No statistical differences were found between dry and wet mats, both bare and coated.

The Young's moduli of ePET mats, bare or L-PPE:N-coated, are still above those of natural arteries (see **Table 4.2**) but they can be advantageous in comparison to ePTFE and woven structures of highly oriented PET; furthermore, the characteristics can be adjusted by chemical means [130], or by plasma etching (to be published), if required. Tensile strength is similar to published values for various arteries and veins, indicating that the burst pressure would also be in the same range. Elongation at break was found to be greater than that of arteries in all cases, but not believed to be problematic. However, while uni-axial tensile tests allow one to estimate elastic properties of the fabricated scaffolds, they do not directly provide their compliance (a multi-axial property). Therefore, further tests would be desirable, in particular ones designed to assess compliance and fatigue resistance of tubular multilayered grafts; this is the subject of future work.

Table 4.2 Mechanical properties of bare and L-PPE:N-coated electro-spun PET mats under dry and wet conditions (three experiments, at least 12 samples in each experiment). Young's modulus was calculated in the linear portion of the stress-strain curve. Data are presented in comparison with values from the literature.

Sample	Young's Modulus (MPa)	Yield Strength (MPa)	Yield Strain (%)	Tensile Strength (MPa)	Elongation at Break (%)
ePET (dry)	20±6(*)	0.85±0.1(*)	7±2(*)	1.7±0.2(*)	247±88(*)
ePET- L-PPE:N (dry)	34±7(*)	1.2±0.2(*)	5±1.1(*)	2.1±0.3(*)	164±39(*)
ePET (wet)	21±8	1.0±0.3	6.2±2.2	1.9±0.5	211±27
ePET- L-PPE:N (wet)	28±9	1.1±0.3	4±0.7	1.9±0.4	139±23
Human Saphenous Vein [254]	15	-	-	1	-
Human Femoral Artery [255]	9-12	-	-	1-2	63-76
Human Coronary Artery [89]	-	-	-	1.4–11	55-99

* Significant difference at the 0.05 level between two mat-types (bare and L-PPE:N-coated)

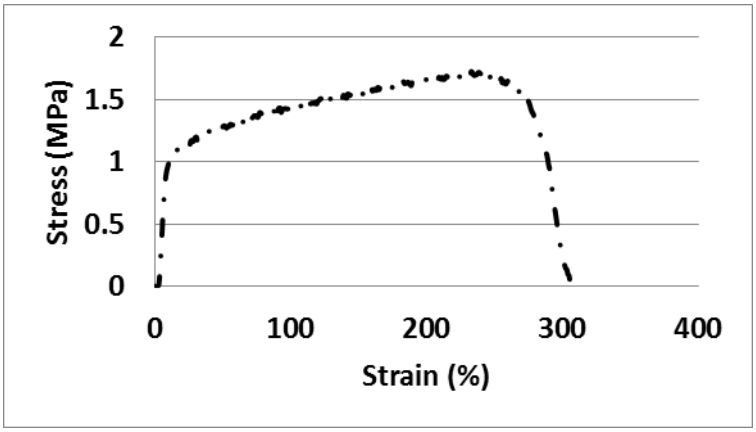

Figure 4.4 Typical tensile test (stress-strain) results for a nano-fibre mat; curves corresponding to bare and L-PPE:N-coated samples had very similar characteristics.

4.3.1.4 Chemical Properties of Bare and L-PPE:N-Coated Mat Samples

4.3.1.4.1 *Chemical Composition and Its Depth-Dependence*

Using the special L-PPE:N-coated 2-layer mat sample described earlier, XPS measurements were carried out on top ([a]: 0 µm), in the middle ([b]: 45 µm) and on bottom ([c]: 90 µm) positions, respectively (n = 3). Respective values of [N] in each of those three locations were as follows: [a]: 13 %; [b]: 5 %; [c]: 5 %. Although [N] is seen to have decreased with increasing depth, it was clearly non-zero in positions [b] and [c], several tens of micrometers below the surface of the mat during its exposure to the plasma. This reveals beyond doubt that active species from the plasma penetrated through the mat's porous structure.

4.3.1.4.2 *Ageing under Wet Conditions*

Figure 4.5 shows ageing behavior (surface-chemical changes) of L-PPE:N-coated mats following immersion in Milli-Q water for 1, 3 and 7 days: We first note an appreciable increase in [O], accompanied by a decrease in [N] during the first 3 days, after which changes became smaller; as expected, [NH_2] also decreased somewhat during immersion. The latter is due to reactivity of primary amines with oxygen and humidity; amides, ketones and aldehydes are the likely main reaction products, as revealed by earlier research in these laboratories [247, 248]. Despite this small decrease, [NH_2] remained at a relatively high value (above 4 %) compared to other functionalization techniques, for example by plasma modification [256, 257]. This is of key importance, because [NH_2] plays an essential role in promoting cell-adhesion.

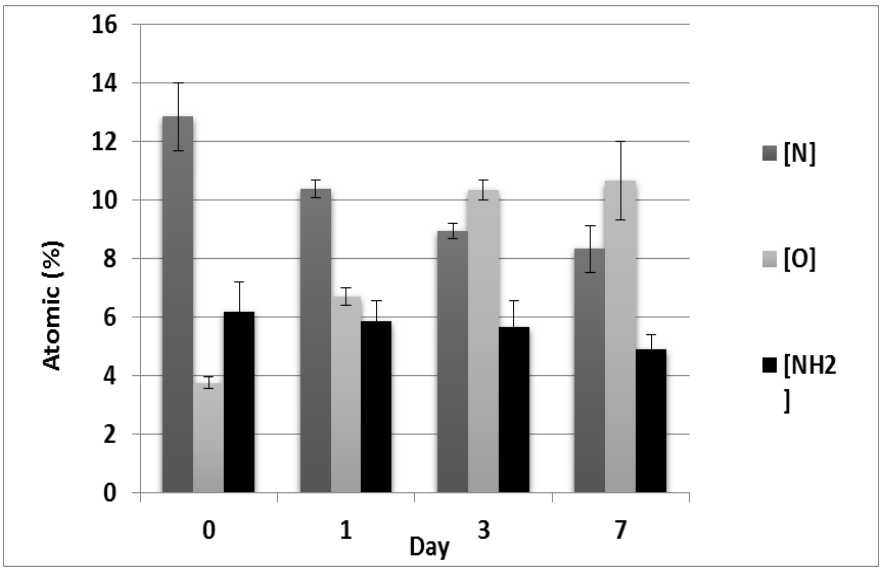

Figure 4.5 Ageing of L-PPE:N-coated mats after immersion in Milli-Q water for various durations, namely 1, 3, and 7 days (XPS; n=3).

4.3.2 Cell Adhesion, Viability and Proliferation on Bare and L-PPE:N-Coated Mat Substrates

HUVEC response to the electrospun mat scaffolds (ePET), to woven PET (Dacron®, "wPET"), and to PCP (as positive control) was investigated by measuring the ability of cells to adhere and proliferate on the various materials, both bare and L-PPE:N-coated, see **Figure 4.6**. Adhesion after 24h (day 1) on the bare mat (ePET) was significantly less than on PCP. ePET-LPPE:N significantly increased adhesion ($p < 0.05$), to the point of being the same as on PCP. In other words, plasma-coating of the electrospun mat resulted in a much greater population density of adhering cells. This was presumably due the much enhanced surface activity of L-PPE:N resulting from its primary amine groups, also evidenced by previously published research from these and other laboratories [167, 168, 246, 248].

HUVEC growth at days 4, 7, 14 and 21 was also found to be significantly ($p < 0.05$) higher on the plasma-coated mat than on the bare one (compare data "ePET" and "ePET-LPPE:N"). In actual fact, AlamarBlue reduction induced by cells on a bare mat was observed to even *decrease* between days 1 and 7, but it then rose on days 14 and 21; Ma et al. [155] reported similar behavior for human coronary artery endothelial cells on electrospun PET nano-fibrous mats with

and without gelatin-coating. Here, however, L-PPE:N coating enhanced HUVEC density during the entire culture period, days 1 to 21 (see "ePET-LPPE:N"). Adhesion was even higher than on the positive control, gelatin-coated PCP. The higher values obtained with PCP at days 14 and 21 should not be taken into consideration, because in PCP wells cells could migrate during the growth period and cover a larger area, ~1.9 cm^2, compared with only ~1 cm^2 in the case of ePET mats.

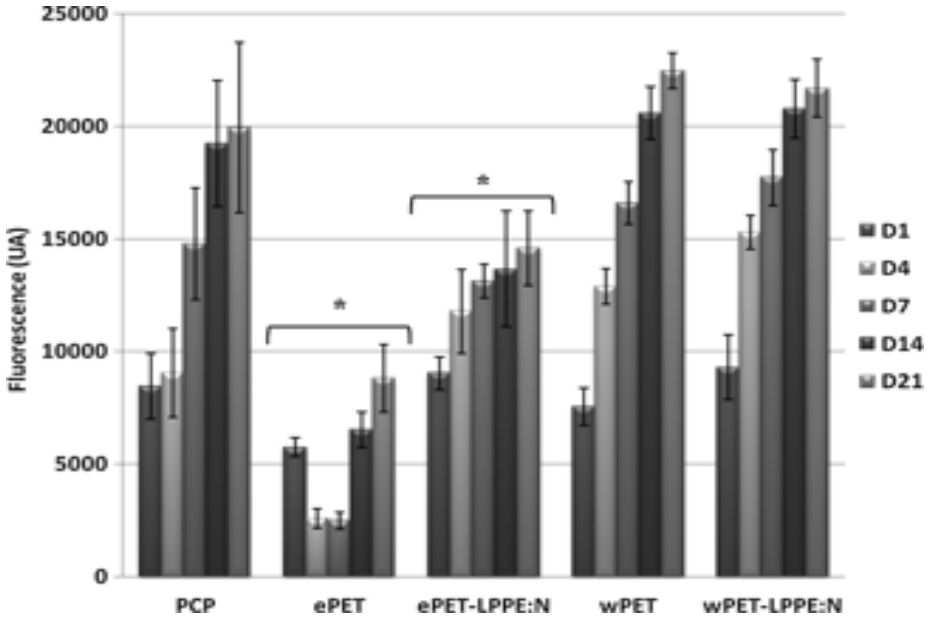

Figure 4.6 Growth of HUVECs on different bare and L-PPE:N-coated substrate surfaces, after different culture times (PCP: tissue-culture polystyrene; ePET: electrospun mats; wPET: woven Dacron® fabric; LPPE:N: L-PPE:N-coated) (n= 9 for each)

* Significant difference between bare and L-PPE:N-coated ePET ($p<0.05$)

In comparison with ePET, the bare and plasma-coated Dacron® exhibited even higher cell numbers at each time point (except day 1) ($p < 0.05$). This was not unexpected, because this material's large pores enabled cell migration into those, as observed here by confocal and scanning electron microscopy. In contrast, the smaller (2.5 - 3.5 µm) pores of electrospun mats restrain cells to the topmost surface, an important advantage for forming a confluent monolayer of endothelial cells on the lumen side of a graft. Confocal microscopy images are presented in **Figure 4.7**, where the upper portion portrays planar views of cell populations on the different

substrates, on days 1, 7 and 21. On each of the surfaces the numbers of dead cells (red) was very small. Both the planar (upper) and the Z-stack (lower portion of Figure 7) images confirmed that on Dacron® (wPET), the cells penetrated inside the scaffold, while on ePET, where they remained confined *at* the surface, fluorescence is seen to have remained concentrated on a surface layer of ca. 10 μm thickness. This was also confirmed by SEM images, which show a near-confluent monolayer of endothelial cells on the coated electrospun mat at day 21 (**Figure 4.8**): **Figure 4.8(a,b)** clearly reveals the flat, spread morphologies of HUVECs after 21 days on the pristine [8(a)] and L-PPE:N-coated [8(b)] electrospun PET mats, respectively. Fewer cells are observed on the bare mat (ePET) than on its coated counterpart, ePET-LPPE:N, in qualitative agreement with earlier-mentioned results by others. [133, 155, 258] **Figure 4.8(c,d)** shows that HUVEC penetrated inside the voids of bare (wPET) and coated Dacron® (wPET-LPPE:N), as already pointed out while discussing **Figure 4.7**.

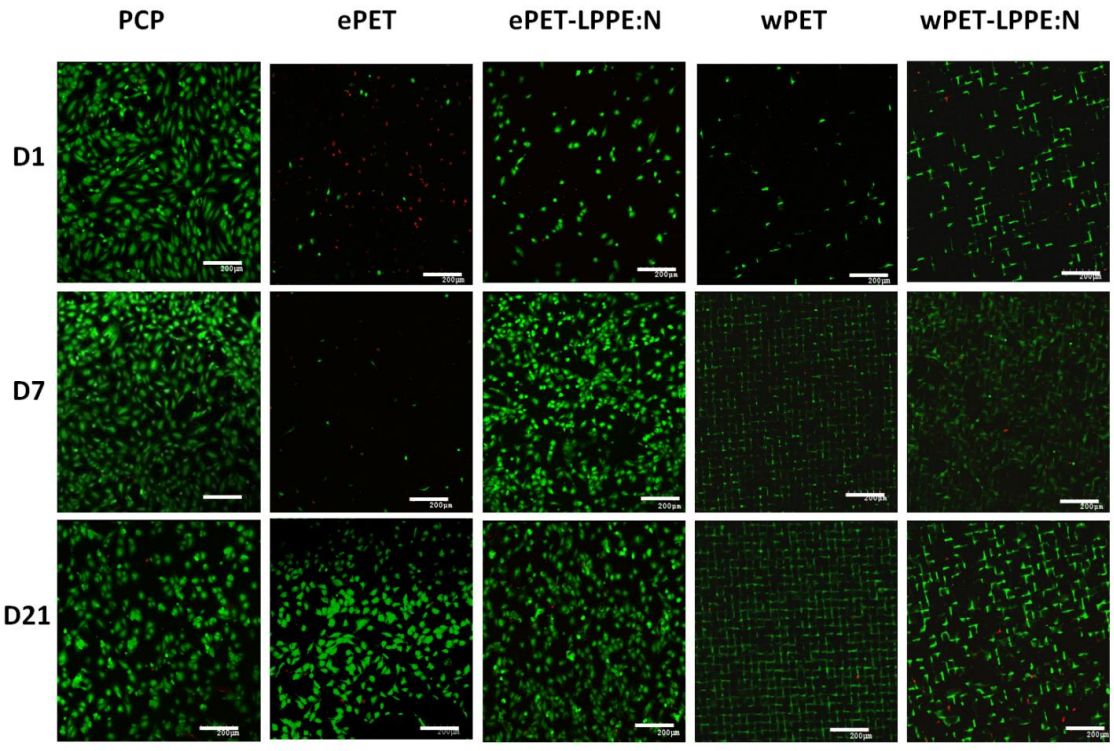

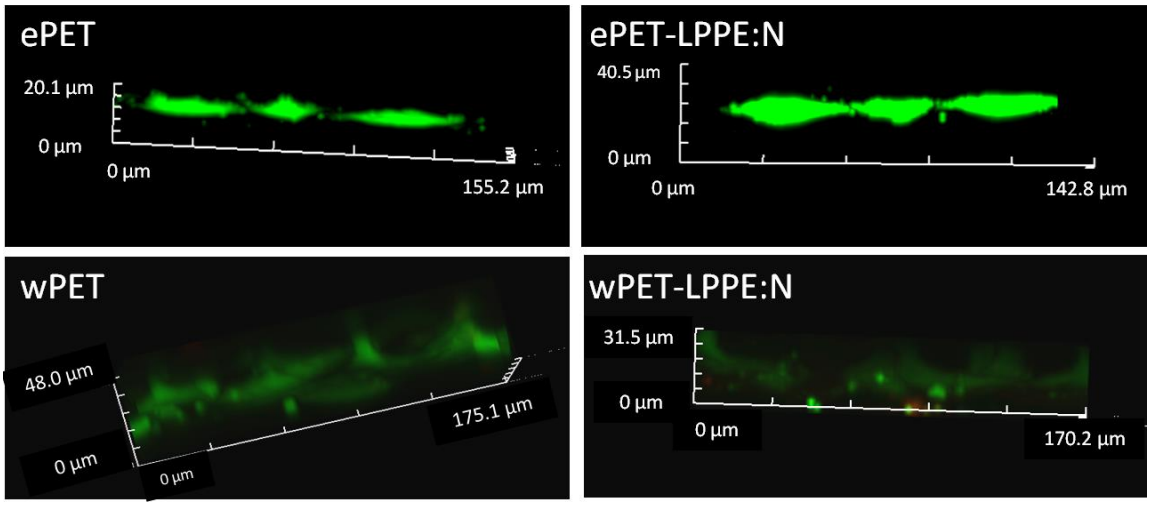

Figure 4.7 Confocal microscopy images of immunofluorescence-stained HUVECs on the various substrates identified at the top; different rows represent days 1, 7 and 21 of culture (scale bar: 200 µm). The bottom row shows Z-stack images after 21 days.

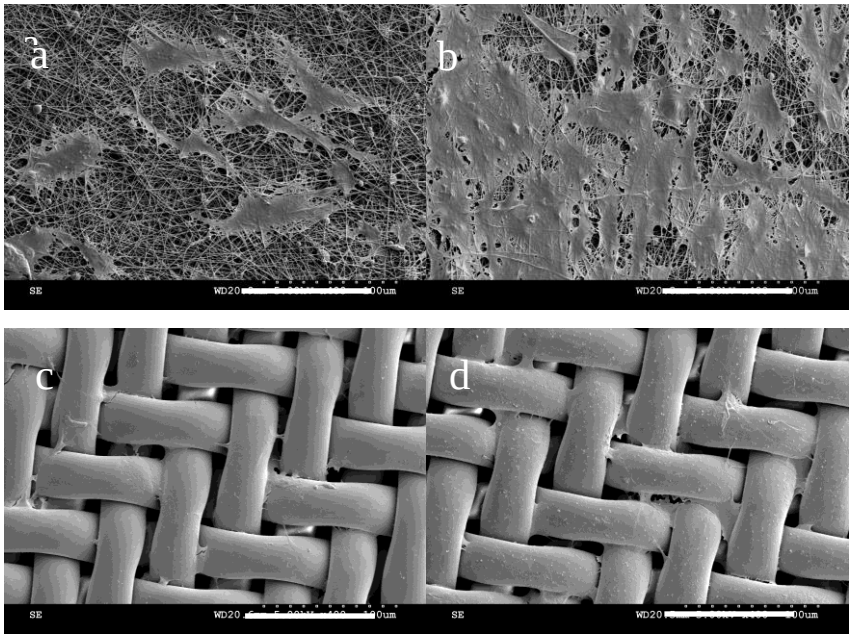

Figure 4.8 SEM micrographs of electrospun nanofiber mats with HUVECs after 21 days of growth: a) bare mat (ePET); b) mat after L-PPE:N coating; c) bare woven PET (wPET, Dacron®); d) woven PET after L-PPE:N coating (scale bar: 100µm)

Together, these results therefore tend to confirm our hypothesis that electrospun nanofiber scaffolds can provide a structure akin to the base-membrane of natural arteries [89, 258, 259]. However, while cell adhesion, viability and proliferation allow one to estimate the biocompatibility and non-cytotoxicity of the fabricated scaffold, more detailed studies would be desirable to evaluate its efficacy as a graft material.

4.3.3 Cell Resistance to Laminar Shear Stress

HUVEC retention on bare and L-PPE:N-coated ePET mats was investigated using the parallel-flow chamber with a typical physiological shear stress value of 15 dynes cm^{-2}, for 1 hr. **Figure 4.9** shows AlamarBlue results after 48 hrs of adhesion and growth, subjected or not to shear. Cell retention was found to be promising for L-PPE:N-coated mats, with approximately 70 ± 4% and 30 ± 10% of the cells remaining on coated and bare mats, respectively ($p < 0.05$). Once again, in this experiment L-PPE:N coating was also found to have increased the initial adhesion and 48 hrs growth of cells under static conditions. However, the difference with bare ePET was less marked, probably due to the fact that large numbers of cells were seeded, 10^6 cells per mat. It has been reported [260] that the influence of the substrate on cell adhesion can be reduced when cell density is very high, possibly due to cell-cell interactions that may dominate over those with the substrate. After exposure to shear, cell densities were significantly greater on ePET-LPPE:N than on bare (ePET) samples ($p < 0.05$), as also confirmed by SEM observation (**Figure 4.10**). This agrees with earlier-published results from these laboratories [184, 246], which showed strong adhesion and retention of endothelial cells on L-PPE:N coated flat substrates.

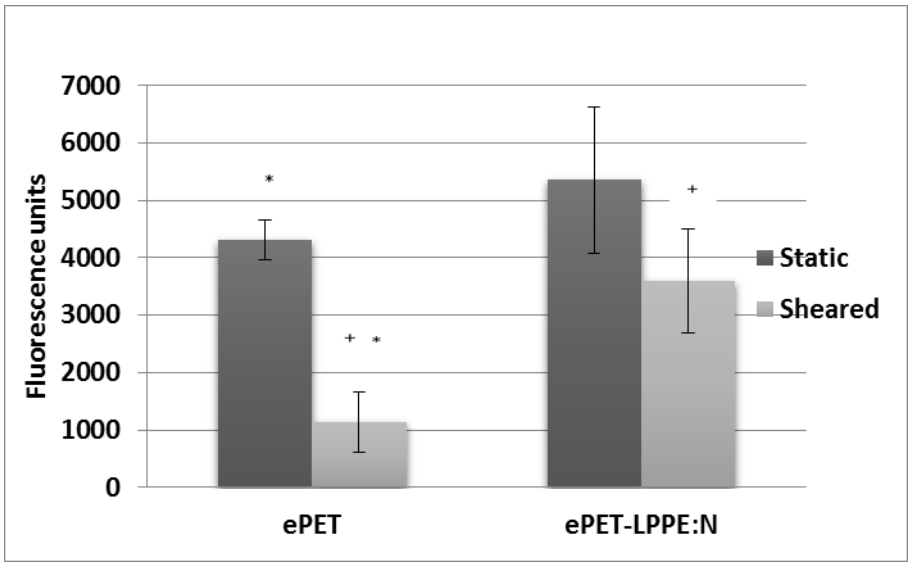

Figure 4.9 HUVECs' resistance to laminar shear stress (15 dynes/cm^2, 1h), evaluated by AlamarBlue assay (n= 12 for each mat). * Significant difference at the 0.05 level between ePET mats under static and shear conditions. + Significant difference at the 0.05 level between bare and L-PPE:N-coated ePET mats under shear condition.

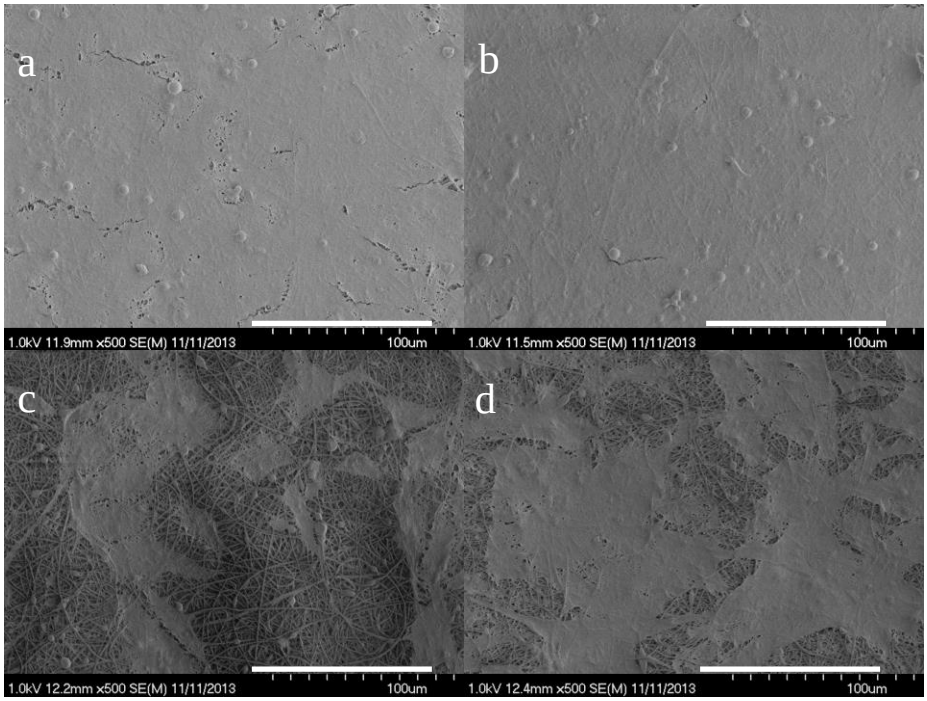

Figure 4.10 SEM micrographs of bare (a,c) and L-PPE:N-coated (b,d) electrospun nanofiber (ePET) mats: a,b) under static conditions; c,d) under shear (scale bar: 100µm)

4.4 General Discussion and Conclusion

The primary requirements for a synthetic functional vascular graft (VG) are biocompatibility, bioactivity, and favorable mechanical properties [229]. The current generation of VGs is mainly limited by inadequate mechanical properties that lead to mismatch and intimal hyperplasia, and by lacking spontaneous endothelialization of the lumen surface. Pre-endothelialization of the lumen has shown promise as a strategy to improve small-diameter VGs, but it is still handicapped by poor adhesion and retention of endothelial cells (ECs) [261, 262].

In the present study two well-documented techniques, electrospinning and plasma polymerization (PP) of an amine-rich coating, were combined to address the issues mentioned above, that is, to create an effective scaffold for subsequent EC-seeding. Electrospun 3D PET mats (ePET) with random fiber orientation were prepared, PET being chosen because it is stable, cost-effective and cytocompatible, with tunable properties and because several PET-based vascular implants have already received FDA-approval [263]. Electrospun PET exhibits relatively low stiffness and favorable strength that can be of interest for VG applications, its tensile properties being comparable to those of natural arteries [130, 133, 231, 264].

Although further investigation is warranted, present results reveal no deleterious effect of L-PPE:N coating on the properties of ePET mats, thanks to the mild plasma conditions employed (low power, 10 W; pressure, 600 mTorr; and temperature, ~300 K).

The morphology of our electrospun PET 3D nanofibre network proved suitable for forming a near-confluent endothelial cell (EC) monolayer lining, see Figure 8b and 10. Indeed, the fabrication conditions yielded high porosity and small pore size (Figure 1) that enable exchange of nutrients and gas molecules, while restricting EC growth to the topmost (eventual lumen) surface [265]. This is greatly advantageous compared with presently used ePTFE and woven PET grafts, where cells penetrate and do not readily form such a complete EC monolayer (see Figure 7 and 8d).

Cell adhesion, -growth and -retention under flow-induced shear stress were shown to be limited on bare ePET mats, but L-PPE:N coating helped overcome this limitation to a large extent. Earlier work in these laboratories had already proven L-PPE:N to be highly effective,

reproducible and sufficiently stable over time for cell culture applications [164, 247, 266]. Here, the greatly-enhanced cell density on L-PPE:N-coated scaffolds compared with bare samples (see Figure 6) confirmed the coating as an excellent pre-treatment for the requisite HUVEC response; this was not surprising in view of similar observations we reported for HUVEC, but also for vascular smooth muscle cells (VSMCs), fibroblasts and mesenchymal stem cells (MSC) [164, 165, 189, 246]. It also agrees with other groups' findings that functionalized PP coatings can enhance cell adhesion, growth and proliferation on diverse electrospun substrates [7, 267]. PP with appropriate chemical functionalities, primary amine (-NH_2) groups in the case of L-PPE:N, rapidly attract and bind proteins in bio-fluids or culture media; integrin receptors on cells' outer membrane surfaces, in turn, "recognize" and bind to certain of these proteins. In aqueous solution at physiological pH values, the protonated amine group possesses a localised positive charge which helps attract the negatively-charged biomolecules (proteins) and cells [268]. Because L-PPE:N promotes the attachment of many different cell types, pre-seeding with endothelial cells should precede *in-vivo* implantation. On the other hand, it can also serve to create complete tissue-engineered vascular grafts (TEVG).

There have recently been several reported efforts to create TEVGs based on electrospining, for example bilayered scaffolds or hybrid scaffolds made by combining natural and synthetic polymer mats. Let us mention bilayered scaffolds of PCL-collagen blend [104], elastin, type I collagen and poly (D,L-lactide-co-glycolide) (PLGA) [269], multi-layered type I collagen, gelatin, segmented polyurethane and poly(ethylene oxide) [270], and collagen/ chitosan/thermoplastic polyurethane nanofibrous scaffolds [271]. Although collagen is known to increase cell adhesion, its possible immunogenic effects, rapid degradation, and cost of synthetic collagen constitute important challenges [272]. L-PPE:N can be deposited on any type of surface and could be used with other electrospun material, resorbable or not. As a logical future step, the combination presented here (electrospinning + PP) will be used to add a more porous electrospun outer layer, either of PET or of a biodegradable polymer, to favor growth of a thick VSMC layer and obtain a *complete* scaffold for TEVG.

In conclusion, the combination of electrospinning and primary-amine rich plasma polymer coating proposed in this research can provide an adequate scaffold for the luminal side of small-diameter vascular prostheses; more precisely, it enables finely-controlled structural, mechanical and surface properties that are required for confluent, flow-stable pre-endothelialization of VGs

or TEVG. These improvements may help overcome the clinical complications encountered when using current generations of off-the-shelf VG prostheses.

Acknowledgments

This research is being supported by grants from the Natural Sciences and Engineering Research Council of Canada (NSERC) and the Canadian Institutes of Health Research (CIHR) (CPG 87497). One of us (H.S.) gratefully acknowledges the Fonds de recherche du Québec-Nature et technologies (FQRNT) for the award of its Merit Scholarship. The authors also thank C. Cerclé, N. MacDonald, S. Poulin, J. Lefebvre, Y. Leblanc (Ecole Polytechnique), K. Hamelin, B. La Colla (CHUM), as well as S. St-Amour and S. Sauriol (FPInnovations) for technical support during experiments.

CHAPTER 5 ARTICLE 2: PLASMA-ETCHING FOR CONTROLLED MODIFICATION OF STRUCTURAL AND MECHANICAL PROPERTIES OF ELECTROSPUN PET SCAFFOLDS

Houman Savoji, Sophie Lerouge, Abdellah Ajji, Michael R. Wertheimer*

_____

Houman Savoji, Prof. Abdellah Ajji, Prof. Michael R. Wertheimer

Institute of Biomedical Engineering, École Polytechnique de Montréal, Montreal, QC, H3C 3A7, Canada

Houman Savoji, Prof. Sophie Lerouge

Laboratory of Endovascular Biomaterials (LBeV), Research Centre, Centre Hospitalier de l'Université de Montréal (CRCHUM), Montreal, QC, Canada

Prof. Sophie Lerouge

Department of Mechanical Engineering, École de technologie supérieure, Montreal, QC, H3C 1K3, Canada

Prof. Abdellah Ajji

Department of Chemical Engineering, École Polytechnique de Montréal,

Houman Savoji, Prof. Michael R. Wertheimer

Department of Engineering Physics, École Polytechnique de Montréal, Montreal, QC, Canada

*E-mail: michel.wertheimer@polymtl.ca

_____

This paper has been published in "Plasma Processes and Polymers 2015, 12, 314–327" [11].

Abstract

Aligned electrospun poly(ethylene terephthalate) (ePET) nanofiber mats that mimic the media layer of arteries have been fabricated. In order to bring their mechanical and surface properties in line with those of natural blood vessels, we have used three different plasma etching techniques: (i) atmospheric pressure ("HP") corona discharge in air; low-pressure (ii) radio-frequency discharge ("LP") and (iii) discharge in a microwave plasma asher, the latter two in pure oxygen (O_2) gas, or O_2 mixture with Ar or CF_4. Substantial reduction in Young's modulus has been attained after as little as 5 min. treatment in (iii), without visible damage to the fibers. Changes in surface composition and drastic improvement in surface wettability / wicking have also been observed, which resulted in promoting adhesion and growth of smooth muscle cells (SMCs).

Keywords: Nanofibers, Electrospinning, Plasma-etching, Poly(ethylene terephthalate), Mechanical property, Surface chemistry, Vascular graft

5.1 Introduction

The quest for improved functional small-diameter vascular grafts is great and growing. Currently, the use of autologous grafts from the patient is considered the gold-standard, especially for small-diameter blood vessels. However, their availability has in practice been a limiting factor due to insufficient or defective donor tissue and danger of patient morbidity associated with harvest surgery [27]. Synthetic grafts such as woven poly(ethylene terephthalate) (PET, Dacron^{R}) and expanded poly(tetrafluoroethylene) (ePTFE) have been widely used to replace large-diameter vessels. However, these have shown limited patency when applied to small-diameter (< 6 mm) vessels due to the mechanical and compliance mismatch that lead to intimal hyperplasia [27, 273].

The native artery wall is composed of three distinct layers: the intima, media, and adventitia [274] [275]. Each layer contributes its own biomechanical role, while being subjected to axial, circumferential and torsion forces. The extracellular matrix (ECM), comprising a basement membrane and a complex, chemically and physically cross-linked network of proteins, glycosaminoglycans, collagen and elastin fibers with nanoscale features, plays an important role in controlling cell behavior in living systems [274, 275]. It is known that the media layer, which contains smooth muscle cells (SMCs), collagen fibrils and elastic lamellae, comprises long, parallel and circumferentially aligned fibers. These are essential for arterial contraction and dilation and they facilitate the control of blood pressure and tissue homeostasis [276].

Primary requirements for a functional synthetic vascular graft (VG) are biocompatibility, bioactivity and, most important, favorable mechanical properties [27, 229]. The current generation of VGs is limited by (i) inadequate (excessive) mechanical stiffness that leads to compliance mismatch and intimal hyperplasia; and by (ii) lack of spontaneous endothelialization of the lumen surface [277]. Therefore, fine-tuning of the mechanical properties will directly affect the performance of an engineered VG after implantation.

Electrospinning has the potential to produce fiber-based scaffolds similar to the protein fibers of the ECM, with diameters that can range from 50-5000 nm, and consisting of a 3D structure with high porosity and large surface area; this technique uses polymer solutions or -melts under high electric field [278, 279]. An important challenge in attempting to engineer a synthetic vascular graft is to achieve optimum morphological, mechanical and biological properties in each layer.

Regarding the media layer, the versatility of electrospinning allows one to organize and orient fibers so that they can guide the migration and elongation of cells [229].

Aligned fibrous mat-scaffolds from selected natural and/or synthetic polymers are under investigation to mimic the media layer, by directing SMCs in a circumferentially aligned orientation similar to that in natural vessels. In addition, aligned fibers can provide the requisite mechanical strength to resist the high pressure encountered *in-vivo* [279-284]. Electrospun PET (ePET) is an excellent candidate, because it is non-toxic, has good mechanical properties, bio-durability, biocompatibility and low cost; however, most important is the fact that PET vascular grafts have already been FDA-approved and clinically used for several decades. Therefore, a number of research groups, including the present authors, have elected to use PET as their vascular biomaterial [10, 133, 235, 285, 286].

We have recently shown that tensile properties, including Young's modulus, of random ePET mats are higher than those of natural arteries, but that they can be better than ePTFE, woven or knitted PET in the present context.[10] Moreover, those characteristics can be modified by wet-chemical [130] or dry (plasma-based) etching, if desired. Wet-chemical treatment (e.g. hydrolysis with concentrated NaOH, among others) has so far been the only method proposed in the literature for this purpose [130, 287-289], but it generally entrains problems of toxicity, environmental impact, and associated costs, among others [290]. Furthermore, macroscopic damage can result to fibers in contact with NaOH, when the ester linkage of PET is broken (leading to formation of a sodium carbonate salt and ethane1, 2diol) [291, 292].

On the contrary, rapid, clean, highly reproducible and environmentally benign plasma etching may offer an attractive alternative to fine-tune the mechanical and surface-chemical properties of ePET fibers. This can be accomplished by controlling treatment parameters such as gas type and flow, power, pressure and treatment time. Cold plasma treatments, both at low- and atmospheric pressure are widely used to modify the inert surfaces of polymers so as to enhance their wettability, roughness and biocompatibility, for example, and to adapt them for biomaterials applications, generally without changing their bulk properties [293-297]. Keller et al. reported a comprehensive study of plasma-based and wet-chemical removal of manufacturing residuals from PET multifilament fibers, concluding that radio-frequency plasma in He/O_2 is the best option for various reasons [298]. Verdonck et al. used SEM to investigate the influence of O_2

plasma etching on the morphological properties and fiber diameter distribution of electrospun polyacrylonitrile (PAN) fibers, including etch mechanisms in the reactive-ion etching (RIE) mode. They concluded that etching was more rapid in the presence of ion bombardment and for smaller-diameter nanofibers [299]. Zandén et al. also used O_2 plasma treatments of electrospun polyurethane (PU), for durations up to 7 minutes, to investigate changes in surface morphology, chemistry and wettability. They observed fiber diameter reduction, increased porosity and modified fiber surface texture, accompanied by structural degradation after longer exposure times. The initially hydrophobic membranes were observed to become hydrophilic and water-absorbing, but the authors found that neither pristine nor plasma-modified samples had an effect on the shape of red blood cells (RBC), the function of which remained intact [300]. Finally, a very recent study by Jeon et al. reported O_2 plasma-based creation of sub-micrometer sized surface patterns, with the aid of special templates, on mats of electrospun poly(e-caprolactone) (PCL) fibers. The authors showed SEM images corresponding to plasma exposures up to 120 minutes. Stress-strain tests revealed weakening (decrease in Young's modulus, strength and elongation at break), attributed to the fibers' roughened surfaces. Finally, they described enhanced attachment and proliferation of (MG63) osteoblast-like cells, claiming the materials' suitability for tissue engineering applications [301].

Clearly, some of the above-cited work has utilized O_2 plasma to etch or surface-modify various electrospun fibrous mats for cell-biological purposes. However, none of the authors have specifically mentioned plasma-etching as a potential process to fine-tune the mechanical properties of electrospun fiber mats, certainly not in the context of vascular grafts. Therefore, the objective of the present study has been to investigate the effects of low- and high (atmospheric-) pressure plasma-etching on mechanical, morphological, chemical and biocompatibility properties of partially aligned electrospun PET mat scaffolds, specifically destined for VG applications.

5.2 Experimental Part

5.2.1 Fabrication of Aligned Nanofibrous PET Scaffolds

5.2.1.1 Electrospinning

Partially aligned nanofibrous PET mats (ePET) were prepared by electrospinning of 12.5 wt/vol% polymer solution [231]. The polymer solution was prepared by dissolving PET pellets (DuPont selar PT 7086, intrinsic viscosity of 1) in a 1:1 mixture of analytical grade dichloromethane (CH_2Cl_2) / trifluoro-acetic acid (TFA) (both from Sigma Aldrich), and gently stirring for 24 h. Two (2) ml of polymer solution was electrospun at a rate of 10 ml/h with the aid of a syringe pump, in an enclosure with controlled ambient humidity and temperature. The power supply provided a constant voltage, 30 kV, between the tip of the grounded spinneret needle (size 18G) and the rotating collector. The latter, a drum rotating at 1000 RPM, was placed at a distance of 13 cm from the needle tip. The actual nano-fibre mat was collected on a non-stick aluminum foil wrapped around the metal drum. Electrospun mats were first dried in ambient air for ca. 3 days, then cut into pieces and carefully peeled from the aluminum foil for subsequent experiments. The pieces of scaffolds were stored in a desiccator until further use. Process conditions are summarized in **Table 5.1**.

Table 5.1 Process conditions used to produce the present electrospun aligned PET mats.

	Process parameters				Collector				Ambient conditions	
					Dimension		Speed			
Polymer solution concentration (% w/v)	Needle size (G)	Tip-Collector distance (cm)	Voltage (kV)	Flow rate (mL/h)	Length (cm)	Radius (cm)	Linear velocity (m/s)	RPM	RH (%)	Temp. (°C)
12.5	18	13	30	10	35	10	10.3	1 000	8–25	20–25

5.2.1.2 Plasma Etching

5.2.1.2.1 *Low-Pressure*

Nano-fibre mats were etched in a low-pressure ("LP") capacitively coupled radio-frequency (r.f., 13.56 MHz) glow discharge plasma reactor[162], using (i) Argon (Ar) / 10% Oxygen (O_2) gas mixture, or (ii) pure oxygen (O_2) (both from Air Liquide Canada Ltd., Montreal, QC). Etch treatments were performed at 100 milliTorr (13.3 Pa) pressure in the cylindrical aluminum/steel reactor chamber, flows of the feed gases being controlled using electronic flow meter/controllers (Vacuum General Inc., San Diego, CA), and admitted into the chamber via a shower-head gas distributor of 10 cm diameter. The flow rate of gas was kept constant at 20 standard cubic centimeters per minute (sccm) for both cases (i) and (ii) above. The treatment was performed at constant power, P = 50 W (corresponding d.c. bias voltage, V_B = - 40 V), for different durations, namely 3, 6, 12, and 15 minutes, samples being placed on the (10 cm diameter) powered electrode. Clearly, the maximum energy of ions impinging on the samples' surfaces, a key parameter in plasma etching, did not exceed some tens of eV, as indicated by the above-cited value of V_B. In reference 18 we pointed out that at this low pressure, active plasma species can penetrate through the entire depth of the highly porous mats.

5.2.1.2.2 *Atmospheric Pressure*

The high-("HP", atmospheric)-pressure dielectric barrier discharge (DBD) apparatus was described and illustrated earlier, and it was operated in atmospheric air in the so-called corona mode [302, 303]. Briefly, the system comprised a cylindrical, dielectric-coated stainless steel high-voltage (HV) electrode and a grounded, planar Al electrode on which reposed a 300 × 240 mm^2, 2 mm-thick glass plate that served both as substrate and as a second dielectric layer (the gap between the two was typically 1 mm). The lower (planar) electrode and glass plate were moved back and forth under the HV electrode at precisely controlled speed, depending on the desired treatment (etching) time. The roughly 1 cm wide plasma (filamentary corona) zone was generated with a commercial power source and transformer (Enercon Industries, model LM2727-03, 450 kVA maximum output) at a typical frequency of 10 kHz and peak-to-peak voltage of 18 kV.

5.2.1.2.3 *Plasma Asher*

A low-pressure microwave plasma ashing system (GIGAbatch 360 M, PVA TePla A.G., Germany), designed to remove organic photoresist during the manufacture of integrated circuits, was also used here to etch nanofibrous PET mats. The density of microwave plasma, ca. 10^{11} cm^{-3}, is much greater than that of its r.f. counterpart, typically 10^{9} cm^{-3}, resulting in a greatly increased etch rate [304, 305]. As in earlier work [304, 305] (i) a mixture of O_2 / 20% CF_4, but also (ii) pure O_2 were used at 1000 mTorr (133.3 Pa) pressure, and at 200 W of microwave power for 1 min and 5 min, respectively. The optimal etching conditions, ones presumably leading to highest yields of O and F atoms, were taken from previously published research by this laboratory [305].

5.2.2 Materials Characterization

5.2.2.1 Scanning Electron Microscopy (SEM)

Selected samples were examined by field-emission scanning electron-microscopy (FE-SEM) using a JEOL model JSM-7600 TFE instrument (JEOL Ltd., Tokyo, Japan) at a voltage of 1 kV and a working distance of 13.3 mm, at different magnifications. Nano-fiber mat surfaces were sputter-coated under vacuum with a thin layer of gold in a dedicated coater for 50 seconds, and were then mounted on a suitable sample holder using double-sided tape. The diameters and diameter distributions of 400 randomly-selected fibers (at least two experiments with triplicate samples of both pristine and etched mats) were examined by SEM. Micrographs were analyzed using image analysis software (NIH Image software).

5.2.2.2 Mat Thickness

The mats' thicknesses were measured using a digital gauge (Film Master, Qualitest, designed for film thickness measurements with better than 10 μm resolution). To minimize possible error resulting from compression of the mats during measurements, they were sandwiched between two rigid PET films.

5.2.2.3 Quantification of Fiber Alignment

Fast Fourier Transform (FFT) was used to characterize the alignment of the fibers. Here, we merely present the essentials, because details have been described elsewhere [270, 306]. The FFT function converts spatial information into an optical data image in a mathematically defined frequency domain. The resulting FFT output image reflects the degree of fiber alignment present in the selected area. A square region of 512 × 512 pixels on the SEM image was randomly selected and processed for FFT using image analysis software (NIH Image software) supported by an oval profile plug-in. All FFT data was normalized to a baseline value of 0 and plotted in arbitrary units, allowing different data sets to be directly compared.

5.2.2.4 Porosity

Porosity properties of nanofiber mats were determined using a liquid (ethanol) intrusion method [96, 131]. Dry mats were weighed before being immersed in 100% ethanol overnight for complete wetting. Mats were then gently wiped to remove excess ethanol and weighed again. Porosity is defined as the volume of the ethanol entrapped in the pores divided by the total volume of the wet mats (ethanol + mat). In our previous study,[10] we also measured porosity of mats by two other alternative methods, namely gravimetric and mercury intrusion porosimetry. It is worth noting that they gave similar results, with no significant difference compared with the liquid (ethanol) intrusion method.

5.2.2.5 X-Ray Photoelectron Spectroscopy

X-Ray photoelectron spectroscopy (XPS) analyses were performed in a VG ESCALAB 3MkII instrument, using non-monochromatic Mg Kα radiation. The size of the analyzed area was about 1 mm^2, the sampling depth being in the 1-5 nm range on account of the fibers' geometries. Spectra were acquired at 0° emission angles (normal to the mat surface), and charging was corrected by referencing all peaks to the carbon (C1s) peak at binding energy, *BE* = 285.0 eV. The X-ray source was operated at 15 kV, 20 mA. Quantification of data was performed using Avantage v4.12 software (Thermo Electron Corporation) by integrating the area under a specific peak after a Shirley-type background subtraction, and using sensitivity factors from the Wagner

table. Data acquired by XPS survey spectra were combined to calculate [O], [O]/[C], and other quantities of interest.

5.2.2.6 Static Contact Angle (SCA) Measurements

Static contact angle (SCA) of water was measured using a VCA Optima Surface Analysis System (AST Products, Billerica, MA) at room temperature (approximately 23°C). The sample was fixed on a glass slide, a 2 µL drop of MilliQ water was placed on the sample surface using a micro-syringe, and SCA was measured using the VCA software provided by the manufacturer. The measurement was repeated at five different locations on selected samples; each experiment was carried out in triplicate to ensure reproducibility, the values were averaged, and the standard deviation was calculated.

5.2.2.7 Wicking Properties

Since the nanofiber mats possess irregular structure with high porosity, it is difficult to precisely measure the wetting properties by contact angle measurements. As an alternative, wicking behavior of the mats can provide sufficiently accurate information about the wetting behaviour. According to the ISO9073-6 standard test method, wicking can be expressed as the height of capillary rise measured for a predetermined time, or the time required for a liquid to reach a predetermined height. We measured the time of capillary rise to 2 cm height in a vertically suspended specimen strip (2 cm × 1 cm) along the fiber direction, while the lower end was dipped into water colored with methylene blue.

5.2.2.8 Tensile Testing

Tensile properties of the mats were evaluated using a uniaxial tensile testing machine (Instron, ElectroPuls™ E3000). Samples were prepared by cutting mats into 0.5 cm x 2 cm strips; a given sample was then inserted into the Instron's jaws, the distance between the upper and the lower jaw being set at 1 cm. The tensile test was performed using a 250 N load cell, at a controlled rate of 10 mm/min. Young's modulus, yield strength, yield strain, tensile strength and elongation at break were calculated manually using Stress-Strain curves. Samples were tested in the "dry" state

(in ambient air). Experiments were repeated three times; at least 12 samples were used in each experiment to test reproducibility.

5.2.2.9 Low-cycle Strain-controlled Accelerated Fatigue Testing

In addition, low-cycle strain-controlled fatigue testing was carried out on the samples which had the closest mechanical properties to those of natural arteries (ePET-Asher-O_2-5min, see further below). Pristine and plasma-etched samples were cut into strips (6 mm × 20 mm), and placed between the grips of a uniaxial tensile tester (Bose, Electroforce 3200 instrument, 22 N load cell). Cyclic uniaxial tensile testing was performed in the elastic domain with a strain-controlled loading (initial linear part of the stress–strain curve, see below). Mat-samples were stretched using a cross-head speed of 0.17 mm/s to an initial strain of 0.25% (pre-conditioning), and were then subjected to 1,000,000 continuous sinusoidal cycles at 10 Hz, in strain ranges of ±1%, whereby the maximum strain, ε_{max}, did not exceed the yield strain.

5.2.2.10 Intrinsic Viscosity and Molecular Weight

Solution viscosity measurements were performed with pristine and plasma-etched ePET samples, to determine their intrinsic viscosity and molecular weight [307, 308]. In accordance with ASTM-D 4603, a Cannon-Ubbelohde viscometer was used for this purpose: A solvent mixture of phenol / 1,1,2,2-tetrachloroethane (60/40 w/w) was employed to dissolve 0.125 g of the PET samples in 25 mL of solvent at 110 °C for 1 hr. Once the samples were completely dissolved, the solutions were first filtered, then tested at 30 °C in a water bath, as follows: From the flow times of the pure solvent mixture (t_0) and the polymer solutions (t, at least three measurements), inherent and intrinsic viscosities were determined from the following equations:

$$\eta_{inh}\ {}^{30°C}_{0.5\%} = \frac{\ln \eta_r}{C} \qquad (1),$$

where:

$\eta_{inh}\ {}^{30°C}_{0.5\%}$: inherent viscosity at 30°C and at polymer concentration of 0.5 g/dL

η_r : relative viscosity = t/t_0

t: average solution flow time, s

t_0: average solvent flow time, s

C: polymer solution concentration, g/dL

The intrinsic viscosity was calculated by using the Billmeyer relationship:

$$\eta = 0.25(\eta_r - 1 + 3\ln\eta_r)/C \quad (2),$$

By means of the Mark-Houwink equation, it is possible to determine the viscosity molecular weight, M_v, from the above-calculated intrinsic viscosity:

$$[\eta] = KM_v^a \quad (3),$$

where the constants "K" and "a" at 30 °C are 2.37×10^{-4} and 0.73, respectively [308].

5.2.2.11 Differential Scanning Calorimetry (DSC)

Melting and crystallization behaviors of pristine and plasma-etched samples were carried out in pure nitrogen atmosphere using a differential scanning calorimeter (Model Q2000, TA Instruments Co., New Castle, DE, USA) equipped with a universal analysis 2000 program (Model Q1000, TA Instruments). About 10 mg of polymer was weighed and crimped into an aluminum pan; then, a heat-cool-heat programming protocol was used with a rate of 10°C min^{-1} over the temperature range from 30°C to 300°C, that was expected to include crystallization, melting and glass transitions of all samples. Heat flow and temperature were calibrated using an indium metal standard.

5.2.3 Biological Testing

5.2.3.1 Cell Culture and Seeding

Vascular smooth muscle cells (VSMCs) from rat embryonic thoracic aorta (a7r5 cell line, ATCC, Manassas, VA) cultured in Dulbecco's Modified Eagle's Medium/ Nutrient Mixture F-12 Ham's Media (DMEM/F12; Invitrogen, Burlington, ON) supplemented with 10% fetal bovine serum (FBS; Medicorp, Montreal, QC) were used between passages 4 to 15. Samples from pristine and plasma-etched electrospun mats (Asher-O_2; 5 min; n=6 each) were cut into disks with a punch (*D*

= 1 cm), placed into 48-well polystyrene culture plates, sterilized in 70% ethanol for 5 min, followed by a rinse with sterile water. Samples were dried overnight under a laminar hood. Next day, cloning glass cylinders (0.8 cm inner diameter; 1 cm height) were placed on the samples to prevent cell adhesion on the outside. VSMCs were detached with 0.05% trypsin/EDTA (Invitrogen, 25300-054), counted and diluted to obtain a suspension of 100,000 cells/ml. Next, 200 µL of this suspension (20,000 cells) was added to each well. As control, cells were also cultured directly on polystyrene culture plates (hereafter "PCP"). After a 24h culture period, cloning cylinders and medium were removed, and 500 µL of fresh complete medium was added to each well. The plates were incubated for 1 and 7 days, the culture medium (DMEM/F12 supplemented with 1% penicillin–streptomycin (Pen–Strep; Invitrogen) being changed every 2 days.

5.2.3.2 Cell Adhesion and Growth

5.2.3.2.1 *AlamarBlue Assay*

Cell adhesion and growth was assessed using AlamarBlue reduction assay (Cedarlane, 30025-1(BT)), during which cell metabolic activity reduces resazurin dye (blue) to resorufin (pink). At days 1 and 7, culture medium was removed and 500 µL of complete medium plus 50 µL of AlamarBlue were added to each well and incubated for 4 h at 37 °C, 5% CO_2. After 4 h, 150-µL aliquots were pipetted into 96-well plates (Corning) in triplicate, and the plates were examined at excitation/emission wavelengths of 560/590 nm in a fluorescence plate reader (BioTek, Synergy 4). The experiment was repeated three times to assure reproducibility. To confirm these data, the density and homogeneity of cells on the mats were directly observed after staining cells by crystal violet solution (0.075% w/v in a 3% v/v acetic acid solution) for 15 min, rinsed 3 times with Milli-Q water and air-dried prior to capture by microscopy (not shown here).

5.2.3.2.2 *Scanning Electron Microscopy (SEM)*

To visualize cell morphology on controls and plasma-etched scaffolds, some samples with cells grown for 7 days were fixed at room temperature for 1 hr with 3% glutaraldehyde (diluted in PBS), before rinsing twice with PBS. Thereafter, they were dehydrated in successive ethanol

solutions of different concentrations (30, 50, 70, 95 and twice 100%; 10 min each). Samples were air-dried under a hood overnight, then gold-coated (Coater: Emitech, K550X) for 2 min for SEM observation (Hitachi, S-3600N).

5.2.4 Statistical Analysis

All data are expressed as mean values ± SD. Statistical analysis was carried out using independent t-test when comparing two groups only (for example, pristine versus plasma-etched). Values of *p* lower than 0.05 were considered significant for all tests.

5.3 Results and Discussion

5.3.1 Physical Properties of Pristine and of Etched Samples

5.3.1.1 Fiber Alignment and Mat Thickness

Partially aligned nanofibrous PET mats were prepared by electrospinning, the mandrel being rotated at 1000 rpm. The height and shape of the 2D FFT plot derived from an SEM micrograph of a pristine mat bear witness to a high degree of fiber alignment (**Figure 5.1 A,B**): The higher and narrower the peak, the more precisely aligned are the fibers along a single direction. The frequency plot, **Figure 5.1C,** shows greatest intensity in the direction of fiber orientation on the micrograph, while sharp peaks near 90° and 270° confirm that the vast majority of fibers were preferentially oriented in the direction of mandrel rotation, that is, perpendicular to the axis of rotation.

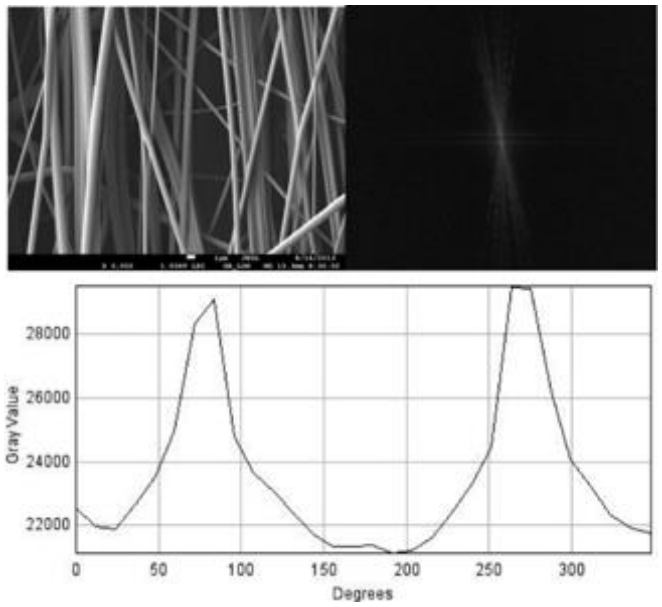

Figure 5.1 Two-dimensional FFT analysis of scaffold anisotropy; (A) SEM micrograph of pristine aligned electrospun nanofiber sample; (B) Image frequency plot; (C) 2D FFT alignment plot for the corresponding SEM micrograph.

Mat thickness measurements revealed significant variation from the center to the edges (70-100 μm). Therefore, samples for later experiments were taken exclusively from the central portions.

5.3.1.2 Measurements of Pore Parameters and Porosity

Porosity results from pristine and plasma-etched samples (**Table 5.2)** were obtained by ethanol intrusion porosimetry. The high porosity of pristine mats, 78%, is highly desirable for the intended media layer of vascular grafts, readily enabling the transport of nutrients, metabolic wastes and gases. Moreover, the pore size is large enough to allow SMC penetration into the scaffold. As expected, the porosity was seen not to change significantly after plasma etching.

Table 5.2 Average fiber diameter and porosity of electrospun mats, pristine and plasma-etched.

Sample (etch time)	Average fiber diameter [nm]	Porosity (%)
Pristine ePET	890 ± 350	78
LP-Ar-O_2 (15 min)	690 ± 430[a)]	75
LP-O_2 (15 min)	770 ± 340[a)]	74
HP-Corona (15 min)	720 ± 350[a)]	77
Asher-O_2 (5 min)	830 ± 395[a)]	76
Asher-O_2-CF_4 (1 min)	670 ± 350[a)]	78

[a)]Significant differences between pristine and plasma-etched ePET ($p < 0.05$).

5.3.1.3 Scanning Electron Microscopy (SEM)

SEM micrographs of untreated and plasma-etched samples are shown in **Figure 5.2**; all are seen to possess structures with large open spaces. The pristine mats clearly show smooth fibers with diameters ranging between 400 and 2000 nm, the average value being 890±350 nm. Average fiber diameters for plasma-etched samples are shown in **Table 5.2**: After O_2 and Ar /10% O_2 "LP"-type plasma etching, one notes reduced diameters accompanied by progressively rougher surface features for shorter treatment times (up to12 min), while longer-duration (15 min) exposure caused degradation of the fiber structure and increased friability of the mats. In the case of "HP" (corona) discharge, surface roughening in the form of tiny pits and micro-cracks accompanied a reduction in the average fiber diameter after 15 min. exposure (**Table 5.2**). For both "LP" and "HP"-treated samples the density, depths and sizes of pits and micro-cracks increased with rising exposure time. In the case of "LP", vacuum ultraviolet (VUV) radiation ($\lambda <$ 200 nm) and ion bombardment may have contributed, in addition to erosion by reactive oxygen species. Somewhat surprisingly, the plasma-asher was found not to significantly alter the fibers' morphology, while nevertheless significantly reducing the average fiber diameter (**Table 5.2**). We did not investigate longer treatment durations with the plasma asher, because 1 or 5 min of exposure was sufficient to adequately reduce the mechanical properties (see below).

The influence of plasma etching on porosity is only minor, but etching clearly leads to fiber diameter reduction, changes to fiber texture and to network morphology. It is worth pointing out that some similar observations had already been reported in earlier literature, notably preferential etching of small-diameter fibers [298], and surface roughening [298-300].

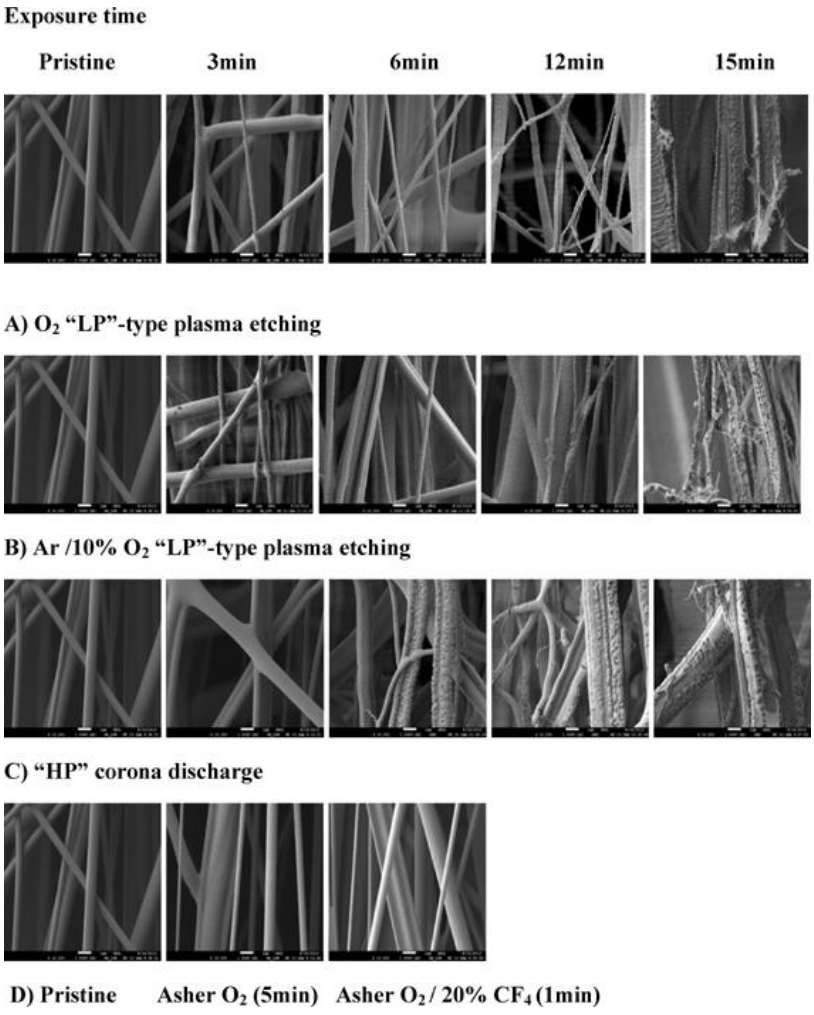

Figure 5.2 SEM micrographs of electrospun aligned PET nano-fiber mats; effects of different plasma-etch treatment processes: (A) O_2 "LP"-type plasma etching; (B) Ar/10% O_2 "LP"-type plasma etching; (C) "HP" corona discharge; D) Plasma-asher (scale bar: 1 μm).

5.3.2 Surface-Chemical (XPS) Analyses

The surface-chemical compositions of pristine and plasma-treated mats were obtained by XPS analyses, **Table 5.3** Surface-near C and O concentrations of pristine samples were 70.5 % and 29.5 %, respectively, but plasma-etched ones displayed higher O/C ratios, as expected. “LP”-type O_2 plasma etching led to higher O/C than its Ar-10% O_2 counterpart, while “HP” corona created mostly O-containing groups, but some N- containing ones, as well. Plasma ashing, on the other hand, resulted in the highest O/C ratio. This is presumably caused by very high atomic oxygen content in the microwave-excited plasma. Plasma-ashing with the O_2 / 20% CF_4 mixture was found to result in low F concentration at the surface.

Table 5.3 Surface-chemical compositions of pristine and plasma-etched electrospun mats.

	C1s	O1s	N1s	F1s	[O]/[C]
ePET (pristine)	70.5	29.5	–	–	0.4
LP—Ar—O_2 (15 min)	65.4	34.7	–	–	0.5
LP—O_2 (15 min)	62	38	–	–	0.6
HP Corona (15 min)	64	34.5	1.5	–	0.5
Asher-O_2 (5 min)	52.8	47.2	–	–	0.9
Asher-O_2-CF_4 (1 min)	54.8	40.5	–	4.8	0.7

5.3.3 Contact Angle (SCA) Measurements

The water SCA results are summarized in **Table 5.4**. It can be clearly seen that plasma etching dramatically changes the surface response from hydrophobic to fully hydrophilic (~ 0°). The water droplets spread and immediately penetrated into all plasma-etched mats once they were placed on the surfaces. This can be due to capillary effects, surface roughness, porosity and high surface oxygen content as seen from XPS data (**Table 5.3**), which can be mainly assigned to polar carbonyl and carboxyl groups.

5.3.3.1 Wicking Properties

As explained earlier, SCA measurements alone do not enable one to fully understand the hydrophilicity of nanofibrous materials. Therefore, wicking was proposed as a complementary method of investigation. Wicking is the spontaneous uptake of a liquid into a porous substrate, driven by capillary forces. **Table 5.4** presents the wicking time for a 2 cm liquid rise in plasma-etched ePET mats, compared with the pristine "non-wetting" one, for which no capillary rise was observed. This supports SCA measurements, which showed that plasma etching significantly increased the wettability of electrospun PET mats.

Table 5.4 Static contact angle and wicking time of pristine and plasma-etched electrospun mats.

	Static Contact Angle (°)	Wicking time (s)
ePET	137±3	N.A. (non-wetting)
LP—Ar—O_2	0	4.5
LP—O_2	0	5
HP Corona	0	8.5
Asher-O_2	0	8.5
Asher-O_2-CF_4	0	9

5.3.4 Tensile Tests

The tensile properties of pristine and plasma-etched mats were measured in the length direction of the 0.5 cm x 2 cm sample strips. The effects of plasma etching by "LP, "HP" and asher at different treatment times are depicted in **Figure 5.3** and **Figure 5.4**; the latter also shows selected literature data for ePET after NaOH wet-chemical etching [133], and for femoral artery [309], for comparison. Young's modulus, tensile strength and elongation at break were all found to decrease significantly with rising treatment time (**Figure 5.3)**. Interestingly, shorter treatment times sufficed for the plasma asher to achieve similar reduction in Young's modulus as with LP and HP plasma (**Figure 5.4**). For this reason, no longer treatment duration was investigated with plasma asher. We had noted earlier that LP and HP plasma etching both introduced micro-pit surface defects, and that they led to fiber degradation after longer exposure times (see **Figure**

5.2). Thus, observed decreases in tensile properties with rising treatment times are not unexpected. Surprisingly, as also noted earlier, micro-pits and -cracks were not observed on fibers treated in the plasma asher, even though the PET erosion rate was high [304, 305], especially for O_2-CF_4 etch (**Table 5.2**). Here too, plasma etching resulted in significant decrease in Young's modulus, tensile strength and elongation at break. These might be due to more intense short-wavelength VUV irradiation in the microwave plasma, resulting in more chain scissions. This may be particularly significant for the present highly porous nano-fibrous mats, because plasma can be sustained inside the pores and VUV can affect a significant fraction of the fibers' volume in spite of its shallow penetration depth (a few tens of nm [141, 295, 310, 311]). To further examine possible chain scission effects, intrinsic viscosity and molecular weight measurements were carried out; the results are discussed in the following section.

Young's modulus was calculated from the linear portion of the stress-strain curve, and data are presented in comparison with values from the literature. Young's moduli and tensile strengths of plasma-etched PET mats are comparable to those of natural arteries (see **Figure 5.4**). On the other hand, elongation at break was found to be less than that of arteries in all cases. However, even though uni-axial tensile testing allows one to assess elastic properties of the fabricated scaffolds, it does not provide a direct measure of compliance (a multi-axial property). Therefore, further tests are desirable, particularly ones designed to evaluate compliance and fatigue resistance of tubular multilayered graft prototypes; this is the subject of ongoing work.

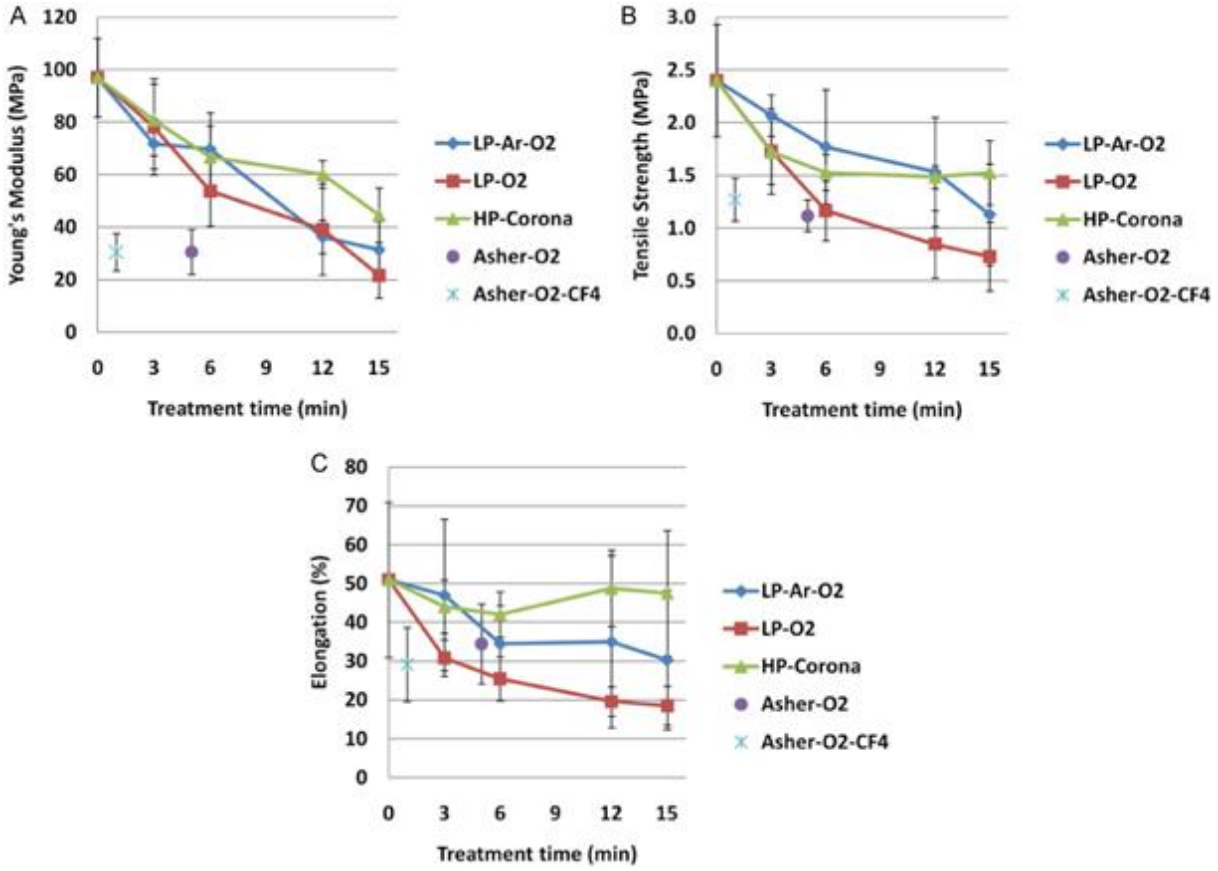

Figure 5.3 Effect of etch duration on mechanical properties of pristine and plasma-etched aligned ePET mats (three experiments, at least 12 samples in each experiment). (A) Young's modulus; (B) tensile strength; (C) elongation at break.

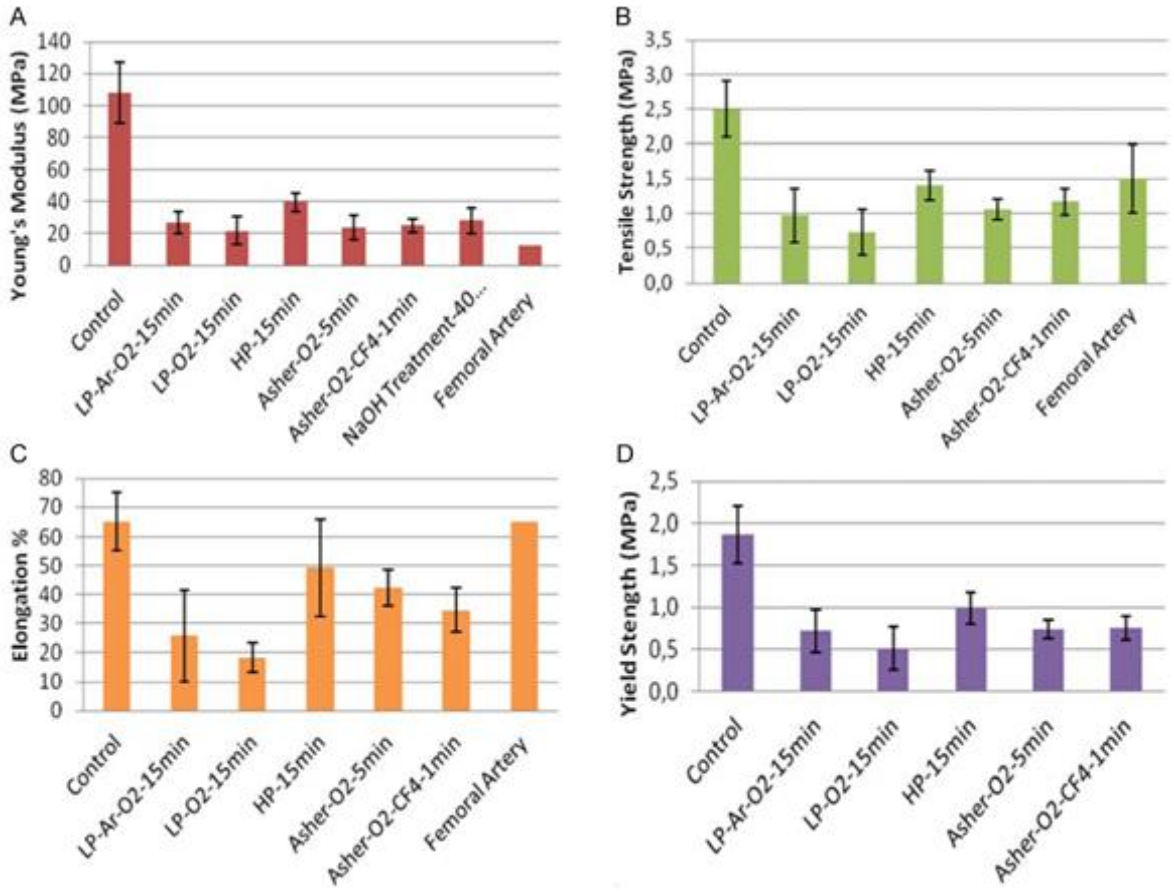

Figure 5.4 Mechanical properties of pristine and plasma-etched aligned ePET mats (three experiments, at least 12 samples in each experiment). (A) Young's modulus; (B) tensile strength; (C) elongation at break; (D) yield strength. Yield strain did not change significantly for plasma-etched samples compared with pristine ones.

5.3.4.1 Low-cycle Strain-controlled Accelerated Fatigue Testing

For further experiments, an asher-etched ePET mat (Asher-O_2, 5min) was chosen, because it provides similar reduction of Yong Modulus as other etch treatments, but for short treatment duration, no significant alteration of the fibers' morphology and no F content. Stress-strain curves (N=1; 1,000,000 cycles) of pristine ePET and of mats etched with the plasma-asher (Asher-O_2) are depicted in **Figure 5.5**. The loading / unloading curves did not change with increasing numbers of cycles. Therefore, after a large number of 10 Hz cycles the samples' mechanical properties were unchanged, which is of course highly desirable for the application considered in this study. In addition, some minor hysteresis (a possible difference between loading and

unloading, which represents energy loss in the system) did not significantly change with the number of cycles at this frequency, as evidenced by the constant area between loading and unloading curves. No signs of sample damage (buckling and deformation) were observed during experiments. However, while fatigue testing of planar mats does allow one to assess fatigue behavior, more detailed studies on tubular multilayered prototype grafts will be desirable to understand their behavior in the real applications.

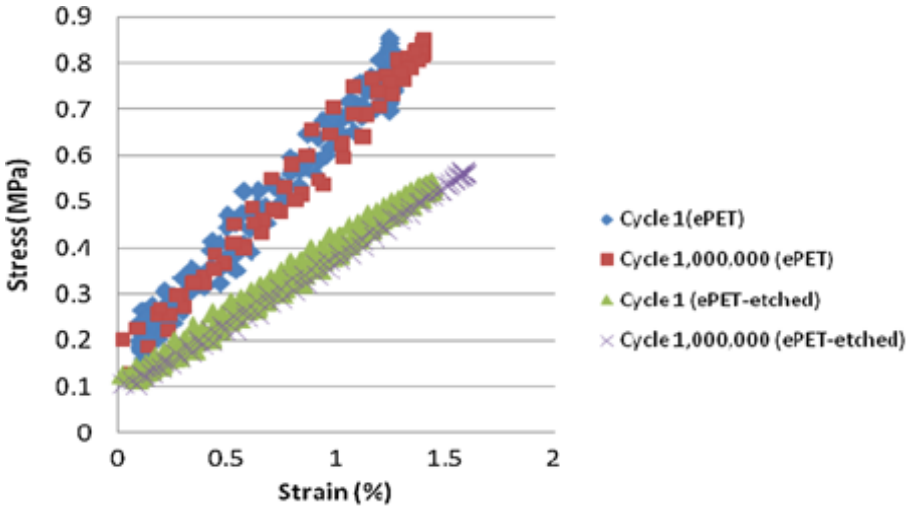

Figure 5.5 Strain-stress diagrams (loading and unloading) for pristine and plasma-etched aligned ePET mats, at cycle numbers 1 and 1 000 000.

5.3.4.2 Intrinsic Viscosity and Molecular Weight

In the preceding section, we postulated that plasma etching might entrain chain scissions, leading to lower average chain lengths (reduced molecular weight). This might originate from both ion bombardment (LP-type plasma) and VUV irradiation, for example the 130 nm emission from atomic oxygen [168, 305] and /or energetic photons from excited argon or fluorine in certain LP and plasma-asher treatments. Such effects are greatly enhanced when the samples' surface-to-volume ratio is large, clearly the case for electrospun material.

Table 5.5 shows significant reductions in intrinsic viscosities and viscosity M_v values for the cases of plasma-etched mats after different plasma-etching procedures. These results agree with SEM images of the treated mats, where surface degradation was observed for samples etched by

LP-plasma in O_2 and Ar+O_2 mixture. Decreases are also seen to be appreciable for HP- and asher-etched samples, compared with the pristine sample values. This would therefore confirm that the nanofibrous polymer was indeed subject to chain scissions, resulting in reduced average chain lengths and lower values of elastic modulus [168, 297, 312].

Table 5.5 Inherent and intrinsic viscosities and viscosity molecular weights for pristine and plasma-etched mats

	ePET (pristine)	LP—O_2 15 min	LP—O_2-Ar 15 min	HP 15 min	O_2—CF_4-asher 1 min	O_2-asher 5 min
Inherent viscosity [$dL \cdot g^{-1}$]	0.94	0.31	0.24	0.57	0.54	0.64
Intrinsic viscosity [$dL \cdot g^{-1}$]	1.00	0.32	0.24	0.59	0.55	0.67
Viscosity Mv [$g \cdot mol^{-1}$]	92 450	19 500	13 275	44 620	41 255	53 490

5.3.5 Differential Scanning Calorimetry (DSC)

DSC measurements were performed on all samples. Presumably, the glass transition (T_g), cold crystallization and melting point temperatures correspond to the three peaks on the DSC thermograms (**Figure 5.6**), in order of rising T, all for first heating runs. Cold crystallization and melting peaks occurred at 127 °C and 252 °C in the thermograms of both pristine and etched nanofibers, but no cold crystallization peak was observed for the case of a PET pellet since it was already partially crystalline. However, the melting temperature (252 °C) of the pellet and ePET were the same. Hence, no major differences in thermal properties were observed between pristine and plasma-etched samples, suggesting that crystallinity did not change appreciably in the course of plasma exposure. Differences between PET mats and pellets (particularly T_g) are probably due to very rapid solidification during solvent evaporation while electrospinning: this presumably does not allow enough time for macromolecular ordering.

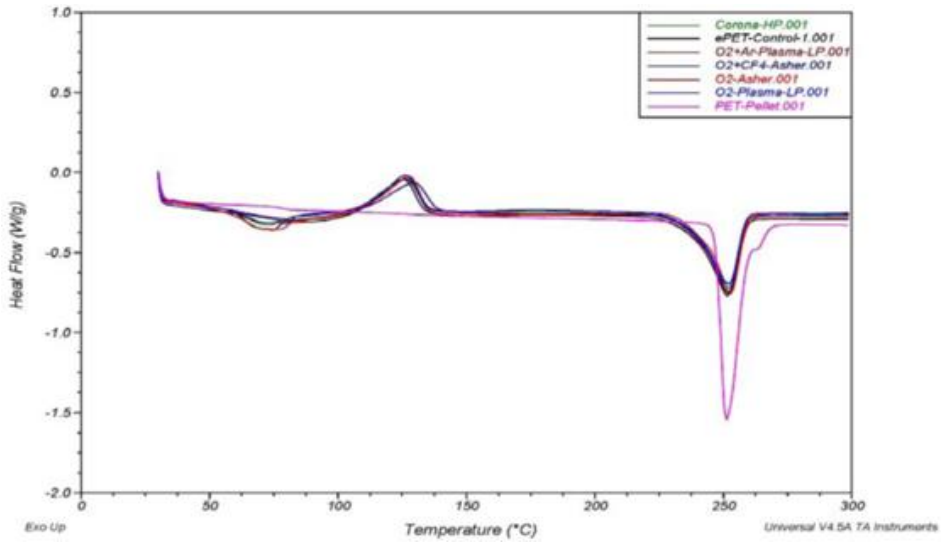

Figure 5.6 DSC thermograms for PET pellet, pristine and plasma-etched ePET mats, during first heating.

5.3.6 Cell Adhesion, Viability and Proliferation on Pristine and Plasma-Etched Substrates

5.3.6.1 Cell Adhesion and Growth

Cell adhesion and -growth was observed on both pristine and plasma-etched mats (Asher-O_2, 5 min) using the AlamarBlue assay. As already pointed out above, asher-etched ePET mat (O_2, 5 min) was chosen because its mechanical properties are comparable to those of natural arteries, and because the fibers' surface morphology was unchanged (see **Table 5.3**). No significant difference in cell adhesion was observed between pristine and plasma-etched samples, which showed similar results as control PCP 24h after seeding (**Figure 5.7**).

Cell growth after 7 days was quite limited on pristine ePET, but significantly (p <0.05) greater on the plasma-etched mat (**Figure 7**). Even more cells were found on PCP (p <0.05) on day 7, but this should not be taken into account, because cells could migrate in PCP wells during the growth period and cover all areas of the well. In contrast, ePET mats were transferred to new wells before the Alamar-Blue assay, to prevent counting cells which migrated and grew on the bottoms of wells. The observed high cell count on plasma-etched mats was expected, because a similar increase had already been observed following wet-chemical or plasma treatments in O_2, CO_2 or

air, for the case of both polymer films and electrospun mats [133, 153, 313]. It is probably due to their different surface properties (hydrophilicity, O-containing functional groups, and somewhat increased surface roughness). These may improve cell adhesion and growth via increased adsorption of proteins from the culture medium or from cell secretions, in agreement with other studies [133, 301].

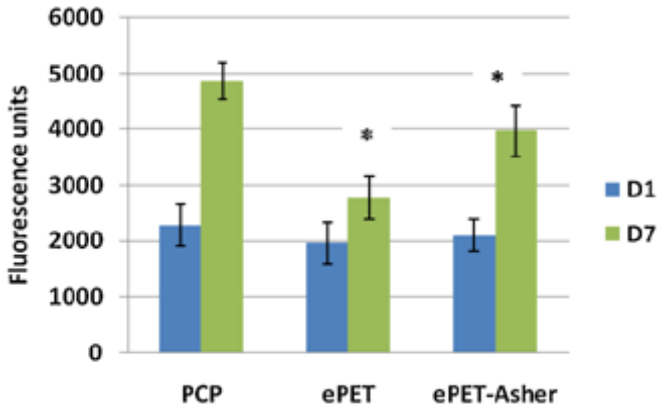

Figure 5.7 Adhesion 24 h and growth 7 d of VSMCs on pristine and plasma-etched substrate (PCP: tissue-culture polystyrene; ePET: electrospun mats; e-PET-Asher: plasma-etched mats) ($n = 8$ for each). * Significant difference between pristine and plasma-etched ePET at day 7 ($p < 0.05$).

5.3.6.2 Cell Morphology

Cell morphology was visualized on the pristine and plasma-etched mats at day 7 by SEM (**Figure 5.8)**. Cells spread on both mats and oriented along or bridged between neighboring fibers. Also, they displayed a spindle-like contractile phenotype and multicellular network, and they penetrated inside the voids of both types of mats. This observation agrees with other studies that show cell migration towards the inside of nano- or micro-fibrous matrices with large pore sizes [284] [106, 133, 314]. However, SEM images merely allow one to observe cell infiltration into the very top layers of the mats; additional study by confocal microscopy is required to evaluate their deeper penetration.

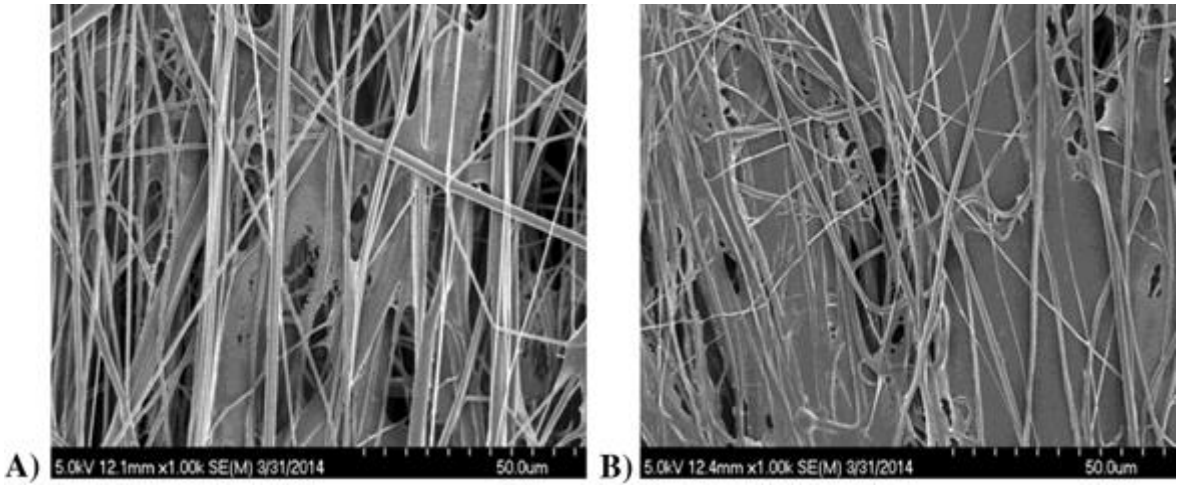

Figure 5.8 SEM micrographs of electrospun nanofiber mats with VSMCs after 7 d of growth: (A) pristine mat (ePET); (B) mat after plasma-etching (scale bar: 50 μm).

5.4 General Discussion and Conclusions

Mimicking the mechanical properties and structure of the media layer of blood vessels plays a key role in the clinical outcomes of engineered vascular graft (VG). Fabrication of a biocompatible, compliant matrix with defined structure that enables the growth of circumferentially-oriented smooth muscle cells (SMCs) remains a challenge [275]. Orientation is the key requirement for SMCs, because they are spindle-shaped and circumferentially aligned [106].

In the present study, cost-effective and easily-implemented electrospinning with a high speed rotating mandrel was used to approximate morphology and mechanical properties of the VG's SMC layer. Highly porous electrospun PET mats (ePET) were prepared with fibers well-aligned along the mandrel's circumference, advantageous for SMC growth. PET was selected because it is stable, inexpensive and cytocompatible, with tunable properties, and because several PET-based vascular implants already received FDA-approval [10, 133]. The main challenge has been excessively-high mechanical properties in the circumferential direction of the spin-aligned mats (most particularly, their high Young's modulus). Therefore, an environmentally benign process, plasma-etching, was chosen to fine-tune the mats' mechanical and surface-chemical properties.

Significant decreases in Young's modulus were observed following LP-, HP-, and asher-induced plasma etching (**Figure 5.4**). Moreover, although there is a reduction in elongation at break, the obtained tensile strengths are similar to those of natural arteries. These changes could be related to the reduction in fiber diameters and to nano/micro-pit surface defects observed after extended LP and HP plasma treatments. Chain scissions and concomitant decreases in molecular weight were also observed with all three etching techniques, according to intrinsic viscosity measurements (**Figure 5.6**). These can be attributed to reactive oxygen erosion, accompanied by ion bombardment and VUV-induced reactions. These are responsible for the majority of chemical alterations present, namely chain scissions accompanied by molecular weight reduction, cleavage of the polymer backbone, and possibly some cross-linking, along with surface oxidation. Prolonged etching duration could entrain deleterious effects on the ePET mats' morphology, as shown in **Figure 5.2** for LP- and HP-plasma etched samples. Interestingly and fortunately, short-duration treatments in the plasma-asher enabled one to attain a similar decrease in Young's modulus (**Figure 5.4**) without observable damage of the fibers, which remained smooth. In addition, the average fiber diameter was reduced (**Table 5.2**) accompanied by a sharp increase in concentration of O-bearing functional groups (**Table 5.3**). Therefore, plasma etching can offer good control for tuning mechanical, morphological and surface-chemical properties of electrospun fibrous mats [299, 300, 315]. The likely presence at etched surfaces of some low molecular weight oxidized residues is not considered problematic, because they occur in very low concentration, are unlikely to be cytotoxic and, in any event, dissolve upon immersion in (aqueous) cell-culture media.

The morphology of the present aligned ePET mats (pristine and asher-etched (O_2, 5 min)) proved to be suitable for deep inward penetration of SCMs, for them to spread between fibers and along their lengths, see **Figure 5.8**. Indeed, the fabrication conditions used yielded high porosity and a relatively large average fiber diameter (**Figure 5.2** and **Table 5.2**). This, and the ability of plasma to be sustained deep within the porous mats facilitated the infiltration of SMCs; of course, the open structure also enables ready exchange of nutrients and gas molecules. In addition to changes in mechanical characteristics, which allow the present etched ePET mats to more closely mimic natural blood vessels, plasma etching was also shown to have a large effect on wettability, observed by SCA and wicking time of a dye solution (**Table 5.4**), turning the originally hydrophobic mats into hydrophilic ones [300, 316, 317]. Increased wettability is, of course,

favorable for cell adhesion and –growth: The polar chemical functionalities created by plasma-etching, for example hydroxyl, carbonyl or carboxylic groups, are known to favor cell adhesion and growth through increased protein adsorption [318, 319], which integrin receptors on cells' outer membrane, in turn, "recognize" and bind to. Moreover, microscopic or sub-micrometer surface roughness can also significantly affect the materials' wettability and protein adsorption [300, 315]. These combined effects showed a strong influence on cell growth after 7 days, compared with the pristine ePET mats (**Figure 5.7)**. Additional modification with bioactive factors can further improve the scaffolds for VG applications, and this is the subject of ongoing investigations.

To conclude, in the present work LP- and HP-plasma etching, along with microwave plasma ashing, have been applied to fine-tune the mechanical and surface properties of aligned electrospun PET (ePET) mat scaffolds. The effects on morphology, mechanical properties, surface chemistry / wettability and bioactivity have been studied and reported here. Among the three etch techniques, the plasma asher (with pure oxygen) seems to be most advantageous in terms of rapidity, minimal apparent damage to fiber surfaces, along with efficacy in changing mechanical properties. Thus, the combination of electrospinning and appropriate plasma-etching can provide an adequate (3D) scaffold for the media layer of small-diameter vascular prostheses; more precisely, it enables one to achieve finely-controlled structural, mechanical and surface properties that are required for VG applications.

Acknowledgments

This research is being supported by grants from the *Natural Sciences and Engineering Research Council of Canada* (NSERC) and the *Canadian Institutes of Health Research* (CIHR) (CPG 87497). One of us (H.S.) gratefully acknowledges the *Fonds de recherche du Québec-Nature et technologies* (FQRNT) for the award of its Merit Scholarship. The authors thank C. Cerclé, N. MacDonald, S. Poulin, Dr. J. Lefebvre, Y. Leblanc (all at *École Polytechnique de Montréal*), and Dr. M. Maire (*CR-CHUM*) for skilled technical support and help during some of the experiments, and École's Microfabrication Laboratory (LMF) for providing access to the plasma-ash apparatus.

CHAPTER 6 ARTICLE 3: COMBINING ELECTROSPUN FIBER MATS AND BIOACTIVE COATINGS FOR VASCULAR GRAFT PROSTHESES

Houman Savoji[1,2,5], Marion Maire[2], Pauline Lequoy[2,4], Benoît Liberelle[3],

Gregory De Crescenzo[1,3], Abdellah Ajji[1,3], Michael R. Wertheimer[1,5], Sophie Lerouge[2,4,*]

École Polytechnique de Montréal, Montreal, QC, Canada ([1]Institute of Biomedical Engineering, [3]Department of Chemical Engineering, [5]Department of Engineering Physics)

[2] Laboratory of Endovascular Biomaterials (LBeV), Research Centre, Centre Hospitalier de l'Université de Montreal (CRCHUM), Montreal, QC, Canada

[4] Department of Mechanical Engineering, École de technologie supérieure, Montreal, QC, Canada

Corresponding author:

Sophie Lerouge, Department of Mechanical Engineering, École de technologie supérieure,

1100 Notre-Dame Ouest, Montreal, QC, H3C 1K3, Canada

E-mail: sophie.lerouge@etsmtl.ca

This manuscript has been published in "Biomacromolecules 2017, 18 (1), pp 303–310" [12].

Abstract

The patency of small-diameter (< 6 mm) synthetic vascular grafts (VGs) is still limited by the absence of a confluent, blood flow-resistant monolayer of endothelial cells (ECs) on the lumen, and of vascular smooth muscle cell (VSMC) growth into the media layer. In this research, electrospinning has been combined with bioactive coatings based on chondroitin sulfate (CS) to create scaffolds that possess optimal morphological and bioactive properties for subsequent cell seeding. We fabricated random and aligned electrospun poly(ethylene terephthalate), ePET, mats with small pores (3.2 ± 0.5 or 3.9 ± 0.3 μm,), then investigated the effects of topography and bioactive coatings on EC adhesion, growth and resistance to shear stress. Bioactive coatings were found to dominate the cell behavior, enabling creation of a near-confluent EC monolayer that resisted physiological shear-flow conditions. CS is particularly interesting since it prevents platelet adhesion, a key issue to avoid blood clot formation in case of an incomplete EC monolayer or partial cell detachment. Regarding the media layer, circumferentially oriented nano-fibers with larger pores (6.3 ± 0.5 μm) allowed growth, survival and inward penetration of VSMCs, especially when the CS was further coated with tethered, oriented epidermal growth factor (EGF). In summary, the techniques developed here can lead to adequate scaffolds for the luminal and media layers of small-diameter synthetic VGs.

Keywords: electrospinning; vascular graft; bioactive coatings; chondroitin sulfate; EGF immobilization; endothelialization; shear-induced flow; VSMC survival

6.1 Introduction

Primary requirements for functional synthetic small-diameter vascular grafts (VGs) or tissue engineered blood vessels for coronary or femoral artery bypass are favorable compliance and hemocompatibility [27]. To achieve long-term patency, a VG should thus possess a continuous and stable monolayer of endothelial cells (ECs) on its lumen, with significant resistance to physiological shear stress [320]. Yet, stable endothelialization of VGs remains a so-far unmet objective, in spite of great efforts during the past decade. *In vitro* seeding of autologous ECs or *in situ* capture of endothelial progenitor cells on the luminal layer of grafts have been tested [321], but due to weak EC adhesion the implanted grafts lacked adequate long-term patency. This is partly due to the inability of conventional VGs to reproduce the morphology and cell-matrix interactions of native tissues. In the extracellular matrix (ECM), topographical cell guidance is assured thanks to various combinations of pores, ridges and fibers at micro/nanoscale levels. Additionally, the ECM is known to orchestrate time- and spatially-controlled delivery of biochemical cues that trigger specific cell signaling pathways to finely tune tissue growth and homeostasis [322, 323].

Electrospinning has been used to design highly porous scaffolds that mimic topological cues of the ECM within native arteries [14, 229, 324]. Nano/microfiber scaffolds with different degrees of fiber- alignment and -diameter have therefore been developed to optimize structural and mechanical properties of VGs in an effort to regulate cell adhesion, shape, spreading, and migration [99, 133, 325].

Our team has investigated how electrospun polyethylene terephthalate (ePET) mat properties such as fiber diameter, orientation and surface characteristics affect EC adhesion, spreading, infiltration and migration [10, 11, 133, 231]. PET was selected for its good mechanical properties, stability, biocompatibility, and low cost. Furthermore, large diameter woven PET VGs have already been FDA approved and clinically used for many years [10, 27, 231]. The results of above-cited studies demonstrated that mats with small diameter fibers were appropriate to form an EC monolayer on the lumen of a VG [133], but a completely confluent monolayer could not be achieved under shear stress [10, 14].

A promising method to further enhance EC adhesion, growth and resistance to shear stress is to combine electrospun fibers with a bioactive coating [6]. We have recently shown that a primary

amine-rich, low-pressure plasma-polymerized coating (hereafter “LP”) was able to significantly increase EC growth and retention [10, 246], but that retention was still not entirely complete. Moreover, LP was found to promote platelet adhesion and aggregation, that is, increased risk of thrombosis if the endothelial lining partially detaches under shear [13]. Our team also demonstrated [13, 190] that chondroitin sulfate (CS), a sulfated glycosaminoglycan that is abundant in the ECM of native blood vessels [326], once grafted on LP coating, also promotes EC adhesion and growth, but strongly reduces protein adsorption, platelet adhesion and aggregation [13]. Therefore, we propose here to combine electrospun mats with a bioactive coating that includes CS, in order to achieve a complete, stable endothelial lining.

Electrospinning may also help to achieve a porous structure for constructing the media layer of a synthetic blood vessel, a layer which contains circumferentially-aligned fibres and the vascular smooth muscle cells (VSMC) responsible for contraction, dilation and blood pressure control [327, 328]. Therefore, the combination of an electrospun scaffold with a bioactive coating was also evaluated here as a mean to enhance VSMC growth and infiltration into porous mats. In addition to CS, epidermal growth factor (EGF), a 6-kDa mitogenic protein known to enhance VSMC growth, was also tethered on CS-grafted surfaces in an oriented manner, because this strategy is known to improve GF potency compared with random covalent binding [185, 189, 329].

We here report the cooperative effects of topological and biochemical features (the degree of alignment of electrospun nano-fibers, and the use of bioactive coatings) using three-dimensional (3D) ePET nanofiber scaffolds, upon cell growth of luminal (EC) and media (VSMC) layers for VGs. First, we combined LP+CS coatings with smaller pore-size random (hereafter “RL”) and aligned (hereafter “AL”) ePET mats for the luminal layer, then evaluated their ability to favor human umbilical vein EC (HUVEC) adhesion, growth and resistance to shear-induced flow. Next, we combined bioactive coatings (LP+CS+oriented tethered EGF) with aligned mats having somewhat larger pore-size for the media layer (hereafter “AM”), and investigated their bioactivity and ability to favor VSMC adhesion, growth and infiltration.

6.2 Materials and Methods

6.2.1 Materials

PET pellets were obtained from DuPont selar PT 7086 (intrinsic viscosity of 1), and ethylene (C_2H_4; 99.5%) and ammonia gas (NH_3, 99.99%) from Air Liquide Canada Ltd. (Montreal, Canada). Chondroitin sulfate (CS), bovine serum albumin (BSA, 66 kDa) were purchased from Sigma-Aldrich Canada Ltd; DuoSet ELISA kits were obtained from R&D Systems, Minneapolis, MN. When not mentioned otherwise, chemical products were purchased from Sigma-Aldrich Canada Ltd.

6.2.2 Fabrication of Random and Aligned Bioactive Nano-fibrous Scaffolds

6.2.2.1 Electrospinning

Optimized ePET mats for luminal and medial layers of VGs were prepared on a rotating mandrel, using a homemade electrospinning set-up. As previously described [10, 11], PET pellets were dissolved in 1:1 mixture of analytical grade dichloromethane (CH_2Cl_2)/trifluoro-acetic acid (TFA), and gently stirred for 24 h at room temperature. Two milliliters (mL) of polymer solution were electrospun with the aid of a syringe pump, in an enclosure at ambient humidity and temperature. Electrospinning parameters (**Table 6.1**) were adjusted to fine-tune the morphology of the mats for HUVEC and VSMC culture, i.e. random and aligned ePET mats with smaller pores for the luminal layer (RL and AL), and aligned mat with larger pore-size for the media layer (AM). The mandrel velocity was increased to obtain more aligned fibers for the luminal layer. On the other hand, a partially aligned, larger-pore mat for the media layer was obtained using higher PET concentration, a larger needle and relatively high drum speed. The fabricated electrospun scaffolds were dried in ambient air for 3 days to remove any residual solvent.

Table 6.1 Process conditions used to produce the electrospun random and aligned ePET mats

Mat type	PET solution concentration (% w/v)	Process parameters				Collector	Ambient conditions	
		Needle size (G)	Tip-Collector distance (cm)	Voltage (kV)	Flow rate (mL/h)	Mandrel velocity (RPM)	RH (%)	Temp (°C)
RL	9	22	15	15-17	0.5	175	8-25	20-25
AL	9	22	15	20	0.5	2000	8-25	20-25
AM	12.5	18	13	30	10	1000	8-25	20-25

RL: random mat for luminal layer; AL: aligned mat for luminal layer; AM: aligned mat for media layer

6.2.2.2 Plasma-Polymerization

Primary-amine rich plasma polymer (LP) coatings were deposited on the surface of the nano-fiber mats in a low-pressure ("L") capacitively-coupled radio-frequency (r.f., 13.56 MHz) glow discharge plasma reactor, using ethylene (C_2H_4) / ammonia (NH_3) gas mixture [160, 247]. The coatings were deposited under partial vacuum (p = 80 Pa) using constant flow rates of C_2H_4 "monomer" and ammonia, NH_3, $F_{C_2H_4}$ and F_{NH_3}, with a mixture ratio $R = F_{NH_3}/ F_{C_2H_4} = 0.75$. The deposition was performed for 8 min duration under mild plasma conditions (power, P = 10 W, d.c. bias voltage, V_B = - 40 V). These conditions were previously shown to provide high nitrogen and amine concentrations, [N] and [NH_2], and good stability (insolubility) in aqueous solutions [247].

6.2.2.3 CS Grafting on the LP-coated Mats

Circular samples (1 cm^2) of the amine-rich LP-coated ePET mats were punched to fit into 48-well plates. CS was dissolved in Milli-Q water at 0.1 $g.mL^{-1}$, and the resulting solution was filtered (200-µm PTFE filter) to remove aggregates. CS was covalently grafted on the mats by way of carbodiimide chemistry (NHS/EDC-based chemistry) [185]: The mats were incubated in 200 µL

of solution containing 0.01 $g.mL^{-1}$ CS, 40% v/v EtOH, 50 mM MES, 22.8 mM EDC, 4.6 mM NHS for 1 h at room temperature, then finally rinsed once with PBS (10 mM, pH 7.4) and twice with Milli-Q water for 2 min in an ultrasonic bath.

6.2.2.4 EGF Oriented Immobilization

Oriented immobilization of EGF on CS-grafted surfaces was performed [185] using the Ecoil and Kcoil peptides that hetero-dimerize with high specificity and affinity [215, 329]. Cysteine-tagged Kcoil peptides were synthesized by the peptide facility at the University of Colorado (Denver, CO, USA). Ecoil-tagged EGF (E-EGF) was produced in human embryonic kidney (HEK) 293 cells and purified [213]. Kcoil was grafted on CS-grafted mats using EMCH linker that reacts with the carboxyl groups of CS and the thiol group of the cysteine-terminated Kcoil [185]. Mats covered with covalently bound Kcoil were incubated overnight in a 10% solution of fetal bovine serum (FBS) in PBS to remove any unbound peptide. After rinsing with PBS, surfaces were incubated for 1 h with 200 µL of E-EGF solution at 22 nM concentration in 10 mM PBS containing 1% BSA. This concentration was chosen based on our previous experiments on PET film surfaces [185]. After capture of the Ecoil-tagged protein, mats were rinsed with PBS.

6.2.3 Characterization of Bioactive Scaffolds

6.2.3.1 Mat Morphology

Electrospun nano-fiber structure and morphology were evaluated by scanning electron microscopy (SEM) using a JSM-7600 Field Emission instrument (JEOL Ltd., Tokyo, Japan) at 0.5 kV. Mat surfaces were first sputter-coated with gold for 45 s; images were analyzed using ImageJ (NIH, USA) software, and diameters were calculated based on at least 100 fibers (at least two experiments with triplicate samples). The fiber alignment was characterized using the directional plugin of ImageJ to obtain Fast Fourier Transformation (FFT) of SEM images [11]. The porosity of nanofiber mats was determined using a liquid (ethanol) intrusion method [96]. In addition, the average pore size was evaluated by SEM with the ImageJ software, assuming elliptical pore shapes and taking an average of major and minor axes of the best-fitting ellipses.

6.2.3.2 Chemical Composition

X-ray photoelectron spectroscopy (XPS) analyses of bare and modified mats were performed in a VG ESCALAB 3MkII instrument, using non-monochromatic Mg Kα radiation. To assess possible chemical composition gradients across the thickness of the mat, a two-layer scaffold was created by a two-step electrospinning approach. The first ply (ca. 50 µm, half of the final thickness) was fabricated and dried overnight; the second ply (approx. 50 µm) was then electrospun on top of the first. A LP+CS coating was created on top of the two-layer mat and XPS survey spectra were taken at different depths of this composite sample, namely, top ([a]: 0 µm), mid-plane ([b]: 50 µm), and bottom ([c]: 100 µm).

6.2.3.3 Protein Adsorption Measurements

Since CS has low-fouling properties [13], CS grafting throughout the scaffold thickness was examined by protein adsorption using Texas Red fluorescent-labeled bovine serum albumin (BSA), using the two-layer mat described above. Briefly, the two layers were gently separated and immersed in labeled BSA (0.2 mg/mL in PBS) for 2 h under static ambient conditions in the dark. Fluorescence intensity was measured after thorough washing with PBS to remove unbound protein. Images were analyzed using ImageJ software and the background auto-fluorescence was subtracted for each sample.

6.2.3.4 E-EGF Quantification by ELISA

E-EGF immobilized on the mats was quantified by direct enzyme-linked immunosorbent assay (ELISA) according to the manufacturer's instructions. The optical density (O.D.) was measured at 630 nm. The slopes corresponding to the initial O.D. variation in the wells over time were calculated, and the value obtained for a surface with no growth factor was subtracted from all signals.

6.2.4 Biological Testing

6.2.4.1 HUVEC Adhesion and Growth

HUVECs (Cell Applications Inc.) were cultured in 1% gelatin-coated flasks, in complete medium EGM-2 bullet Kit (Lonza, CC-3162) and used at passage 3 - 5. Random and aligned 1 cm-diameter disk samples from bare, LP-coated, and CS-grafted mats were placed in 48-well polystyrene culture plates (hereafter "PCP") and sterilized in 70% ethanol for 5 min, rinsed with sterile water, then dried overnight under a laminar hood. Cloning glass cylinders (0.8 cm inner diameter, 1 cm height) were placed on the disk samples to prevent their movement after cell seeding and to prevent cell adhesion elsewhere. 200 µL of HUVEC suspension (20,000 cells) was added to each well; as positive controls, cells were also cultured directly on PCP coated with 1% gelatin. After a 4h period of adhesion, cloning cylinders and medium were removed, and cells were left to grow for 1, 7, 14 and 21 days in 500 µL of complete medium supplemented with 1% penicillin–streptomycin (Pen–Strep; Invitrogen). HUVEC adhesion and growth on the various surfaces was evaluated using AlamarBlue (10 %v/v) reduction assay (Cedarlane, 30025-1(BT), four samples each). The experiment was carried out in triplicate to ensure reproducibility. To assess cell viability and distribution in the 3D mats, Live-Dead assays were performed by incubating in calcein-AM (2 µM) and ethidium homodimer-1 (5.5 µM, Invitrogen) for 45 min at 37 ºC in the dark, before rinsing with PBS and imaging under a Laser Confocal Scanning Microscope (Olympus multiphoton FV-1000 MER, Olympus, Canada).

Immunostaining was performed to visualize actin microfilaments, focal adhesions and cell-cell contact points according to well-established procedures [186, 246]. Briefly, cells were fixed and permeabilized with 3.7% paraformaldehyde and 0.1% TRITON X-100 solution in PBS, respectively, then incubated with primary antibodies, namely anti-mouse vinculin (Millipore, MAB3574, diluted 1:100) and anti-mouse VE-cadherin (Millipore, diluted 1:100). Following this, the scaffolds were incubated with secondary antibody, goat anti-mouse Alexafluor 546 (Invitrogen, A-11018, diluted 1:200), then with the corresponding Alexa (Molecular Probes) Phalloidin Alexa-488 anti-mouse (Invitrogen, A-11029, diluted 1:40). Finally, cell nuclei were stained with Draq5 (diluted 1:1000). Samples were examined using a Leica TCS SP2 confocal laser-scanning microscope (Leica Microsystems, Wetzlar, Germany).

6.2.4.2 Cell Alignment and Morphology

Cell alignment was calculated from immunostained images using ImageJ software, based on the angle difference between the long axis of each nucleus (presumed elliptical) and the average fiber direction (100 nuclei in total), following which alignment angles were categorized in 10° increments. Cells with angles < 30° were considered aligned [330, 331]. In addition, the cell elongation was evaluated using ImageJ software by its shape index (circularity = $4*\pi*\text{area}/\text{perimeter}^2$) for each cell on random and aligned scaffolds, shape index 1 corresponding to a perfect circle [332]. SEM was also used to visualize cell morphology on controls and modified scaffolds.

6.2.4.3 HUVEC Resistance to Laminar Shear Stress

To study HUVEC resistance to shear, cells (250 µL in complete medium, 10^6 cells/mat) were seeded and left to adhere on mats (10 mm×22.5 mm) for 48 h so as to obtain a confluent monolayer. They were then subjected to laminar flow-induced shear stress of ca. 15 dynes cm^{-2} (similar to an actual physiological value [333]) for 1 h in a parallel-flow chamber (Glycotech, C 31-001, Gaithersburg MD) [10]. The influence of fiber alignment (random vs. aligned mats) and surface composition (bare, LP and LP+CS-coated mats) on cell retention was studied by AlamarBlue and SEM.

6.2.4.4 VSMC Adhesion, Growth and Survival

VSMCs from rat embryonic thoracic aorta (a7r5 cell line, ATCC, VA, USA), cultured in Dulbecco's Modified Eagle's Medium/ Nutrient Mixture F-12 Ham's Media (DMEM/F12; Invitrogen) supplemented with 10% fetal bovine serum (FBS; Medicorp, Quebec, Canada), were used between passages 4 to 15. For cell growth and survival experiments, 20,000 and 30,000 cells/mat, respectively, were seeded in complete media on pristine and modified aligned mats (LP, LP+CS, LP+CS+EGF), as was done in the case of HUVECs. Cell growth was assessed in complete media and cell survival in serum-free medium (DMEM/F12; Invitrogen), both using AlamarBlue. The media was changed every other day. For conditions designated as ''soluble EGF'', 10 $ng.mL^{-1}$ of EGF was supplemented in the culture medium.

6.2.4.5 Histology

In order to evaluate cellular infiltration into the electrospun mats after 21 days of incubation, samples were rinsed with PBS and fixed with 10% neutral buffer formalin for 24h at room temperature. After embedding in paraffin, 6 µm thick microtomed sections were stained using Hematoxylin-Eosin (H&E) and imaged.

6.2.5 Statistical Analysis

Each experiment was carried out in triplicate to examine reproducibility. All data are expressed as mean values ± SD. Statistical analyses were carried out using ANOVA with Tukey's post hoc analysis, or by independent t-test when comparing two groups only. Values of $p < 0.05$ were considered significant for all tests.

6.3 Results and discussion

6.3.1 Morphology of Random and Aligned Scaffolds for Lumen

In blood vessels, ECs are well known to be aligned and elongated in the flow direction, which results in maximized cell retention under blood flow-induced shear stress [333]. To stimulate EC alignment by topographical cues, aligned scaffolds with small pore-size (AL) were compared with their random counterparts (RL) in regard to formation of an EC monolayer. SEM images (**Figure 6.1**A and B) confirm uniform, smooth fiber morphology with interconnected open structure, and average diameters of ca. 550 ± 90 nm and 500 ± 140 nm for random and aligned nanofibers, respectively (n=200). The overall porosity was similar (87%) in both cases, mean respective pore diameters being ca. 3.2 ± 0.5 and 3.9 ± 0.3 µm. The 2D FFT frequency images (**Figure 6.1**A and B, inset) show that only the aligned (AL) scaffolds exhibited an oriented structure. The fiber alignment was also quantified by the 2D FFT plot (see supplemental data **Figure E1**) which shows greatest intensity in the direction of fiber alignment on the micrograph, while sharp peaks at 90° and 270° confirm that the majority of fibers were oriented in a specific direction (perpendicular to the mandrel axis during electrospinning).

6.3.2 Morphology of Aligned Scaffolds for Medial Layer

Aligned scaffolds (AM) with greater pore size were fabricated in order to mimic the media layer (**Figure 6.1**C), respective average fiber diameter, pore diameter and porosity being 890 ± 350 nm, 6.3 ± 0.5 μm and 78%. Greater pore sizes were desirable in this case to allow SMC infiltration into the bulk of the scaffold. The 2D FFT frequency image (**Figure 6.1**C, inset) and quantified plot (supplemental data **Figure E1**) also confirm the fiber alignment.

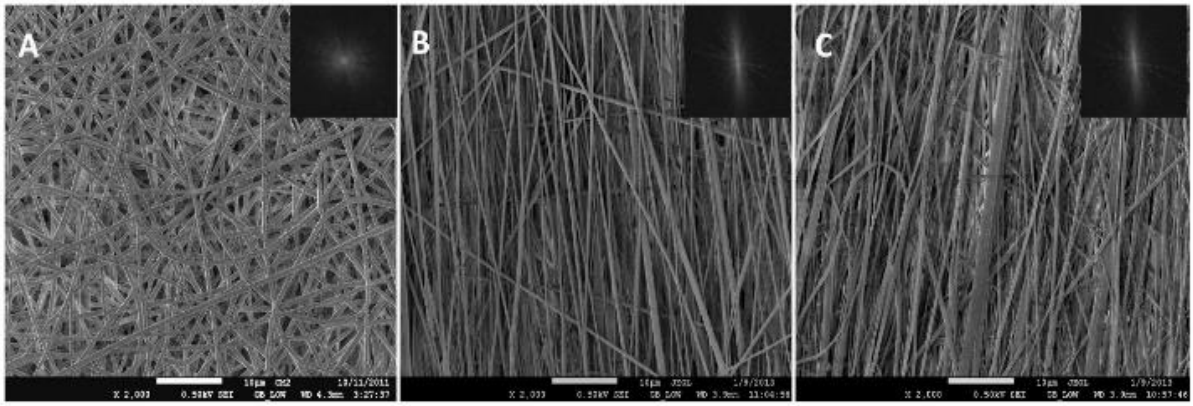

Figure 6.1 SEM and 2D FFT images (insets) of (A) random (RL), (B) aligned (AL) mat for the luminal layer; and (C) aligned (AM) mat for the media layer (scale bar: 10 μm).

6.3.3 Surface Chemistry and Depth-Dependence

XPS-based elemental composition of an AM mat after LP deposition and CS grafting is presented in **Table 6.2**. From our earlier work it is known that LP is stable and that it comprises high values of [N] and [NH_2] [10, 334], reconfirmed here ([N] = 11.2%). The presence of sulfur (S) also confirmed successful grafting of CS on the LP-coated mats. Furthermore, the ability to coat fibers with LP and LP+CS in the sample bulk was examined using the two-layer mat sample, on top [a]: 0 μm; in the middle, [b]: 50 μm; and at the bottom, [c]: 100 μm (n = 3, **Table 6.2**). Although [N] decreased with increasing depth, it was clearly measurable in cases [b] and [c], many tens of micrometers below the surface, confirming that active plasma species penetrated through the porous structure. After CS grafting, [N] decrease and [S] increase at each level of the mats are a first confirmation that CS was grafted across the mat thickness.

Table 6.2 XPS-based chemical compositions of bare and coated aligned mats for the media layer (AM) and their depth-dependence (n=3)

2-layer AM bare mat			
Depth	**[a]: 0 µm**	**[b]: 50 µm**	**[c]: 100 µm**
Elements	**Avg. (%)** ±SD	**Avg. (%)** ±SD	**Avg. (%)** ±SD
C	70.5	70.5	70.5
N	0	0	0
O	29.5	29.5	29.5
S	0	0	0
2-layer AM+LP-coated mat			
C	84.3±1.4	74.4±1	74.5±0.8
N	11.2±0.9	7.2±0.1	5.1±0.8
O	4.6±2.4	18.4±1.1	20.4±0.0
S	0	0	0
2-layer AM+LP+CS grafted mat			
C	69.3±1.4	69.8±0.5	71.3±1.4
N	8.7±1.2	5.8±0.1	4.4±0.3
O	21.3±0.2	23.6±0.3	23.6±1.2
S	0.7±0.1	0.8±0.0	0.8±0.1

6.3.4 Protein Adsorption

CS grafting throughout the thickness of the AM mats was confirmed by BSA adsorption on the same two-layer mats. Protein adsorption can serve as an indirect indicator for CS grafting thanks

to the earlier-demonstrated low-fouling properties of CS [13]. As shown in **Figure 6.2**, LP coating *increased* albumin adsorption compared with bare ePET mats, as previously demonstrated on film substrates [13], while CS grafting significantly decreased it. As expected, these effects are less pronounced at the bottom (case [c]), which confirms lower [NH_2] after plasma (**Table 6.2**) and consequently less grafted CS.

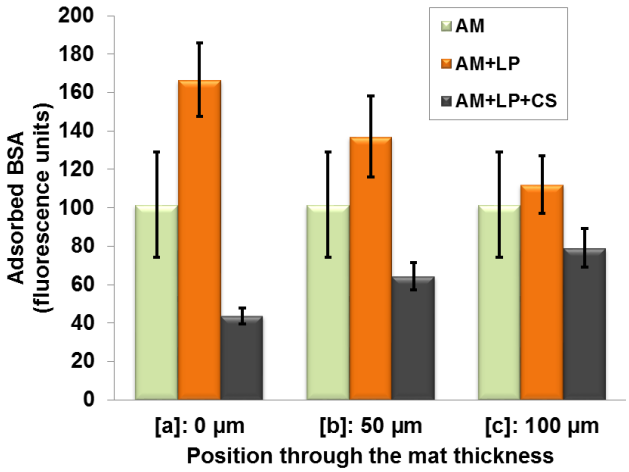

Figure 6.2 Fluorescence intensity of adsorbed Texas Red-BSA (0.2 mg/mL) on bare AM, AM+LP-, and AM+LP+CS-coated mats as a function of depth (n=10).

6.3.5 Effect of Fiber Orientation and Bioactive Coatings on HUVECs

Figure 6.3 presents adhesion and growth results for HUVECs on the various surfaces, assessed by their metabolic activity. Adhesion and growth on bare RL and AL scaffolds were found to be similar at each time point ($p > 0.05$). Interestingly, metabolic activity was found to drop sharply at day 7, but then it increased again, a type of behavior reported before by our team [10] and another group [155]. LP coating significantly increased cell adhesion and growth on both scaffolds ($p < 0.05$), in agreement with previous studies on various 2D and 3D substrates [10, 13, 246]. CS-grafted scaffolds showed similar initial adhesion as LP ($p > 0.05$), but more rapid growth thereafter, as shown by significantly higher values at day 7, 14 and 21 (**Figure 6.3**, **Figure 6.4**).

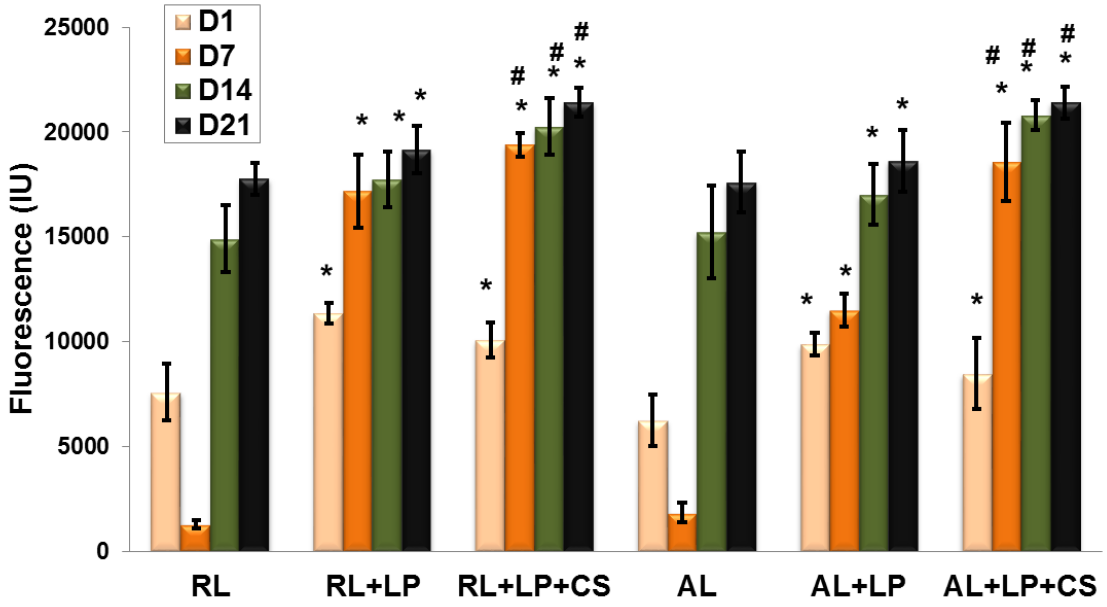

Figure 6.3 Adhesion (day 1) and growth (day 7, 14 and 21) of HUVECs on bare and coated random (RL) and aligned (AL) mats. Mean ± SD ($n \geq 6$).

(* $p < 0.05$ with bare surfaces; # $p < 0.05$ with LP-coated surfaces at the same time point).

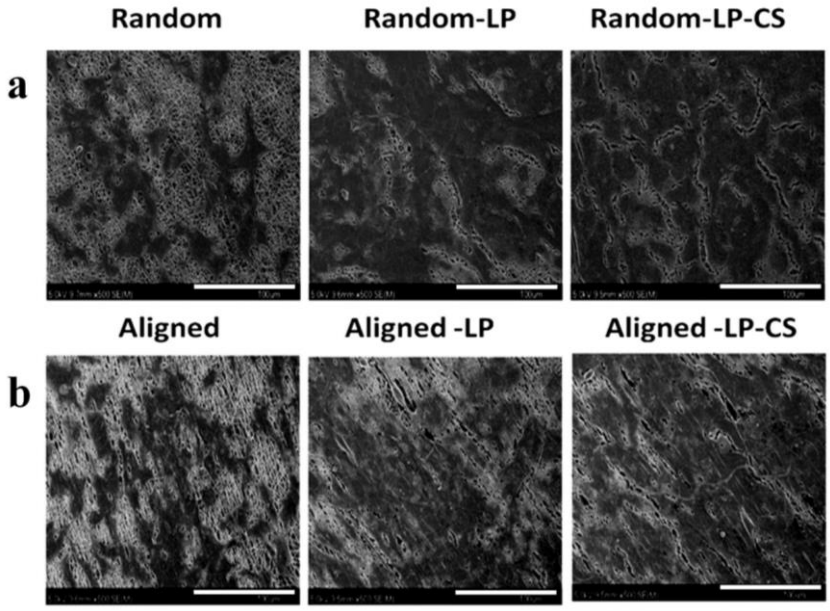

Figure 6.4 SEM images of HUVECs after 21 days of cell culture on a) bare and coated random (RL); b) bare and coated aligned (AL) ePET mats (scale bar: 100µm).

The z-stack confocal images in **Figure 6.5**a confirm a monolayer of endothelial cells on both RL and AL scaffolds, with no sign of cell penetration into the bulk. Moreover, at locations where confluency occurred, VE-cadherin protein expression is noted at cell-to-cell contact regions, indicating that neighboring cells interacted in a coherent manner (**Figure 6.5**d). This would confirm that these nano-fibrous structures are indeed well adapted for forming confluent monolayers of endothelial cells.

Vinculin immunostaining showed no significant difference between the various mat morphologies. Even on the latter we observed only limited focal adhesion complexes, mostly at the polarized cell edges (**Figure 6.5**e). This agrees with other studies [335, 336], demonstrating weak focal points between cells and the electrospun nano- fibers.

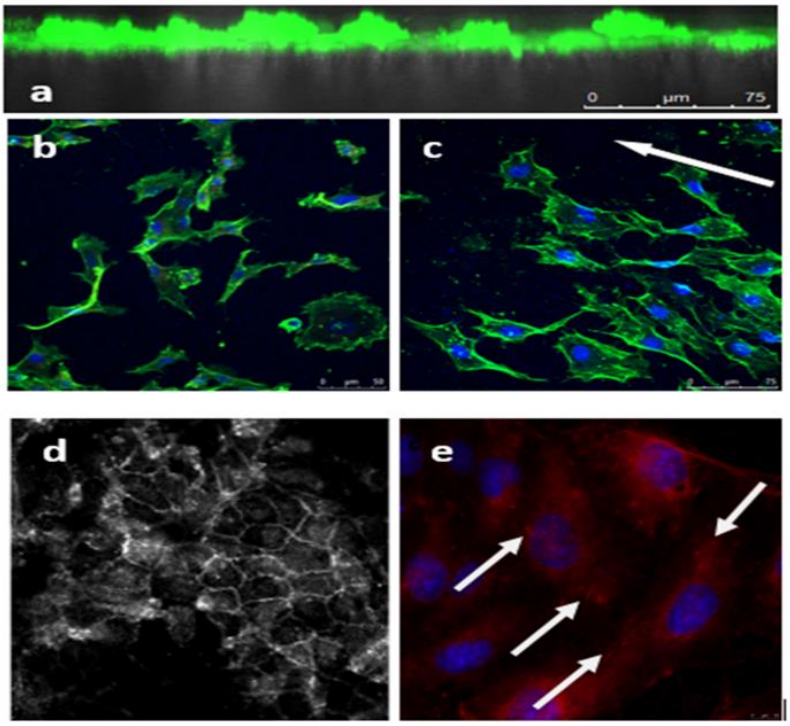

Figure 6.5 a) z-stack confocal micrograph of HUVECs grown (D21) on an AL mat (live cells in green); b, c) confocal micrographs of HUVEC adhered (at D1) on LP-coated (b) random (RL) and (c) aligned (AL) mats (cytoskeletal F-actin in green, nucleus in blue, electrospun fiber direction indicated by arrow); d) typical cell-cell interactions (VE-cadherin, in white); e) cell focal adhesion points (vinculin, in red) on LP-coated random (RL) mat at D7 (scale bar: 75 µm).

Finally, cell retention after shear stress was tested on bare and coated mats (**Figure 6.6**). The percentage of cells remaining after shear was very low on bare mats (25-30%), but much greater for LP and LP+CS coated ones, both random and aligned (LP+CS > LP > bare; $p < 0.05$). The performance was slightly (but not significantly) better on the aligned scaffolds, ones coated with LP+CS showing up to 82 % cell retention.

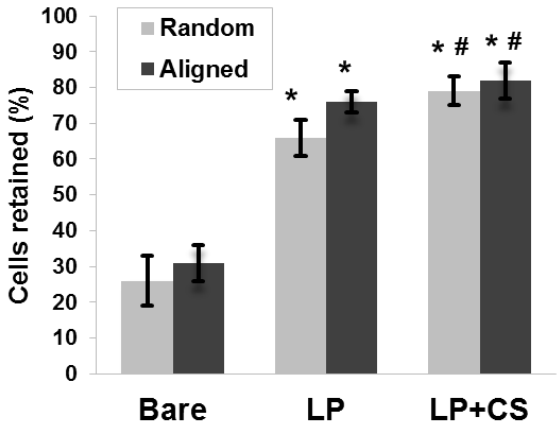

Figure 6.6 HUVEC retention after laminar shear stress (15 dynes.cm $^{-2}$,1h), evaluated by AlamarBlue assay (n=4).

*, $^{\#}$ $p < 0.05$ with reference to bare and LP-coated surfaces under shear, respectively.

Some cell alignment was observed on the AL mats, as shown on **Figure 6.5c** by parallel-oriented F-actin microfilaments, in contrast with the irregular cell shape observed in **Figure 6.5**b for the random (RL) mats. This was confirmed by quantitative analysis of the nuclear alignment: 80% of the cells aligned with the AL fiber direction (angles < 30°, see supplemental data, **Figure E2** and **Table E1**), contrary to random cell orientation for the RL scaffolds. Furthermore, there were significant differences in cell elongation between the RL and AL mats (circularity 67±12% versus 33±20%, respectively, $p < 0.05$).

6.3.6 VSMCs: Bioactivity of Coatings on Scaffolds for the Media Layer

6.3.6.1 Kcoil Grafting and EGF Capture - Quantification by ELISA

For the media layer, EGF was additionally immobilized on a LP-CS coating. ELISA confirmed successful tethering of the EGF using the Kcoil-Ecoil system, the optical density on CS+Kcoil+EEGF being much greater than on other surfaces (9, 12 and 18-fold higher compared with simple CS, simple Kcoil and CS incubated with Ecoil EGF in absence of Kcoil, respectively, $p < 0.05$) (**Figure E3**, Supplemental data). This confirmed the specificity of the E/K coiled-coil interaction, as well as its suitability to capture EGF on CS.

6.3.6.2 VSMC Adhesion and Growth

Metabolic activity of VSMCs after 1 and 7 days on bare and coated mats is illustrated in **Figure 6.7**. At day 7, the number of cells was quite small on pristine ePET (see "AM"), but significantly greater on the bioactive coatings, increasing in the order: LP, LP+CS and LP+CS+EEGF ($p<0.05$).

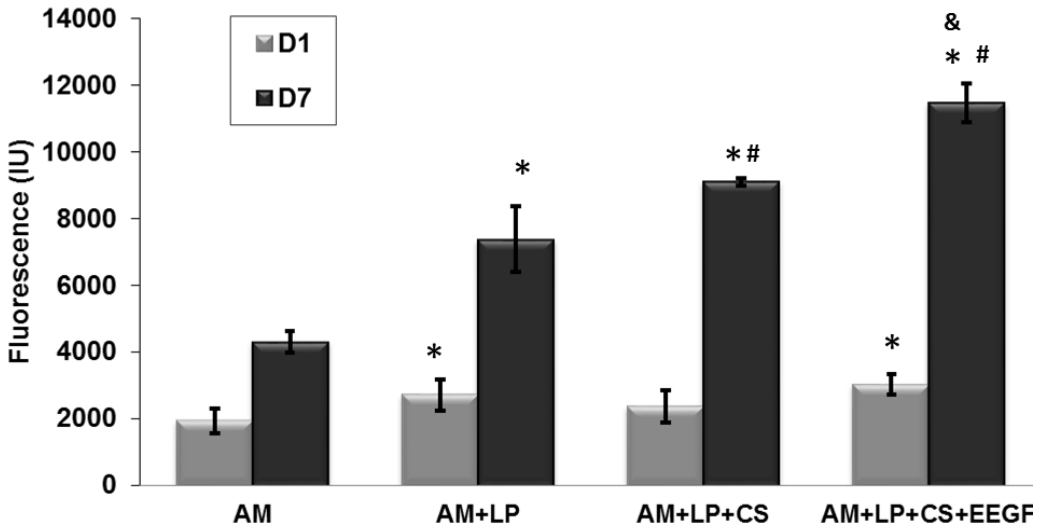

Figure 6.7 Adhesion after 24 h (D1) and growth after 7 days (D7) of VSMCs on bare and coated substrates [AM: bare aligned mats; (n=8 for each)].

*, #, & $p < 0.05$ with reference to bare, LP, and LP+CS-coated surfaces, respectively.

Histological examination (**Figure 6.8**) confirmed cell infiltration into the bulk of aligned ePET (AM) mats, presumably thanks to their larger pore size, albeit to a limited extent since most cells were encountered on top. Greater penetration might occur by increasing pore size even more or by using dynamic cell seeding.

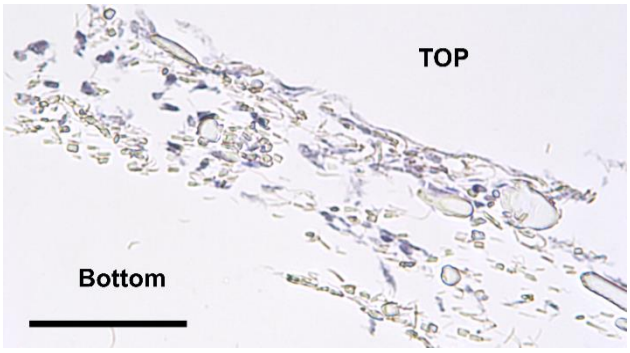

Figure 6.8 Histological section of an LP-coated AM mat, demonstrating cell infiltration (day 21; H&E staining, scale bar: 100 µm).

6.3.6.3 VSMC Survival in Serum-Free Medium

Figure 6.9 presents VSMC survival after 1, 3 and 5 days in serum-free medium on bare and coated mats, assessed by the AlamarBlue assay. A very strong decrease in cell number is observed after 5 days on bare and LP surfaces (only ~ 5% survival), indicating that LP did not improve cell survival, even though it increased their initial adhesion. VSMC survival increased on LP+CS (39% of initial cell count after 5 days; $p<0.05$ compared to bare and LP), and was still further improved by EGF, 49% and 55% of the cells remaining with soluble and immobilized EGF, respectively ($p<0.05$ compared to LP+CS; without significant difference between immobilized and EGF in solution). This indicated that EGF triggered cell survival mechanisms and that oriented immobilization is at least as efficient as EGF in solution, even though the latter was renewed every 2 days.

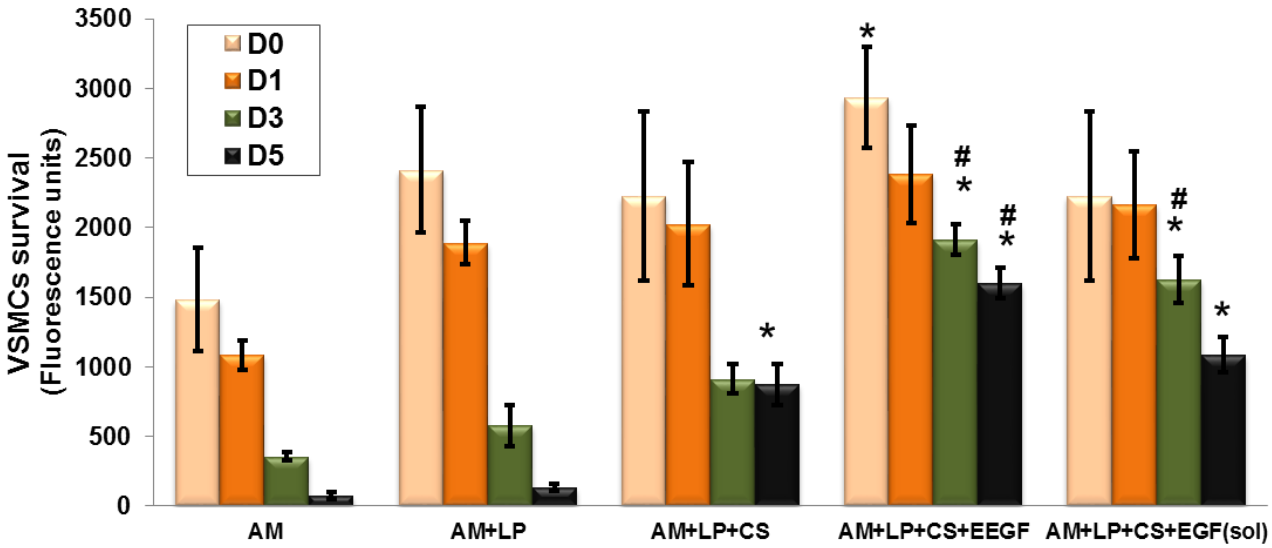

Figure 6.9 VSMC survival on bare and coated aligned (AM) substrates (LP+CS+EEGF: EGF immobilized on LP+CS-coated mats; AM+LP+CS+EGF(sol); LP+CS-coated mats with soluble EGF added in medium) (mean + SD; n=6). Except LP at D3 and D5, all coatings were significantly better than bare mats at each time point ($p<0.05$, not indicated on the graph)

* $p<0.05$ compared to LP; $^{\#}$ $p<0.05$ compared to LP+CS

6.3.7 Combining Bioactive Coatings and Electrospun Mats: A Promising Approach for VG

In this research, we fabricated random and aligned bioactive electrospun PET mats as scaffolds for the luminal and media layers of small-diameter synthetic vascular grafts. Electrospinning enabled us to mimic the ECM morphology, and to control porosity, favouring either monolayer formation (HUVEC) or cell penetration into the bulk (VSMC). We have in addition investigated the effect of fiber alignment, since there is still controversy in the literature regarding the effect of nano-fiber alignment on cell spreading and –proliferation, some studies reporting increased HUVEC growth on aligned mats [14, 99] while others show better results with random scaffolds [100]. In the present work, nanofiber alignment was found to have slightly influenced HUVEC alignment and elongation, with minor impact (not significant) on cell retention under flow. The effect of the bioactive coating clearly dominated over the mat topography: Indeed, LP and LP+CS coatings greatly affected cell adhesion, growth and retention on both RL and AL

scaffolds. We showed that HUVEC adhesion, growth, and retention under flow-induced shear stress were increased by LP coating on ePET mats and smooth PET films [10, 246], but that cell retention was not complete. The present results demonstrated that grafting CS further enhanced HUVEC adhesion, growth and, most important, their resistance to detachment. The fact that CS promotes low platelet adhesion, despite its high propensity for HUVEC adhesion [13] is a clear advantage. Such a non-thrombogenic under-layer could help prevent thrombotic events, should the endothelium lining be incomplete or partially detach under shear-flow. In contrast, other coatings such as simple LP, fibronectin or collagen proposed in the literature are thrombogenic [41]. Thanks to its low thrombogenicity, the potential of our coating to capture *in situ* endothelial progenitor cells (EPC) to form a complete monolayer on the lumen could also be studied, because it offers a promising alternative to *in vitro* pre-seeding of cells [41].

The LP+CS coating was also found to be an excellent coating for the medial layer of vascular grafts of tissue constructs. In addition, the oriented immobilization of EGF enabled strong increase in VSMC survival in serum-free media, mimicking the lack of nutrients on the abluminal side of the graft. Immobilization of biomolecules has demonstrated great promise by their resulting durability and stability, which in turn leads to enhanced and continuous cell response [175, 187].

An additional advantage of these coatings is their versatility, since they can be created on any electrospun material thanks to the plasma polymerization process, in contrast to chemical modifications that require optimization as a function of substrate chemistry. In this project, electrospun PET was used for practical and regulatory reasons. However their mechanical properties may not be ideal in regard to compliance. Our previous studies [10, 11] have shown that the Young's moduli of ePET mats, random and aligned, were respectively about 20 MPa and 100 MPa, well above those of natural arteries. Compliance being indirectly related to Young’s modulus, we would expect that of the present electrospun mats to be low. We already proposed to resolve this particular issue by chemical means [133] (hydrolysis with concentrated NaOH), or by plasma etching [11], if required. But other electrospun materials such as PU or PU/PCL mixture may be used instead [337].

6.4 Conclusions

In this project, the combination of electrospinning, plasma polymerization and CS grafting was found to promote the formation of a stable endothelial layer. CS is particularly interesting because it is stable, biocompatible and it prevents platelet adhesion, a key issue to avoid blood clot formation in case of an incomplete EC monolayer or partial cell detachment. Moreover, the versatility of these technologies enables one to adapt them to other polymeric biomaterials, in order to optimize compliance and biodegradation rate, depending on the application. While further work is needed to combine the luminal and medial layers, and to optimize the material for compliance, the present results suggest that the combination of electrospinning and bioactive coatings can provide adequate scaffolds for small-diameter vascular prostheses.

6.5 Supporting Information

Cumultive data for endothelial cell orientation on aligned (AL) mats (**Table E1)**, Typical 2D FFT alignment plot of aligned mats (**Figure E1)**, Histogram of endothelial cell orientation on aligned (AL) mats (**Figure E2)**, Apparent surface densities (absorbance) of oriented tethered EGF, measured by direct ELISA; $p < 0.05$ compared to all other surfaces (n=3) (**Figure E3)**.

Acknowledgments

This research was supported by grants from the Natural Sciences and Engineering Research Council of Canada (NSERC) and the Canadian Institutes of Health Research (CIHR) (CPG 127764). H.S. gratefully acknowledges the Merit Scholarship from the *Fonds de recherche du Québec-Nature et technologies* (FQRNT) and an award from the Jane and Frank Warchol Fund of the Society of Vacuum Coaters (SVC) Foundation. The authors also thank C. Cerclé, Dr. J. Lefebvre, Y. Leblanc (École Polytechnique), Micheline Fortin (IRIC-Histology) and the CR CHUM Microscopy Platform for skilled technical support and help during some of the experiments.

Supporting Information

I. Supplementary Table

Table E1: Cumultive data for endothelial cell orientation on aligned (AL) mats

Fiber angle	*Frequency*	*Cumulative %*
0	0	0.00%
10	38	37%
20	32	67%
30	15	82%
40	11	92%
50	4	96%
60	1	97%
70	1	98%
80	2	100%
90	0	100%
More	0	100%

II. Supplementary Figures

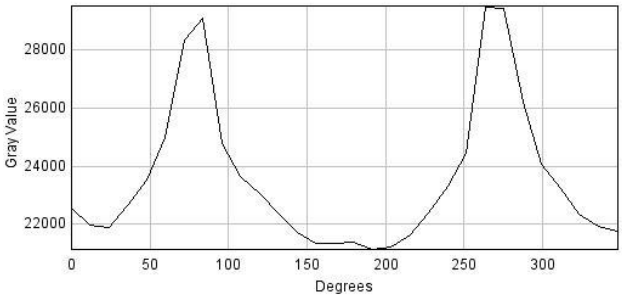

Figure E1: Typical 2D FFT alignment plot of aligned mats.

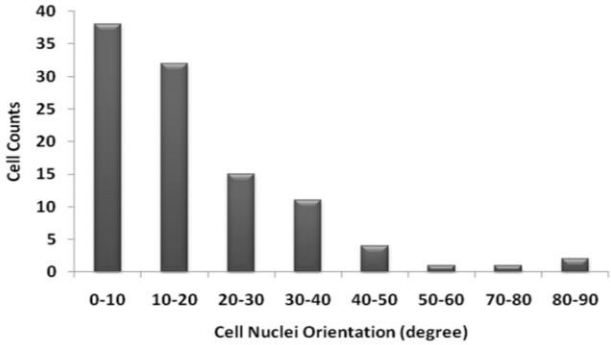

Figure E2: Histogram of endothelial cell orientation on aligned (AL) mats.

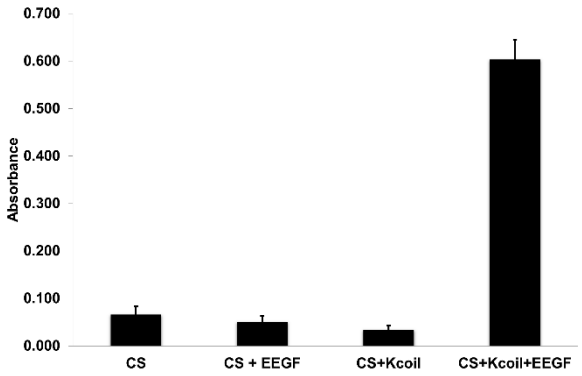

Figure E3: Apparent surface densities (absorbance) of oriented tethered EGF, measured by direct ELISA; $p < 0.05$ compared to all other surfaces (n=3).

CHAPTER 7 GENERAL DISCUSSION AND RECOMMENDATIONS FOR FUTURE RESEARCH

In this Ph.D. thesis, we proposed to develop vascular prostheses combining 3D electrospun nanofiber matrices and bioactive coatings prepared by plasma-polymerization in order to tackle the limitations of present day SDVGs, namely graft occlusion due to the lack of compliance and thrombogenicity. We have chosen to use PET since it possesses stability, biocompatibility, and low cost, but foremost due to the fact that PET VGs have already been FDA-approved and clinically used for a few decades. Moreover, literature data suggest that the best anti-thrombogenic surface is a complete and stable endothelium which inhibits coagulation, suppresses platelet aggregation, and stimulates fibrinolysis [338]. Therefore, our approach was to create a lumen surface which promotes such endothelium lining by using *in vitro* pre-seeding techniques, or eventually *in situ* endothelialization.

This research has been divided into four different steps: (1) combine (i) electrospun nano-fiber mats (random and aligned) with (ii) bioactive coatings to generate novel types of scaffolds for VG applications; (2) optimize them so as to match mechanical and bio-performances of natural blood vessels; (3) evaluate them in terms of EC adhesion, growth, and resistance to flow-induced shear for the luminal layer; (4) evaluate them in regard to VSMC adhesion, growth, survival, and infiltration of the media layer.

7.1 Electrospun Nanofiber Scaffolds and Plasma Polymerization for VG applications

For the luminal layer of SDVGs, as explained in detail in **Chapter 4**, we have first combined two techniques, namely electrospinning and low-pressure plasma polymerization (L-PPE:N / LP coating), to come up with a solution to promote the *in vitro* endothelialization and to improve mechanical properties for SDVGs. Therefore, ***our first hypothesis was that electrospinning of PET can create nanofibrous structures that are more compliant and favor the formation of a EC monolayer compared to conventional woven PET or ePTFE structures***.

Random ePET mats with small pore size were shown indeed to present a nanostructure that prevents EC infiltration and promotes the formation of an EC monolayer. This is a more effective structure compared with currently used ePTFE and woven Dacron (PET) grafts, where cells infiltrate and do not readily form a complete EC monolayer [10]. Our observation by the z-stack confocal images confirms a monolayer of ECs on our scaffolds. Neighboring cells interacted with each other as well as with the underlying scaffold in a coherent manner, confirmed by the expression of specific proteins including VE-cadherin and vinculin.

In terms of mechanical properties, the Young's moduli of ePET mats, bare or plasma-coated, were about 20 ± 6 MPa and 34 ± 7 MPa [10], respectively, therefore above those of natural arteries (human coronary artery: 1.5 MPa [339], human femoral artery: 9-12 MPa [255]) **(Chapter 4)**. The tensile strength is similar to published values for various arteries and veins. Elongation at break was found to be greater than that of arteries in all cases, but not believed to be problematic. [10].

In paper 2 **(Chapter 5)**, Young's modulus was found to be even higher when fabricating ePET with aligned fibers for the media layer of VG, namely more than 100 MPa. As compliance is inversely proportional to Young's modulus, we can expect that the compliance of those electrospun mats will be too low.

In a very recent study by our team [340], a linear analytical model was used to calculate the ratios between the elastic modulus and the ultimate strength of an isotropic electrospun mat required to achieve both the compliance of the native vessel and the burst pressure of a monolayer VG. The results suggest that ePET structures do not meet the mechanical requirements (target ratio: 1.4 compared with 10 and 40 for random and aligned mats) to be used in the fabrication of a VG.

These characteristics can be adjusted by chemical means, or by plasma etching, if required. For example, wet-chemical treatment (e.g., hydrolysis with concentrated NaOH, among others) has so far been the only method proposed in the literature for tuning the mechanical properties of electrospun structures [133], but it generally entrains problems of toxicity, environmental impact and associated costs, among others [341]. Furthermore, macroscopic damage can result to fibers in contact with NaOH [342]. In paper 2 **(Chapter 5)**, we showed that, on the contrary, rapid, clean, highly reproducible and environmentally benign plasma etching would offer an attractive

alternative to fine-tune the mechanical and surface-chemical properties of ePET fibers [11]. This will be discussed further below.

Other electrospun materials could also be used, instead of ePET. One of the promising materials is electrospun polyurethane, which is already commercialized by Nicast Ltd. Electrospun nanofabric AVflo™ is a CE certified polyurethane vascular access graft, which is made of medical grade biocompatible polycarbonate urethane for hemodialysis patients, improving patient care and reducing hospitalization time. It possesses strength, flexibility, durability and excellent patency. It is hydrolytically and oxidatively stable and resistant to biodegradation [113, 343, 344].

The second hypothesis was that plasma coating can improve the biological properties (EC attachment and growth) of electrospun mats.

Therefore, ePET mats alone or combined with LP coating were tested for EC adhesion, growth and retention under flow (**Chapter 4**). EC adhesion and growth were shown to be increased by LP coating. This coating proved to be highly bioactive, reproducible, and sufficiently stable over time for different cell types including VSMCs, fibroblasts, and mesenchymal stem cells [163, 165, 189, 345]. This can be explained by positively-charged chemical functionalities, primary amine ($-NH_2$) groups, which quickly attract and bind negatively-charged proteins in culture media, leading to formation of integrin complexes. Our observation is in agreement with other similar studies which have investigated various plasma-polymerized thin film coatings (e.g. cyclopropylamine, 2-methyl-2-oxazoline, allylamine, ethylenediamine, acetylene-ammonia, etc) for biomedical applications [346-350]. For example, in a recent study [351], plasma deposited 2-methyl-2-oxazoline based coatings were shown to reduce biofilm formation and inflammatory response, but at the same time promote the cellular growth.

The HUVEC resistance to flow-induced shear on LP coating was found to be superior to that of the bare mats ($70 \pm 4\%$ and $30 \pm 10\%$ of the cells remaining on coated and bare mats, respectively ($p < 0.05$)) (**Chapter 4**). Substantial cellular detachment still occurs under flow conditions that resemble the physiological ones. Our observation is in agreement with other studies addressing EC adhesion and retention on various bioactive coated surfaces under physiological shear stress. For example, pre-coated vascular prostheses with cell-adhesive substrates (e.g. gelatin, fibronectin, collagen, laminin, fibrin, fibronectin/fibrin, etc.) showed increased cell attachment

under shear stress [253, 352-355]. Among others, despite different cell seeding densities, our flow-dependent retention results were comparable to those of EC on commercial PET/collagen (78 % after 40 min and 61 % after 120 min) [356]. Feugier et al. [354] also reported cell retention of 66 % and 49 % on type I/III collagen-coated and pristine surfaces, respectively. Moreover, in another study, cell retention on laminin coated surfaces dropped significantly to 55 % after 40 min of flow, and to 50 % after 120 min of flow, compared to static conditions [355].

Although LP coating is a promising functional bioactive coating for VG application, the feasibility of depositing this coating on the lumen of tubular grafts needs to be investigated. Utilizing a plasma jet inside the graft seems to be a plausible solution [357-359], whereby tubular VGs are internally LP-coated using a gas mixture passing through the tube. The deposition is activated by a plasma created within the tube by high-frequency electric energy applied to the precursor gas by means of the plasma jet that could have different configurations (e.g. pen- or needle-like, perforated coil-like, or other).

The originality of this part of the current Ph.D. research is to highlight the feasibility of employing LP coating on electrospun nanofiber mats and to demonstrate its ability to enhance EC adhesion, growth, and resistance to shear. The LP coating is applicable to a wide variety of tissue engineered biomaterials used for vascular applications. This study is the first of its kind to investigate the combination of plasma polymerization and electrospinning process for vascular graft applications. The results of this part of the work were published in Macromolecular Bioscience 2014, 14, 1084–1095 [10]. This was featured by the Editor-in-Chief of the Macromolecular Journals on MaterialsViews on August 13, 2014 under the following title "Overcoming Clinical Complications of Vascular Prostheses". It was also honored with several prestigious awards including the "Étudiants-Chercheurs Étoiles" Award of the "Fonds de Recherche du Québec-Nature et Technologies", in March 2015, as a promising contribution to scientific literature in this field.

7.2 CS Grafting on Plasma-Polymerized Electrospun Mats for Stable Endothelialization

Although LP coating was shown to be a promising one to promote HUVEC adhesion, growth and resistance to shear stress, cell retention is still limited. Moreover, this underlying LP chemistry is thrombogenic and increases the risk of terminal IH through the recruitment of platelets [13].

Bioactive coatings have been developed to inhibit the coagulation cascade, to prevent platelet adhesion and activation, and to promote desirable cell interactions for VG applications[360].

The development of biomaterials with anticoagulant properties has been actively studied in the past. The ECM polysaccharides called glycosaminoglycans (GAGs) have been investigated as potential solutions for VG applications. GAG-based bioactive coatings hold promise for this application due to their growth-inhibitory effects on VSMCs and their anticoagulant activity [361-364]. Among other GAGs, heparin, the most common anticoagulant used clinically, has been used in the fabrication of medical devices. Incorporated heparin, on the surface of grafts through different approaches, is still known as a gold-standard for the bio-functionalization of VGs [365]. Heparin-modified surfaces have shown promising anti-thrombogenic properties including reduced activation of coagulation, and inhibited adhesion of plasma platelets and proteins in the coagulation cascades [55, 365-368].

Immobilization of heparin has been performed through ionic bonding, physical adsorption, bulk material incorporation, and covalent linkage. For example, heparin derivative was used to treat acellular collagen VGs derived from decellularized subintestinal mucosa. Thrombus formation on the heparin-treated grafts after three months was significantly diminished when implanted as rabbit carotid artery interposition grafts [369]. ePTFE VGs with heparin coating improved one-month patency in a rat bypass model [370], while heparin coating on PU grafts also improved the patency of VGs [371].

Despite many attempts to utilize heparin, its decreased bioactivity after the immobilization process is a key issue. This may be due to chemical modification of the heparin, or to physical inaccessibility of its binding site [365, 372]. The use of a hydrophilic spacer such as poly(ethylene glycol) (PEG) has been shown to improve maintaining the biological activity of

heparin by reducing steric hindrance [373, 374]. PEG, itself, can also prevent protein adsorption and platelet adhesion to material surfaces [216].

Additionally, heparin has the ability to bind different biomolecules such as growth factors and ECM proteins [375]. However, heparinized devices can trigger neointima formation due to inflammatory responses.

Now, *chondroitin sulfate* (CS)-containing coatings were already shown to possess anti-apoptotic properties for vascular cells, to prevent nonspecific EGF adsorption, promote hemocompatibility and prevents platelet adhesion (low-fouling and low-thrombogenic), while promoting HUVEC and VSMC adhesion and growth [13, 184, 185]. ***Therefore, our third hypothesis was that CS can further improve the endothelialization and EC resistance to shear stress.***

Therefore, we grafted CS on LP coating deposited on the random and aligned nanofiber substrates so as to tackle the thrombogenic properties of LP in case of partial EC detachment **(Chapter 6)**. We observed that grafting CS on LP-coated electrospun mats can enhance HUVEC adhesion, growth and their resistance to detachment, compared to LP-coated and bare mats ($82 \pm 2\%$ and $76 \pm 1\%$ of the cells remaining on CS-coated and LP mats, respectively ($p < 0.05$)). This is a promising finding since the *in vitro* pre-endothelialization of VGs by ECs prior to implantation has been an alternative to increase the patency rate of the VGs [27, 320], but is known to be limited by poor cell adhesion and retention under shear flow [354]. Our observation is in agreement with other studies using ECM proteins and peptides to reduce the detachment of ECs. For example, RGD peptidomimetics (ligands of the $\alpha_v\beta_3$ integrin) grafted PET showed significant increase in cell retention under shear stress [376].

Several other studies have also explored the use of GAGs such as CS as low platelet adhesion layers to prevent platelet adhesion. For example, CS and hyaluronic acid (HA) were used for the lumen of VGs [176]. HA grafted to PU was shown to diminish protein adsorption and platelet adhesion compared to PEG- or heparin-grafted surfaces. Interestingly, a confluent monolayer of ECs was also formed on HA-grafted surfaces [179]. Further *in vivo* studies are needed to verify their bioactivity and performance in more realistic conditions.

Moreover, EC alignment in the direction of blood flow in the natural arteries is known to increase the cells' capability to resist detachment under shear stress [102, 377]. This is typically achieved by a long and resource-consuming method involving *in vitro* fluid flow preconditioning in a

bioreactor prior to implantation [377]. But recent studies have shown an improvement in EC attachment by tuning the topography (e.g. orientation) of electrospun fibers [14, 333]. We also investigated the effect of fiber alignment on EC adhesion and growth in static culture, and resistance under dynamic shear conditions (**Chapter 6**). To stimulate EC alignment and its resistance to flow-induced shear by topographical cues, aligned scaffolds with small pore-size were compared with their random counterparts in regard to formation of an EC monolayer. We demonstrated that EC resistance to shear stress can be slightly improved if the cells can be oriented by tuning electrospun fiber alignment, but this improvement was not very significant.

From previous studies conducted by our team, it became clear that CS grafting effectively inhibited platelet attachment and -activation on flat surfaces. However, thrombosis is a more complex process: it is the accumulation of circulating platelets at an injury site, as well as the coagulation system that produces thrombin, and ultimately fibrin, to stabilize the clot. It would be necessary to confirm anti-thrombogenic properties of CS on 3D ePET mats by *in vitro* and *in vivo* tests such as specific coagulation cascade measurements, platelet and leukocyte concentration measurements, and thromboelastography, to investigate its blood compatibility [378].

To further extend the investigation, the next logical step could be to examine the potential of CS coating combined with other selective biomolecules to capture endothelial progenitor cells (EPC), to form a complete monolayer on the lumen as a route to achieve anti-thrombogenicity. Generally, *in vitro* endothelialization is very time-consuming and costly. Therefore, *in situ* endothelialization has recently been extensively explored in attempts to find desirable, fast methods [40, 171]. *In vivo* circulating EPCs could potentially be captured onto a functionalized graft for *in situ* endothelialisation [379]. Unlike *in vitro* endothelialization, *in situ* endothelialization provides some advantages such as availably upon demand, simpler surgical procedures and healthy, functional endothelium formation *in vivo* [54, 171, 380]. However, beside its advantages, it necessitates a complex coating technology to capture and home EPCs. The main challenge of *in situ* endothelialisation is to find a more specific and selective EPC capture biomolecule. Once it is selected, the bioactive molecule can be immobilized on the biomaterial's surface via physical adsorption or chemical conjugation [54, 171]. Similar to *in vitro* endothelialization, non-selective cell-adhesive proteins or peptide motifs (collagen [381], fibronectin [192], gelatin [194], RGD peptides [193]) have been used to recruit EPCs from blood circulation. However, these bioactive coatings are not selective for ECs, so that other circulating

cells including platelets, leukocytes and SMCs can also be captured and homed on the lumen, leading to IH [194]. Therefore, those bioactive coatings are not desirable choices for enhancing *in situ* endothelialization. Several growth factors and biomolecules have been studied as promising candidates for promoting ECP cellular activities [195, 196]. To further accelerate the *in vitro* and *in situ* endothelialization process, growth factors (GFs) such as vascular endothelial growth factor (VEGF) and basic fibroblast growth factor (bFGF) can be immobilized as mitogenic factors [189, 197-199]. Other GFs such as stromal cell-derived factor-1α (SDF-1α) [192], brain-derived neurotrophic factors (BDNF) and nerve growth factor (NGF) [382] can also enhance EPC capture and differentiation, and promote endothelialization via paracrine effects. Selective cell-capturing biomolecules primarily include antibodies (e.g. Anti-CD34 antibodies (Ab) [210], Anti-VEGFR2 Ab [383], Anti-VE-cad Ab [384], Anti-CD133 Ab [367]) peptides (e.g. REDV [385], YIGSR [386], TPS [365], CRRETAWAC [387], etc.) and aptamers (i.e. short single-stranded oligonucleotides [388]). Despite a growing number of research efforts on *in situ* endothelialization and its importance in VG engineering, its clinical application is still limited due to the gap between research progress and clinical products. *In situ* endothelialization is therefore still relatively new and complex. The challenge is not only to capture and differentiate EPCs, but also to maintain the proper and durable function of an EC monolayer. An optimal strategy for future success of *in situ* endothelialization would be the combination of capturing biomolecules, growth factors and careful materials selection.

The originality of this part of the current Ph.D. research was to investigate the effects of topography and bioactive coatings on EC adhesion, growth and resistance to shear stress. The results of this part of the research were published in Biomacromolecules, 2017, 18 (1), pp 303–310 [12].

7.3 Combination of Electrospinning and Plasma-Etching for VG Applications

The media layer of native blood vessels contains VSMCs and circumferentially-aligned elastin and collagen fibers, which are essential for maintaining their mechanical strength and vasoactive responsiveness [389]. In addition to the VSMCs' circumferential alignment, their infiltration into

the bulk of the vascular scaffolds is another important factor for the regeneration of SDVGs. For this purpose, suitable pore size and highly interconnected porous structure of the scaffolds are vital [390]. The main obstacle has been excessively high mechanical properties in the circumferential direction of aligned mats (most particularly, their high Young's modulus). For this layer, we thus fine-tuned the processing parameters for electrospinning and plasma etching to improve the morphological, mechanical and biocompatibility properties of the final mats (**Chapter 5**).

Our fourth hypothesis was that combining electrospinning and plasma-etching can create aligned structures that are morphologically and biologically suitable for VSMC infiltration and better compliance.

To this aim, the effects of low- and high (atmospheric-) pressure plasma-etching on mechanical, morphological, chemical, and biocompatibility properties of aligned ePET mat scaffolds was thoroughly studied, specifically for VG applications. We found that our aligned ePET mats with large pore size enable VSMCs to induce partial cellular influx and adhesion to the mats. The final mats enabled the VSMCs to localize to the graft surface and partially migrate within the mats' thickness (as confirmed by histology in **Chapter 6**). While final aligned ePET mats designed for the media layer have demonstrated the ability to facilitate VSMC infiltration within the scaffold bulk, further improvements are still necessary to increase pore size. The latter is necessary to facilitate the infiltration of VSMCs, while also exchanging oxygen and nutrients. Currently, cell infiltration is localized in some sections of the scaffold, while other deeper areas have yet to be infiltrated. This was in agreement with other developments in TEVG of VGs, where robust cellular influx, proliferation, and remodeling ultimately form the medial SMC layer [108]. Therefore, to resolve these issues, we propose to directly combine living cells into fibers, and to generate "living scaffolds"; this will be a versatile new method of bio-fabrication: A revolutionary new technique, electrospinning of cells, could provide *'living fibers'* composed of live cells and a biopolymer, mixed with a variety of other biomolecules (including proteins, growth factors, among others). Many materials can be used to create such electrospun "*living fibers*", including collagen, alginates, chitosan, gelatins, and newly-synthesized materials that mimic certain features of natural ones, with the ability to signal to cells and allow them to infiltrate the finished fibers/scaffolds. This technique will also enable direct handling of a wide range of cells (including primary- and stem cells). The resulting *living fibre* can either be

randomly arranged, or directed to take specific orientations, e.g. for the media layer of a VG. It also has the capacity to handle a wide range of cells without causing genetic, genomic or physiological damage *in vitro* [391, 392].

Our results showed significant decreases in Young's modulus following LP-, HP-, and asher-induced plasma etching (**Chapter 5**). Among the three etch techniques, the plasma asher (with pure oxygen for 5 min) seems to be most advantageous in terms of rapidity, minimal apparent damage to fiber surfaces, along with efficacy in changing mechanical properties (reduction in Young's modulus from 100 MPa to less than 20 MPa). These changes could be related to the reduction in fiber diameters and to nano/ micro-pit surface defects observed after extended LP and HP plasma treatments. Chain scissions, accompanied by molecular weight reduction, were observed with all three etching techniques, according to intrinsic viscosity measurements. On the other hand, elongation at break was found to be less than that of native arteries in all cases. However, even though uni-axial tensile testing allows one to assess elastic properties of the fabricated scaffolds, it does not provide a direct measure of compliance (a multi-axial property). Therefore, further tests are desirable, particularly ones designed to evaluate compliance and fatigue resistance of tubular multilayered graft prototypes. A significant increase in concentration of O-bearing functional groups was also observed. Therefore, plasma etching can offer good control for tuning mechanical, morphological and surface-chemical properties of electrospun fibrous mats. Although this technique is promising, the major limitation of the approach is the multi-steps required for fabrication of a VG prior to implantation.

The originality of this part of this Ph.D. thesis was, for the first time, to investigate the combination of electrospinning and an appropriate plasma-etching technique on (3D) scaffold for the media layer of SDVGs. This enables one to achieve finely-controlled structural, mechanical and surface properties that are required for VG applications. The results of this part were published in Plasma Processes and Polymers 2015, 12, 314–327 [11]. This research was featured on MaterialsViews on December 1, 2014 under the following title "Plasma etching for better vascular grafts".

7.4 CS and Oriented Tethered EGF for Medial Layer of VGs

Oriented immobilization of EGF on CS had been previously developed by our team [185]. We found that: i) this combination was anti-apoptotic for VSMCs, ii) these biomolecules could be immobilized on amine-rich plasma coated PET films; and iii) the coatings improved the survival of rat and human VSMCs in serum-free medium.

Our fifth hypothesis was that oriented immobilization of EGF on CS on 3D aligned electrospun mats can improve VSMC infiltration inside the structures and increase their survival in serum-free medium.

In line with previous research in our team, for the first time, we transferred these novel bioactive coatings (LP + CS + oriented tethered EEGF) on 3D aligned ePET mats with large pore size, so as to increase adhesion, growth, survival and infiltration of VSMCs (**Chapter 6**). Our findings showed that CS+EEGF coatings led to dramatically increased VSMC-growth and -survival in serum-free medium.

This step enabled us to demonstrate that this bioactive coating was transferable to any type of substrate, including 3D ePET which is extremely porous and chemically inert, without having to modify the previously-developed protocol. This work also highlights the versatility of this approach to generate bioactive surfaces through the appropriate selection of bioactive moieties for VG applications.

The originality of this part of this Ph.D. thesis was to transfer innovative bioactive coatings (LP+CS+ oriented tethered EEGF) on 3D aligned ePET mats for media layer of VGs. The results of this part of the work were published in Biomacromolecules, 2017, 18 (1), pp 303–310 [12].

While the results of this part of the project are promising, they also demonstrate important areas where further research is required. To further mimic the dynamic physiological conditions, it is essential to fabricate composite electrospun tubular grafts and evaluate them in a bioreactor, instead of static cell culture conditions. Furthermore, to appropriately challenge these bioactive coated grafts and to assess their efficacy (e.g. endothelialization, anti-clotting, compliance and thrombin generation properties under flow condition), our optimised candidate tubular design

should be directly compared in a large animal model, to both an unmodified tube control and the current bioactive-coated structure.

Although determining the ideal cell culture medium, cell density, and cell lines proved to be challenging tasks, further studies would be necessary to investigate the co-culture of ECs and SMCs.

It would also be necessary to use our bioactive coated scaffolds as cell-free VGs to evaluate *in situ* endothelialisation, by taking advantage of host self-remodeling ability: it possesses more remarkable advantages including avoidance of donor site morbidity, absence of extensive *in vitro* cell culture, easy storage and transport, ready availability, and potentially closer clinical adoption.

Therefore, further long-term *in vivo* investigations need to be done to study the efficacy of the electrospun materials and their porosities, the use of bioactive coatings to inhibit thrombosis and to promote endothelialization. Such studies will help elucidate the true potential of electrospun VGs and enable this proposed VG engineering technology to reach clinical investigation.

CONCLUSION

In conclusion, this study has demonstrated the possible combination of electrospinning, plasma polymerization, plasma etching, and grafting of biomolecules (CS, and EEGF) for engineering VGs that can provide an adequate scaffold for the luminal and media layers of SDVGs. It enables one to achieve the finely-controlled structural, mechanical, and surface properties that are required for VG applications. The improvements proposed in this thesis will create great innovative advances to help overcome the gaps in current VG technologies, inadequate substitutes for the most common occlusion-prone blood vessels (i.e. small-diameter vessels) in the human body. The proposed research not only addresses urgent health problems in the world's aging population, but also helps develop technology for one of the most highly demanding medical device markets. The efficacy of cell attachment to VGs is currently limited by poor resistance to high shear-stress under blood flow, and by compliance mismatch of SDVGs. So far, only the patients' own veins or arteries have been suitable choices for graft material, but these are only effective for 5-10 years and typically have limited success rates. Therefore, synthetic SDVGs remain the best alternative for vascular surgery. Optimization and testing in animal models will benefit transfer to industry and clinics, hence also the economy.

BIBLIOGRAPHY

[1] D. Mozaffarian, E. J. Benjamin, A. S. Go, D. K. Arnett, M. J. Blaha, M. Cushman, *et al.*, "Executive summary: Heart disease and stroke statistics-2016 update: A report from the american heart association," *Circulation,* vol. 133, pp. 447-457, 2016.

[2] R. L. Sacco, "The new american heart association 2020 goal: Achieving ideal cardiovascular health," *Journal of Cardiovascular Medicine,* vol. 12, pp. 255-257, 2011.

[3] A. H. Huang and L. E. Niklason, "Engineering of arteries in vitro," *Cellular and Molecular Life Sciences,* vol. 71, pp. 2103-2118, 2014.

[4] C. Singh, C. S. Wong, and X. Wang, "Medical textiles as vascular implants and their success to mimic natural arteries," *Journal of Functional Biomaterials,* vol. 6, pp. 500-525, 2015.

[5] H. Tian, Z. Tang, X. Zhuang, X. Chen, and X. Jing, "Biodegradable synthetic polymers: Preparation, functionalization and biomedical application," *Progress in Polymer Science,* vol. 37, pp. 237-280, 2012.

[6] J. M. Goddard and J. Hotchkiss, "Polymer surface modification for the attachment of bioactive compounds," *Progress in Polymer Science,* vol. 32, pp. 698-725, 2007.

[7] K. S. Siow, L. Britcher, S. Kumar, and H. J. Griesser, "Plasma methods for the generation of chemically reactive surfaces for biomolecule immobilization and cell colonization-a review," *Plasma Processes and Polymers,* vol. 3, pp. 392-418, 2006.

[8] T. Zhou, Y. Zhu, X. Li, X. Liu, K. W. Yeung, S. Wu, *et al.*, "Surface functionalization of biomaterials by radical polymerization," *Progress in Materials Science,* vol. 83, pp. 191-235, 2016.

[9] F. Intranuovo, R. Gristina, L. Fracassi, L. Lacitignola, A. Crovace, and P. Favia, "Plasma processing of scaffolds for tissue engineering and regenerative medicine," *Plasma Chemistry and Plasma Processing,* vol. 36, pp. 269-280, 2016.

[10] H. Savoji, A. Hadjizadeh, M. Maire, A. Ajji, M. R. Wertheimer, and S. Lerouge, "Electrospun nanofiber scaffolds and plasma polymerization: A promising combination towards complete, stable endothelial lining for vascular grafts," *Macromolecular Bioscience,* vol. 14, pp. 1084-1095, 2014.

[11] H. Savoji, S. Lerouge, A. Ajji, and M. R. Wertheimer, "Plasma-etching for controlled modification of structural and mechanical properties of electrospun PET scaffolds," *Plasma Processes and Polymers,* vol. 12, pp. 314-327, 2015.

[12] H. Savoji, M. Maire, P. Lequoy, B. Liberelle, G. De Crescenzo, A. Ajji, *et al.*, "Combining electrospun fiber mats and bioactive coatings for vascular graft prostheses," *Biomacromolecules,* vol. 18, pp. 303-310, 2017.

[13] P. K. Thalla, H. Fadlallah, B. Liberelle, P. Lequoy, G. De Crescenzo, Y. Merhi, *et al.*, "Chondroitin sulfate coatings display low platelet but high endothelial cell adhesive properties favorable for vascular implants," *Biomacromolecules,* vol. 15, pp. 2512-2520, 2014.

[14] B. M. Whited and M. N. Rylander, "The influence of electrospun scaffold topography on endothelial cell morphology, alignment, and adhesion in response to fluid flow," *Biotechnology and Bioengineering,* vol. 111, pp. 184-195, 2014.

[15] X. Dai, S. Wiernek, J. P. Evans, and M. S. Runge, "Genetics of coronary artery disease and myocardial infarction," *World Journal of Cardiology,* vol. 8, p. 1, 2016.

[16] G. K. Hansson, "Inflammation, atherosclerosis, and coronary artery disease," *New England Journal of Medicine,* vol. 352, pp. 1685-1695, 2005.
[17] K. Yahagi, F. D. Kolodgie, F. Otsuka, A. V. Finn, H. R. Davis, M. Joner, *et al.*, "Pathophysiology of native coronary, vein graft, and in-stent atherosclerosis," *Nature Reviews Cardiology,* vol. 13, pp. 79-98, 2016.
[18] C. Stettler, S. Wandel, S. Allemann, A. Kastrati, M. C. Morice, A. Schömig, *et al.*, "Outcomes associated with drug-eluting and bare-metal stents: A collaborative network meta-analysis," *The Lancet,* vol. 370, pp. 937-948, 2007.
[19] G. Lanzino, A. A. Rabinstein, and R. D. Brown, "Treatment of carotid artery stenosis: Medical therapy, surgery, or stenting?," in *Mayo Clinic Proceedings*, 2009, pp. 362-368.
[20] P. W. Serruys , F. Unger , J. E. Sousa , A. Jatene , H. J. R. M. Bonnier , J. P. A. M. Schönberger , *et al.*, "Comparison of coronary-artery bypass surgery and stenting for the treatment of multivessel disease," *New England Journal of Medicine,* vol. 344, pp. 1117-1124, 2001.
[21] S. Itagaki, P. Cavallaro, D. H. Adams, and J. Chikwe, "Bilateral internal mammary artery grafts, mortality and morbidity: An analysis of 1 526 360 coronary bypass operations," *Heart,* vol. 99, pp. 849-853, 2013.
[22] S. Goldman, K. Zadina, T. Moritz, T. Ovitt, G. Sethi, J. G. Copeland, *et al.*, "Long-term patency of saphenous vein and left internal mammary artery grafts after coronary artery bypass surgery: Results from a department of veterans affairs cooperative study," *Journal of the American College of Cardiology,* vol. 44, pp. 2149-2156, 2004.
[23] M. Slevin and E. Bontas, "Arterial graft failure," in *Coronary Graft Failure*, ed: Springer, 2016, pp. 235-265.
[24] R. E. Harskamp, R. D. Lopes, C. E. Baisden, R. J. de Winter, and J. H. Alexander, "Saphenous vein graft failure after coronary artery bypass surgery: Pathophysiology, management, and future directions," *Annals of Surgery,* vol. 257, pp. 824-833, 2013.
[25] Y. Moshkovitz and E. Raanani, "The art of saphenous vein grafting and patency maintenance," *The Journal of Thoracic and Cardiovascular Surgery,* vol. 151, pp. 300-302, 2016.
[26] W. S. Weintraub, M. V. Grau-Sepulveda, J. M. Weiss, S. M. O'Brien, E. D. Peterson, P. Kolm, *et al.*, "Comparative effectiveness of revascularization strategies," *New England Journal of Medicine,* vol. 366, pp. 1467-1476, 2012.
[27] D. G. Seifu, A. Purnama, K. Mequanint, and D. Mantovani, "Small-diameter vascular tissue engineering," *Nature Reviews Cardiology,* vol. 10, pp. 410-421, 2013.
[28] G. W. Hastings, *Cardiovascular Biomaterials*, 2nd ed.: Springer Science & Business Media, 2012.
[29] S. Sarkar, H. J. Salacinski, G. Hamilton, and A. M. Seifalian, "The mechanical properties of infrainguinal vascular bypass grafts: Their role in influencing patency," *European Journal of Vascular and Endovascular Surgery,* vol. 31, pp. 627-636, 2006.
[30] J. Buján, N. García-Honduvilla, and J. M. Bellón, "Engineering conduits to resemble natural vascular tissue," *Biotechnology and Applied Biochemistry,* vol. 39, pp. 17-27, 2004.
[31] S. G. Friedman, R. S. Lazzaro, L. N. Spier, C. Moccio, and A. J. Tortolani, "A prospective randomized comparison of dacron and polytetrafluoroethylene aortic bifurcation grafts," *Surgery,* vol. 117, pp. 7-17, 1995.

[32] M. R. Jackson, A. T. Ali, C. Bell, J. G. Modrall, M. B. Welborn Iii, E. Scoggins, *et al.*, "Aortofemoral bypass in young patients with premature atherosclerosis: Is superficial femoral vein superior to Dacron?," *Journal of Vascular Surgery,* vol. 40, pp. 17-23, 2004.

[33] V. Catto, S. Farè, G. Freddi, and M. C. Tanzi, "Vascular tissue engineering: Recent advances in small diameter blood vessel regeneration," *ISRN Vascular Medicine,* vol. 2014, 2014.

[34] S. Greenwald and C. Berry, "Improving vascular grafts: The importance of mechanical and haemodynamic properties," *Journal of Pathology,* vol. 190, pp. 292-299, 2000.

[35] F. Hehrlein, M. Schlepper, F. Loskot, H. Scheld, P. Walter, and J. Mulch, "The use of expanded polytetrafluoroethylene (PTFE) grafts for myocardial revascularization," *The Journal of Cardiovascular Surgery,* vol. 25, pp. 549-553, 1983.

[36] Y. Naito, T. Shinoka, D. Duncan, N. Hibino, D. Solomon, M. Cleary, *et al.*, "Vascular tissue engineering: Towards the next generation vascular grafts," *Advanced Drug Delivery Reviews,* vol. 63, pp. 312-323, 2011.

[37] M. Pate, V. Damarla, D. S. Chi, S. Negi, and G. Krishnaswamy, "Chapter 5 - endothelial cell biology: Role in the inflammatory response," in *Advances in Clinical Chemistry*. vol. 52, S. M. Gregory, Ed., ed: Elsevier, 2010, pp. 109-130.

[38] S. I. Fox, *Fundamentals of human physiology*: McGraw-Hill, 2009.

[39] T. Walles, H. Görler, C. Puschmann, and H. Mertsching, "Functional neointima characterization of vascular prostheses in human," *The Annals of Thoracic Surgery,* vol. 77, pp. 864-868, 2004.

[40] A. J. Melchiorri, N. Hibino, and J. P. Fisher, "Strategies and techniques to enhance the in situ endothelialization of small-diameter biodegradable polymeric vascular grafts," *Tissue Engineering Part B: Reviews,* vol. 19, pp. 292-307, 2013.

[41] S. Li and J. J. D. Henry, "Nonthrombogenic approaches to cardiovascular bioengineering," *Annual Review of Biomedical Engineering,* vol. 13, pp. 451-475, 2011.

[42] T. Liu, S. Liu, K. Zhang, J. Chen, and N. Huang, "Endothelialization of implanted cardiovascular biomaterial surfaces: The development from in vitro to in vivo," *Journal of Biomedical Materials Research Part A,* vol. 102, pp. 3754-3772, 2014.

[43] Alexander M. Seifalian, A. Tiwari, G. Hamilton, and Henryk J. Salacinski, "Improving the clinical patency of prosthetic vascular and coronary bypass grafts: The role of seeding and tissue engineering," *Artificial Organs,* vol. 26, pp. 307-320, 2002.

[44] M. Herring, A. Gardner, and J. Glover, "A single-staged technique for seeding vascular grafts with autogenous endothelium," *Surgery,* vol. 84, pp. 498-504, 1978.

[45] M. Deutsch, J. Meinhart, T. Fischlein, P. Preiss, and P. Zilla, "Clinical autologous in vitro endothelialization of infrainguinal ePTFE grafts in 100 patients: A 9-year experience," *Surgery,* vol. 126, pp. 847-855, 1999.

[46] R. F. Kempczinski, J. E. Rosenman, W. H. Pearce, L. R. Roedersheimer, Y. Berlatzky, and G. Ramalanjaona, "Endothelial cell seeding of a new PTFE vascular prosthesis," *Journal of Vascular Surgery,* vol. 2, pp. 424-429, 1985.

[47] F. Hess, S. Steeghs, R. Jerusalem, O. Reijnders, C. Jerusalem, B. Braun, *et al.*, "Patency and morphology of fibrous polyurethane vascular prostheses implanted in the femoral artery of dogs after seeding with subcultivated endothelial cells," *European Journal of Vascular Surgery,* vol. 7, pp. 402-408, 1993.

[48] H. R. Laube, J. Duwe, W. Rutsch, and W. Konertz, "Clinical experience with autologous endothelial cell–seeded polytetrafluoroethylene coronary artery bypass grafts," *The Journal of Thoracic and Cardiovascular Surgery,* vol. 120, pp. 134-141, 2000.

[49] M. Baguneid, D. Murray, H. J. Salacinski, B. Fuller, G. Hamilton, M. Walker, *et al.*, "Shear-stress preconditioning and tissue-engineering-based paradigms for generating arterial substitutes," *Biotechnology and Applied Biochemistry*, vol. 39, pp. 151-157, 2004.

[50] H. J. Salacinski, S. Goldner, A. Giudiceandrea, G. Hamilton, A. M. Seifalian, A. Edwards, *et al.*, "The mechanical behavior of vascular grafts: A review," *Journal of Biomaterials Applications*, vol. 15, pp. 241-278, 2001.

[51] J. Womersley, "Oscillatory flow in arteries. In: The reflection of the pulse wave at junctions and rigid inserts in the arterial system," *Physics in Medicine and Biology,* vol. 2, pp. 313-323, 1958.

[52] J. H. Wendorff, S. Agarwal, and A. Greiner, *Electrospinning: Materials, processing, and applications*: John Wiley & Sons, 2012.

[53] A. de Mel, B. G. Cousins, and A. M. Seifalian, "Surface modification of biomaterials: A quest for blood compatibility," *International Journal of Biomaterials*, vol. 2012, 2012.

[54] A. de Mel, G. Jell, M. M. Stevens, and A. M. Seifalian, "Biofunctionalization of biomaterials for accelerated in situ endothelialization: A review," *Biomacromolecules*, vol. 9, pp. 2969-2979, 2008.

[55] R. A. Hoshi, R. Van Lith, M. C. Jen, J. B. Allen, K. A. Lapidos, and G. Ameer, "The blood and vascular cell compatibility of heparin-modified ePTFE vascular grafts," *Biomaterials*, vol. 34, pp. 30-41, 2013.

[56] G. Delaittre, A. M. Greiner, T. Pauloehrl, M. Bastmeyer, and C. Barner-Kowollik, "Chemical approaches to synthetic polymer surface biofunctionalization for targeted cell adhesion using small binding motifs," *Soft Matter*, vol. 8, pp. 7323-7347, 2012.

[57] B. H. Walpoth, P. Zammaretti, M. Cikirikcioglu, E. Khabiri, M. K. Djebaili, J.-C. Pache, *et al.*, "Enhanced intimal thickening of expanded polytetrafluoroethylene grafts coated with fibrin or fibrin-releasing vascular endothelial growth factor in the pig carotid artery interposition model," *The Journal of Thoracic and Cardiovascular Surgery*, vol. 133, pp. 1163-1170, 2007.

[58] H. P. Greisler, D. J. Cziperle, D. U. Kim, J. D. Garfield, D. Petsikas, P. M. Murchan, *et al.*, "Enhanced endothelialization of expanded polytetrafluoroethylene grafts by fibroblast growth factor type 1 pretreatment," *Surgery*, vol. 112, pp. 244-54, 1992.

[59] A. Eberhart, Z. Zhang, R. Guidoin, G. Laroche, L. Guay, D. De La Faye, *et al.*, "A new generation of polyurethane vascular prostheses: Rara avis or ignis fatuus?," *Journal of Biomedical Materials Research*, vol. 48, pp. 546-558, 1999.

[60] Q. Chen, S. Liang, and G. A. Thouas, "Elastomeric biomaterials for tissue engineering," *Progress in Polymer Science*, vol. 38, pp. 584-671, 2013.

[61] G. Soldani, P. Losi, M. Bernabei, S. Burchielli, D. Chiappino, S. Kull, *et al.*, "Long term performance of small-diameter vascular grafts made of a poly (ether) urethane–polydimethylsiloxane semi-interpenetrating polymeric network," *Biomaterials*, vol. 31, pp. 2592-2605, 2010.

[62] X. Zhang, K. Battiston, J. McBane, L. Matheson, R. Labow, and J. P. Santerre, "Design of biodegradable polyurethanes and the interactions of the polymers and their degradation by-products within in vitro and in vivo environments," *Advances in Polyurethane Biomaterials*, p. 75, 2016.

[63] A. Piozzi, I. Francolini, L. Occhiaperti, M. Venditti, and W. Marconi, "Antimicrobial activity of polyurethanes coated with antibiotics: A new approach to the realization of medical devices exempt from microbial colonization," *International Journal of Pharmaceutics*, vol. 280, pp. 173-183, 2004.

[64] J. M. Rhodes and M. Simons, "The extracellular matrix and blood vessel formation: Not just a scaffold," *Journal of Cellular and Molecular Medicine*, vol. 11, pp. 176-205, 2007.
[65] B. M. Al Meslmani, G. F. Mahmoud, T. Leichtweiß, B. Strehlow, F. O. Sommer, M. D. Lohoff, *et al.*, "Covalent immobilization of lysozyme onto woven and knitted crimped polyethylene terephthalate grafts to minimize the adhesion of broad spectrum pathogens," *Materials Science and Engineering: C*, vol. 58, pp. 78-87, 2016.
[66] X. Wang, B. Ding, and B. Li, "Biomimetic electrospun nanofibrous structures for tissue engineering," *Materials Today*, vol. 16, pp. 229-241, 2013.
[67] S. Ramakrishna, K. Fujihara, W.-E. Teo, T.-C. Lim, and Z. Ma, *An introduction to electrospinning and nanofibers* vol. 90: World Scientific, 2005.
[68] N. Bhardwaj and S. C. Kundu, "Electrospinning: A fascinating fiber fabrication technique," *Biotechnology Advances*, vol. 28, pp. 325-347, 2010.
[69] C. P. Barnes, S. A. Sell, E. D. Boland, D. G. Simpson, and G. L. Bowlin, "Nanofiber technology: Designing the next generation of tissue engineering scaffolds," *Advanced Drug Delivery Reviews*, vol. 59, pp. 1413-1433, 2007.
[70] A. Formhals, "Process and apparatus for preparing artificial threads. Us patent, 1975504," ed, 1934.
[71] D. H. Reneker, A. L. Yarin, E. Zussman, and H. Xu, "Electrospinning of nanofibers from polymer solutions and melts," in *Advances in Applied Mechanics*. vol. Volume 41, A. Hassan and G. Erik van der, Eds., ed: Elsevier, 2007, pp. 43-346.
[72] P. Katta, M. Alessandro, R. Ramsier, and G. Chase, "Continuous electrospinning of aligned polymer nanofibers onto a wire drum collector," *Nano Letters*, vol. 4, pp. 2215-2218, 2004.
[73] A. Eatemadi, H. Daraee, N. Zarghami, H. Melat Yar, and A. Akbarzadeh, "Nanofiber: Synthesis and biomedical applications," *Artificial Cells, Nanomedicine, and Biotechnology*, vol. 44, pp. 111-121, 2016.
[74] S. Torres-Giner, R. Pérez-Masiá, and J. M. Lagaron, "A review on electrospun polymer nanostructures as advanced bioactive platforms," *Polymer Engineering & Science*, 2016.
[75] J. M. Deitzel, J. Kleinmeyer, D. Harris, and N. B. Tan, "The effect of processing variables on the morphology of electrospun nanofibers and textiles," *Polymer*, vol. 42, pp. 261-272, 2001.
[76] W. Zuo, M. Zhu, W. Yang, H. Yu, Y. Chen, and Y. Zhang, "Experimental study on relationship between jet instability and formation of beaded fibers during electrospinning," *Polymer Engineering & Science*, vol. 45, pp. 704-709, 2005.
[77] R. E. Benavides, S. C. Jana, and D. H. Reneker, "Nanofibers from scalable gas jet process," *ACS Macro Letters*, vol. 1, pp. 1032-1036, 2012.
[78] W. K. Son, J. H. Youk, T. S. Lee, and W. H. Park, "The effects of solution properties and polyelectrolyte on electrospinning of ultrafine poly (ethylene oxide) fibers," *Polymer*, vol. 45, pp. 2959-2966, 2004.
[79] N. M. Thoppey, R. E. Gorga, J. R. Bochinski, and L. I. Clarke, "Effect of solution parameters on spontaneous jet formation and throughput in edge electrospinning from a fluid-filled bowl," *Macromolecules*, vol. 45, pp. 6527-6537, 2012.
[80] C. L. Casper, J. S. Stephens, N. G. Tassi, D. B. Chase, and J. F. Rabolt, "Controlling surface morphology of electrospun polystyrene fibers: Effect of humidity and molecular weight in the electrospinning process," *Macromolecules*, vol. 37, pp. 573-578, 2004.

[81] J. Johnson, D. Ohst, T. Groehl, S. Hetterscheidt, and M. Jones, "Development of novel, bioresorbable, small-diameter electrospun vascular grafts," *Journal of Tissue Science & Engineering,* vol. 2015, 2015.

[82] N. L'heureux, J.-C. Stoclet, F. A. Auger, G. J.-L. Lagaud, L. Germain, and R. Andriantsitohaina, "A human tissue-engineered vascular media: A new model for pharmacological studies of contractile responses," *The FASEB Journal,* vol. 15, pp. 515-524, 2001.

[83] A. H. Huang, J. L. Balestrini, B. V. Udelsman, K. C. Zhou, L. Zhao, J. Ferruzzi, *et al.*, "Biaxial stretch improves elastic fiber maturation, collagen arrangement, and mechanical properties in engineered arteries," *Tissue Engineering Part C: Methods,* vol. 22, pp. 524-533, 2016.

[84] T. Stylianopoulos, C. A. Bashur, A. S. Goldstein, S. A. Guelcher, and V. H. Barocas, "Computational predictions of the tensile properties of electrospun fibre meshes: Effect of fibre diameter and fibre orientation," *Journal of the Mechanical Behavior of Biomedical Materials,* vol. 1, pp. 326-335, 2008.

[85] E. Tan, S. Ng, and C. Lim, "Tensile testing of a single ultrafine polymeric fiber," *Biomaterials,* vol. 26, pp. 1453-1456, 2005.

[86] S.-C. Wong, A. Baji, and S. Leng, "Effect of fiber diameter on tensile properties of electrospun poly (ε-caprolactone)," *Polymer,* vol. 49, pp. 4713-4722, 2008.

[87] A. Baji, Y.-W. Mai, S.-C. Wong, M. Abtahi, and P. Chen, "Electrospinning of polymer nanofibers: Effects on oriented morphology, structures and tensile properties," *Composites Science and Technology,* vol. 70, pp. 703-718, 2010.

[88] J.-W. Lu, Z.-P. Zhang, X.-Z. Ren, Y.-Z. Chen, J. Yu, and Z.-X. Guo, "High-elongation fiber mats by electrospinning of polyoxymethylene," *Macromolecules,* vol. 41, pp. 3762-3764, 2008.

[89] W. He, Z. Ma, T. Yong, W. E. Teo, and S. Ramakrishna, "Fabrication of collagen-coated biodegradable polymer nanofiber mesh and its potential for endothelial cells growth," *Biomaterials,* vol. 26, pp. 7606-7615, 2005.

[90] A. Arinstein, M. Burman, O. Gendelman, and E. Zussman, "Effect of supramolecular structure on polymer nanofibre elasticity," *Nature Nanotechnology,* vol. 2, pp. 59-62, 2007.

[91] V. Thomas, M. V. Jose, S. Chowdhury, J. F. Sullivan, D. R. Dean, and Y. K. Vohra, "Mechano-morphological studies of aligned nanofibrous scaffolds of polycaprolactone fabricated by electrospinning," *Journal of Biomaterials Science, Polymer Edition,* vol. 17, pp. 969-984, 2006.

[92] J. L. Lowery, N. Datta, and G. C. Rutledge, "Effect of fiber diameter, pore size and seeding method on growth of human dermal fibroblasts in electrospun poly (ε-caprolactone) fibrous mats," *Biomaterials,* vol. 31, pp. 491-504, 2010.

[93] A. S. Badami, M. R. Kreke, M. S. Thompson, J. S. Riffle, and A. S. Goldstein, "Effect of fiber diameter on spreading, proliferation, and differentiation of osteoblastic cells on electrospun poly (lactic acid) substrates," *Biomaterials,* vol. 27, pp. 596-606, 2006.

[94] G. T. Christopherson, H. Song, and H.-Q. Mao, "The influence of fiber diameter of electrospun substrates on neural stem cell differentiation and proliferation," *Biomaterials,* vol. 30, pp. 556-564, 2009.

[95] M. Chen, P. K. Patra, M. L. Lovett, D. L. Kaplan, and S. Bhowmick, "Role of electrospun fibre diameter and corresponding specific surface area (SSA) on cell attachment," *Journal of Tissue Engineering and Regenerative Medicine,* vol. 3, pp. 269-279, 2009.

[96] S. De Valence, J.-C. Tille, J.-P. Giliberto, W. Mrowczynski, R. Gurny, B. Walpoth, *et al.*, "Advantages of bilayered vascular grafts for surgical applicability and tissue regeneration," *Acta Biomaterialia,* vol. 8, pp. 3914-3920, 2012.

[97] J. Zhao, H. Qiu, D.-l. Chen, W.-x. Zhang, D.-c. Zhang, and M. Li, "Development of nanofibrous scaffolds for vascular tissue engineering," *International Journal of Biological Macromolecules,* vol. 56, pp. 106-113, 2013.

[98] C. Huang, S. Wang, L. Qiu, Q. Ke, W. Zhai, and X. Mo, "Heparin loading and pre-endothelialization in enhancing the patency rate of electrospun small-diameter vascular grafts in a canine model," *ACS Applied Materials & Interfaces,* vol. 5, pp. 2220-2226, 2013.

[99] A. K. Gaharwar, M. Nikkhah, S. Sant, and A. Khademhosseini, "Anisotropic poly (glycerol sebacate)-poly(ϵ-caprolactone) electrospun fibers promote endothelial cell guidance," *Biofabrication,* vol. 7, p. 015001, 2014.

[100] D. E. Heath, J. J. Lannutti, and S. L. Cooper, "Electrospun scaffold topography affects endothelial cell proliferation, metabolic activity, and morphology," *Journal of Biomedical Materials Research Part A,* vol. 94, pp. 1195-1204, 2010.

[101] K. A. Rocco, M. W. Maxfield, C. A. Best, E. W. Dean, and C. K. Breuer, "In vivo applications of electrospun tissue-engineered vascular grafts: A review," *Tissue Engineering Part B: Reviews,* vol. 20, pp. 628-640, 2014.

[102] M. Zhu, Z. Wang, J. Zhang, L. Wang, X. Yang, J. Chen, *et al.*, "Circumferentially aligned fibers guided functional neoartery regeneration in vivo," *Biomaterials,* vol. 61, pp. 85-94, 2015.

[103] E. D. Boland, T. A. Telemeco, D. G. Simpson, G. E. Wnek, and G. L. Bowlin, "Utilizing acid pretreatment and electrospinning to improve biocompatibility of poly (glycolic acid) for tissue engineering," *Journal of Biomedical Materials Research Part B: Applied Biomaterials,* vol. 71, pp. 144-152, 2004.

[104] Y. M. Ju, J. San Choi, A. Atala, J. J. Yoo, and S. J. Lee, "Bilayered scaffold for engineering cellularized blood vessels," *Biomaterials,* vol. 31, pp. 4313-4321, 2010.

[105] E. Pektok, B. Nottelet, J.-C. Tille, R. Gurny, A. Kalangos, M. Moeller, *et al.*, "Degradation and healing characteristics of small-diameter poly (ε-caprolactone) vascular grafts in the rat systemic arterial circulation," *Circulation,* vol. 118, pp. 2563-2570, 2008.

[106] B. M. Baker, A. O. Gee, R. B. Metter, A. S. Nathan, R. A. Marklein, J. A. Burdick, *et al.*, "The potential to improve cell infiltration in composite fiber-aligned electrospun scaffolds by the selective removal of sacrificial fibers," *Biomaterials,* vol. 29, pp. 2348-2358, 2008.

[107] Q. P. Pham, U. Sharma, and A. G. Mikos, "Microfiber and multilayer nanofiber/microfiber scaffolds: Characterization of scaffolds and measurement of cellular infiltration " *Biomacromolecules,* vol. 7, pp. 2796-2805, 2006.

[108] J. Nam, Y. Huang, S. Agarwal, and J. Lannutti, "Improved cellular infiltration in electrospun fiber via engineered porosity," *Tissue Engineering,* vol. 13, pp. 2249-2257, 2007.

[109] G. C. Ingavle and J. K. Leach, "Advancements in electrospinning of polymeric nanofibrous scaffolds for tissue engineering," *Tissue Engineering Part B: Reviews,* vol. 20, pp. 277-293, 2013.

[110] L. J. Villarreal-Gómez, J. M. Cornejo-Bravo, R. Vera-Graziano, and D. Grande, "Electrospinning as a powerful technique for biomedical applications: A critically selected survey," *Journal of Biomaterials Science, Polymer Edition,* vol. 27, pp. 157-176, 2016.

[111] S. Agarwal, J. H. Wendorff, and A. Greiner, "Use of electrospinning technique for biomedical applications," *Polymer,* vol. 49, pp. 5603-5621, 2008.
[112] N. Goonoo, A. Bhaw-Luximon, and D. Jhurry, "In vitro and in vivo cytocompatibility of electrospun nanofiber scaffolds for tissue engineering applications," *RSC Advances,* vol. 4, pp. 31618-31642, 2014.
[113] K. K. Sankaran, A. Subramanian, U. M. Krishnan, and S. Sethuraman, "Nanoarchitecture of scaffolds and endothelial cells in engineering small diameter vascular grafts," *Biotechnology Journal,* vol. 10, pp. 96-108, 2015.
[114] S. Yoshida, K. Hagiwara, T. Hasebe, and A. Hotta, "Surface modification of polymers by plasma treatments for the enhancement of biocompatibility and controlled drug release," *Surface and Coatings Technology,* vol. 233, pp. 99-107, 2013.
[115] M. Tirrell, E. Kokkoli, and M. Biesalski, "The role of surface science in bioengineered materials," *Surface Science,* vol. 500, pp. 61-83, 2002.
[116] H. Chen, L. Yuan, W. Song, Z. Wu, and D. Li, "Biocompatible polymer materials: Role of protein–surface interactions," *Progress in Polymer Science,* vol. 33, pp. 1059-1087, 2008.
[117] T. Desmet, R. Morent, N. D. Geyter, C. Leys, E. Schacht, and P. Dubruel, "Nonthermal plasma technology as a versatile strategy for polymeric biomaterials surface modification: A review," *Biomacromolecules,* vol. 10, pp. 2351-2378, 2009.
[118] R. Förch, A. N. Chifen, A. Bousquet, H. L. Khor, M. Jungblut, L. Q. Chu, *et al.*, "Recent and expected roles of plasma-polymerized films for biomedical applications," *Chemical Vapor Deposition,* vol. 13, pp. 280-294, 2007.
[119] G. Wu, P. Li, H. Feng, X. Zhang, and P. K. Chu, "Engineering and functionalization of biomaterials via surface modification," *Journal of Materials Chemistry B,* vol. 3, pp. 2024-2042, 2015.
[120] P. K. Chu, "Surface engineering and modification of biomaterials," *Thin Solid Films,* vol. 528, pp. 93-105, 2013.
[121] M. C. Boivin, P. Chevallier, S. Turgeon, J. Lagueux, and G. Laroche, "Micropatterning polymer materials to improve endothelialization," in *Advanced Materials Research*, 2012, pp. 777-782.
[122] J. H. Collier and T. Segura, "Evolving the use of peptides as components of biomaterials," *Biomaterials,* vol. 32, pp. 4198-4204, 2011.
[123] K. Vallières, É. Petitclerc, and G. Laroche, "Covalent grafting of fibronectin onto plasma-treated PTFE: Influence of the conjugation strategy on fibronectin biological activity," *Macromolecular Bioscience,* vol. 7, pp. 738-745, 2007.
[124] C. A. Hoesli, A. Garnier, P.-M. Juneau, P. Chevallier, C. Duchesne, and G. Laroche, "A fluorophore-tagged RGD peptide to control endothelial cell adhesion to micropatterned surfaces," *Biomaterials,* vol. 35, pp. 879-890, 2014.
[125] R. S. Benson, "Use of radiation in biomaterials science," *Nuclear Instruments and Methods in Physics Research Section B: Beam Interactions with Materials and Atoms,* vol. 191, pp. 752-757, 2002.
[126] F. Poncin-Epaillard, B. Chevet, and J. C. Brosse, "Modification of isotactic polypropylene by a cold plasma or an electron beam and grafting of the acrylic acid onto these activated polymers," *Journal of Applied Polymer Science,* vol. 53, pp. 1291-1306, 1994.
[127] A. Kurella and N. B. Dahotre, "Surface modification for bioimplants: The role of laser surface engineering," *Journal of Biomaterials Applications,* vol. 20, pp. 5-50, 2005.

[128] Z. Ma, Z. Mao, and C. Gao, "Surface modification and property analysis of biomedical polymers used for tissue engineering," *Colloids and Surfaces B: Biointerfaces,* vol. 60, pp. 137-157, 2007.
[129] T. Von Woedtke, S. Reuter, K. Masur, and K.-D. Weltmann, "Plasmas for medicine," *Physics Reports,* vol. 530, pp. 291-320, 2013.
[130] A. Hadjizadeh, A. Ajji, and M. N. Bureau, "Preparation and characterization of NaOH treated micro-fibrous polyethylene terephthalate nonwovens for biomedical application," *Journal of the Mechanical Behavior of Biomedical Materials,* vol. 3, pp. 574-583, 2010.
[131] H. Savoji, D. Rana, T. Matsuura, S. Tabe, and C. Feng, "Development of plasma and/or chemically induced graft co-polymerized electrospun poly (vinylidene fluoride) membranes for solute separation," *Separation and Purification Technology,* vol. 108, pp. 196-204, 2013.
[132] Z. Y. Ma, Y. P. Guan, X. Q. Liu, and H. Z. Liu, "Synthesis of magnetic chelator for high-capacity immobilized metal affinity adsorption of protein by cerium initiated graft polymerization," *Langmuir,* vol. 21, pp. 6987-6994, 2005.
[133] A. Hadjizadeh, A. Ajji, M. Jolicoeur, B. Liberelle, and G. De Crescenzo, "Effects of electrospun nanostructure versus microstructure on human aortic endothelial cell behavior," *Journal of Biomedical Nanotechnology,* vol. 9, pp. 1195-1209, 2013.
[134] S. Noel, B. Liberelle, A. Yogi, M. J. Moreno, M. N. Bureau, L. Robitaille, *et al.*, "A non-damaging chemical amination protocol for poly (ethylene terephthalate)–application to the design of functionalized compliant vascular grafts," *Journal of Materials Chemistry B,* vol. 1, pp. 230-238, 2013.
[135] P. Cools, N. De Geyter, and R. Morent, "Plasma modified textiles for biomedical applications," *Advances in Bioengineering,* pp. 117-148, 2015.
[136] F. S. Denes and S. Manolache, "Macromolecular plasma-chemistry: An emerging field of polymer science," *Progress in Polymer Science,* vol. 29, pp. 815-885, 2004.
[137] N. Inagaki, *Plasma surface modification and plasma polymerization*: CRC Press, 1996.
[138] C. Sarra-Bournet, S. Turgeon, D. Mantovani, and G. Laroche, "Comparison of atmospheric-pressure plasma versus low-pressure RF plasma for surface functionalization of PTFE for biomedical applications," *Plasma Processes and Polymers,* vol. 3, pp. 506-515, 2006.
[139] E. Bormashenko, G. Whyman, V. Multanen, E. Shulzinger, and G. Chaniel, "Physical mechanisms of interaction of cold plasma with polymer surfaces," *Journal of Colloid and Interface Science,* vol. 448, pp. 175-179, 2015.
[140] N. De Geyter, R. Morent, and C. Leys, "Influence of ambient conditions on the ageing behaviour of plasma-treated PET surfaces," *Nuclear Instruments and Methods in Physics Research Section B: Beam Interactions with Materials and Atoms,* vol. 266, pp. 3086-3090, 2008.
[141] N. De Geyter, R. Morent, and C. Leys, "Penetration of a dielectric barrier discharge plasma into textile structures at medium pressure," *Plasma Sources Science and Technology,* vol. 15, p. 78, 2006.
[142] J.-P. Chen and C.-H. Su, "Surface modification of electrospun PLLA nanofibers by plasma treatment and cationized gelatin immobilization for cartilage tissue engineering," *Acta Biomaterialia,* vol. 7, pp. 234-243, 2011.
[143] C. Sarra-Bournet, S. Turgeon, D. Mantovani, and G. Laroche, "Comparison of atmospheric-pressure plasma versus low-pressure RF plasma for surface functionalization

of PTFE for biomedical applications," *Plasma Processes and Polymers,* vol. 3, pp. 506-515, 2006.

[144] I. Unalan, O. Colpankan, A. Z. Albayrak, C. Gorgun, and A. S. Urkmez, "Biocompatibility of plasma-treated poly (3-hydroxybutyrate-co-3-hydroxyvalerate) nanofiber mats modified by silk fibroin for bone tissue regeneration," *Materials Science and Engineering: C,* vol. 68, pp. 842-850, 2016.

[145] E. Stoleru, M. C. Baican, A. Coroaba, G. E. Hitruc, M. Lungu, and C. Vasile, "Plasma-activated fibrinogen coatings onto poly (vinylidene fluoride) surface for improving biocompatibility with tissues," *Journal of Bioactive and Compatible Polymers: Biomedical Applications,* vol. 31, pp. 91-108, 2016.

[146] C. Sarra-Bournet, G. Ayotte, S. Turgeon, F. o. Massines, and G. Laroche, "Effects of chemical composition and the addition of H_2 in a N_2 atmospheric pressure dielectric barrier discharge on polymer surface functionalization," *Langmuir,* vol. 25, pp. 9432-9440, 2009.

[147] P. Chevallier, R. Janvier, D. Mantovani, and G. Laroche, "In vitro biological performances of phosphorylcholine-grafted ePTFE prostheses through RFGD plasma techniques," *Macromolecular Bioscience,* vol. 5, pp. 829-839, 2005.

[148] K. Park, Y. M. Ju, J. S. Son, K.-D. Ahn, and D. K. Han, "Surface modification of biodegradable electrospun nanofiber scaffolds and their interaction with fibroblasts," *Journal of Biomaterials Science, Polymer Edition,* vol. 18, pp. 369-382, 2007.

[149] S. François, N. Chakfé, B. Durand, and G. Laroche, "A poly (l-lactic acid) nanofibre mesh scaffold for endothelial cells on vascular prostheses," *Acta Biomaterialia,* vol. 5, pp. 2418-2428, 2009.

[150] N. R. Ko, G. Sabbatier, A. Cunningham, G. Laroche, and J. K. Oh, "Air-spun PLA nanofibers modified with reductively sheddable hydrophilic surfaces for vascular tissue engineering: Synthesis and surface modification," *Macromolecular Rapid Communications,* vol. 35, pp. 447-453, 2014.

[151] X. Zhu, K. S. Chian, M. B. E. Chan-Park, and S. T. Lee, "Effect of argon-plasma treatment on proliferation of human-skin–derived fibroblast on chitosan membrane in vitro," *Journal of Biomedical Materials Research Part A,* vol. 73, pp. 264-274, 2005.

[152] S. Siri, P. Wadbua, V. Amornkitbamrung, N. Kampa, and S. Maensiri, "Surface modification of electrospun PCL scaffolds by plasma treatment and addition of adhesive protein to promote fibroblast cell adhesion," *Materials Science and Technology,* vol. 26, pp. 1292-1297, 2010.

[153] T. Jacobs, R. Morent, N. De Geyter, P. Dubruel, and C. Leys, "Plasma surface modification of biomedical polymers: Influence on cell-material interaction," *Plasma Chemistry and Plasma Processing,* vol. 32, pp. 1039-1073, 2012.

[154] Y. Zhu, C. Gao, J. Guan, and J. Shen, "Engineering porous polyurethane scaffolds by photografting polymerization of methacrylic acid for improved endothelial cell compatibility," *Journal of Biomedical Materials Research Part A,* vol. 67, pp. 1367-1373, 2003.

[155] Z. Ma, M. Kotaki, T. Yong, W. He, and S. Ramakrishna, "Surface engineering of electrospun polyethylene terephthalate (PET) nanofibers towards development of a new material for blood vessel engineering," *Biomaterials,* vol. 26, pp. 2527-2536, 2005.

[156] J. Sharma, M. Lizu, M. Stewart, K. Zygula, Y. Lu, R. Chauhan, *et al.*, "Multifunctional nanofibers towards active biomedical therapeutics," *Polymers,* vol. 7, pp. 186-219, 2015.

[157] V. M. Donnelly and A. Kornblit, "Plasma etching: Yesterday, today, and tomorrow," *Journal of Vacuum Science & Technology A,* vol. 31, p. 050825, 2013.
[158] D. L. Flamm, O. Auciello, and R. d'Agostino, *Plasma deposition, treatment, and etching of polymers: The treatment and etching of polymers*: Elsevier, 2012.
[159] R. Morent, N. De Geyter, T. Desmet, P. Dubruel, and C. Leys, "Plasma surface modification of biodegradable polymers: A review," *Plasma Processes and Polymers,* vol. 8, pp. 171-190, 2011.
[160] F. Truica-Marasescu and M. R. Wertheimer, "Nitrogen-rich plasma-polymer films for biomedical applications," *Plasma Processes and Polymers,* vol. 5, pp. 44-57, 2008.
[161] P. L. Girard-Lauriault, F. Mwale, M. Iordanova, C. Demers, P. Desjardins, and M. R. Wertheimer, "Atmospheric pressure deposition of micropatterned nitrogen-rich plasma-polymer films for tissue engineering," *Plasma Processes and Polymers,* vol. 2, pp. 263-270, 2005.
[162] F. Truica-Marasescu and M. R. Wertheimer, "Nitrogen-rich plasma-polymer films for biomedical applications," *Plasma Processes and Polymers,* vol. 5, pp. 44-57, 2008.
[163] A. Gigout, J.-C. Ruiz, M. R. Wertheimer, M. Jolicoeur, and S. Lerouge, "Nitrogen-rich plasma-polymerized coatings on PET and PTFE surfaces improve endothelial cell attachment and resistance to shear flow," *Macromolecular Bioscience,* vol. 11, pp. 1110-1119, 2011.
[164] P. L. Girard-Lauriault, F. Truica-Marasescu, A. Petit, H. T. Wang, P. Desjardins, J. Antoniou, *et al.*, "Adhesion of human U937 monocytes to nitrogen-rich organic thin films: Novel insights into the mechanism of cellular adhesion," *Macromolecular Bioscience,* vol. 9, pp. 911-921, 2009.
[165] S. Lerouge, A. Major, P.-L. Girault-Lauriault, M.-A. Raymond, P. Laplante, G. Soulez, *et al.*, "Nitrogen-rich coatings for promoting healing around stent-grafts after endovascular aneurysm repair," *Biomaterials,* vol. 28, pp. 1209-1217, 2007.
[166] P. Favia and R. d'Agostino, "Plasma treatments and plasma deposition of polymers for biomedical applications," *Surface and Coatings Technology,* vol. 98, pp. 1102-1106, 1998.
[167] R. Wyrwa, B. Finke, H. Rebl, N. Mischner, M. Quaas, J. Schaefer, *et al.*, "Design of plasma surface-activated, electrospun polylactide non-wovens with improved cell acceptance," *Advanced Engineering Materials,* vol. 13, pp. B165-B171, 2011.
[168] A. Guex, F. Kocher, G. Fortunato, E. Körner, D. Hegemann, T. Carrel, *et al.*, "Fine-tuning of substrate architecture and surface chemistry promotes muscle tissue development," *Acta Biomaterialia,* vol. 8, pp. 1481-1489, 2012.
[169] K. A. Meade, K. J. White, C. E. Pickford, R. J. Holley, A. Marson, D. Tillotson, *et al.*, "Immobilization of heparan sulfate on electrospun meshes to support embryonic stem cell culture and differentiation," *Journal of Biological Chemistry,* vol. 288, pp. 5530-5538, 2013.
[170] S. Sarkar, K. M. Sales, G. Hamilton, and A. M. Seifalian, "Addressing thrombogenicity in vascular graft construction," *Journal of Biomedical Materials Research Part B: Applied Biomaterials,* vol. 82, pp. 100-108, 2007.
[171] J. H. Pang, Y. Farhatnia, F. Godarzi, A. Tan, J. Rajadas, B. G. Cousins, *et al.*, "In situ endothelialization: Bioengineering considerations to translation," *Small,* vol. 11, pp. 6248-6264, 2015.

[172] T. Asahara, T. Murohara, A. Sullivan, M. Silver, R. van der Zee, T. Li, *et al.*, "Isolation of putative progenitor endothelial cells for angiogenesis," *Science*, vol. 275, pp. 964-966, 1997.
[173] V. Gauvreau, P. Chevallier, K. Vallières, É. Petitclerc, R. C. Gaudreault, and G. Laroche, "Engineering surfaces for bioconjugation: Developing strategies and quantifying the extent of the reactions," *Bioconjugate Chemistry*, vol. 15, pp. 1146-1156, 2004.
[174] J. Y. Shu, B. Panganiban, and T. Xu, "Peptide-polymer conjugates: From fundamental science to application," *Annual Review of Physical Chemistry*, vol. 64, pp. 631-657, 2013.
[175] B. Joddar and Y. Ito, "Biological modifications of materials surfaces with proteins for regenerative medicine," *Journal of Materials Chemistry*, vol. 21, pp. 13737-13755, 2011.
[176] H. Kito and T. Matsuda, "Biocompatible coatings for luminal and outer surfaces of small-caliber artificial grafts," *Journal of Biomedical Materials Research*, vol. 30, pp. 321-330, 1996.
[177] M. Morra, "Engineering of biomaterials surfaces by hyaluronan," *Biomacromolecules*, vol. 6, pp. 1205-1223, 2005.
[178] C. H. Jou, J. S. Lee, W. L. Chou, D. G. Yu, and M. C. Yang, "Effect of immobilization with chondroitin-6-sulfate and grafting with chitosan on fibroblast and antibacterial activity of polyester fibers," *Polymers for Advanced Technologies*, vol. 16, pp. 821-826, 2005.
[179] T.-W. Chuang and K. S. Masters, "Regulation of polyurethane hemocompatibility and endothelialization by tethered hyaluronic acid oligosaccharides," *Biomaterials*, vol. 30, pp. 5341-5351, 2009.
[180] K. Rajangam, H. A. Behanna, M. J. Hui, X. Han, J. F. Hulvat, J. W. Lomasney, *et al.*, "Heparin binding nanostructures to promote growth of blood vessels," *Nano Letters*, vol. 6, pp. 2086-2090, 2006.
[181] B. E. Uygun, S. E. Stojsih, and H. W. Matthew, "Effects of immobilized glycosaminoglycans on the proliferation and differentiation of mesenchymal stem cells," *Tissue Engineering Part A*, vol. 15, pp. 3499-3512, 2009.
[182] M. S. Lord, W. Yu, B. Cheng, A. Simmons, L. Poole-Warren, and J. M. Whitelock, "The modulation of platelet and endothelial cell adhesion to vascular graft materials by perlecan," *Biomaterials*, vol. 30, pp. 4898-4906, 2009.
[183] M. Wissink, R. Beernink, J. Pieper, A. Poot, G. Engbers, T. Beugeling, *et al.*, "Immobilization of heparin to EDC/NHS-crosslinked collagen. Characterization and in vitro evaluation," *Biomaterials*, vol. 22, pp. 151-163, 2001.
[184] C. Charbonneau, J. C. Ruiz, P. Lequoy, M. J. Hébert, G. De Crescenzo, M. R. Wertheimer, *et al.*, "Chondroitin sulfate and epidermal growth factor immobilization after plasma polymerization: A versatile anti-apoptotic coating to promote healing around stent grafts," *Macromolecular Bioscience*, vol. 12, pp. 812-821, 2012.
[185] P. Lequoy, B. Liberelle, G. De Crescenzo, and S. Lerouge, "Additive benefits of chondroitin sulfate and oriented tethered epidermal growth factor for vascular smooth muscle cell survival," *Macromolecular Bioscience*, vol. 14, pp. 720-730, 2014.
[186] P. Lequoy, F. Murschel, B. Liberelle, S. Lerouge, and G. De Crescenzo, "Controlled co-immobilization of egf and VEGF to optimize vascular cell survival," *Acta Biomaterialia*, vol. 29, pp. 239-247, 2016.
[187] P. Lequoy, H. Savoji, B. Saoudi, A. Bertrand-Grenier, M. R. Wertheimer, G. De Crescenzo, *et al.*, "In vitro and pilot in vivo evaluation of a bioactive coating for stent

grafts based on chondroitin sulfate and epidermal growth factor," *Journal of Vascular and Interventional Radiology,* vol. 27, pp. 753-760. e3, 2016.

[188] P. Laplante, M.-A. Raymond, G. Gagnon, N. Vigneault, A. M.-J. Sasseville, Y. Langelier, *et al.*, "Novel fibrogenic pathways are activated in response to endothelial apoptosis: Implications in the pathophysiology of systemic sclerosis," *The Journal of Immunology,* vol. 174, pp. 5740-5749, 2005.

[189] C. Charbonneau, B. Liberelle, M.-J. Hébert, G. De Crescenzo, and S. Lerouge, "Stimulation of cell growth and resistance to apoptosis in vascular smooth muscle cells on a chondroitin sulfate/epidermal growth factor coating," *Biomaterials,* vol. 32, pp. 1591-1600, 2011.

[190] C. Charbonneau, J. E. Gautrot, M. J. Hébert, X. Zhu, and S. Lerouge, "Chondroitin-4-sulfate: A bioactive macromolecule to foster vascular healing around stent-grafts after endovascular aneurysm repair," *Macromolecular Bioscience,* vol. 7, pp. 746-752, 2007.

[191] K. Kanie, Y. Narita, Y. Zhao, F. Kuwabara, M. Satake, S. Honda, *et al.*, "Collagen type IV-specific tripeptides for selective adhesion of endothelial and smooth muscle cells," *Biotechnology and Bioengineering,* vol. 109, pp. 1808-1816, 2012.

[192] G. De Visscher, L. Mesure, B. Meuris, A. Ivanova, and W. Flameng, "Improved endothelialization and reduced thrombosis by coating a synthetic vascular graft with fibronectin and stem cell homing factor SDF-1α," *Acta Biomaterialia,* vol. 8, pp. 1330-1338, 2012.

[193] W. Zheng, Z. Wang, L. Song, Q. Zhao, J. Zhang, D. Li, *et al.*, "Endothelialization and patency of RGD-functionalized vascular grafts in a rabbit carotid artery model," *Biomaterials,* vol. 33, pp. 2880-2891, 2012.

[194] S. Shindo, S. Motohashi, M. Katsu, S. Kaga, H. Inoue, and M. Matsumoto, "Coated prostheses are associated with prolonged inflammation in aortic surgery: A cost analysis," *Artificial Organs,* vol. 32, pp. 183-187, 2008.

[195] K. S. Masters, "Covalent growth factor immobilization strategies for tissue repair and regeneration," *Macromolecular Bioscience,* vol. 11, pp. 1149-1163, 2011.

[196] K. Vulic and M. S. Shoichet, "Affinity-based drug delivery systems for tissue repair and regeneration," *Biomacromolecules,* vol. 15, pp. 3867-3880, 2014.

[197] Y. H. Shen, M. S. Shoichet, and M. Radisic, "Vascular endothelial growth factor immobilized in collagen scaffold promotes penetration and proliferation of endothelial cells," *Acta Biomaterialia,* vol. 4, pp. 477-489, 2008.

[198] Y. M. Shin, Y. B. Lee, S. J. Kim, J. K. Kang, J.-C. Park, W. Jang, *et al.*, "Mussel-inspired immobilization of vascular endothelial growth factor (VEGF) for enhanced endothelialization of vascular grafts," *Biomacromolecules,* vol. 13, pp. 2020-2028, 2012.

[199] R. J. Smith, M. T. Koobatian, A. Shahini, D. D. Swartz, and S. T. Andreadis, "Capture of endothelial cells under flow using immobilized vascular endothelial growth factor," *Biomaterials,* vol. 51, pp. 303-312, 2015.

[200] H. L. Goel and A. M. Mercurio, "Vegf targets the tumour cell," *Nature Reviews Cancer,* vol. 13, pp. 871-882, 2013.

[201] Y. Ding, M. Yang, Z. Yang, R. Luo, X. Lu, N. Huang, *et al.*, "Cooperative control of blood compatibility and re-endothelialization by immobilized heparin and substrate topography," *Acta Biomaterialia,* vol. 15, pp. 150-163, 2015.

[202] Z. Yang, Q. Tu, J. Wang, and N. Huang, "The role of heparin binding surfaces in the direction of endothelial and smooth muscle cell fate and re-endothelialization," *Biomaterials,* vol. 33, pp. 6615-6625, 2012.

[203] M. I. Castellanos, A.-S. Zenses, A. Grau, J. C. Rodríguez-Cabello, F. J. Gil, J. M. Manero, *et al.*, "Biofunctionalization of REDV elastin-like recombinamers improves endothelialization on CoCr alloy surfaces for cardiovascular applications," *Colloids and Surfaces B: Biointerfaces,* vol. 127, pp. 22-32, 2015.

[204] W. J. Seeto, Y. Tian, and E. A. Lipke, "Peptide-grafted poly(ethylene glycol) hydrogels support dynamic adhesion of endothelial progenitor cells," *Acta Biomaterialia,* vol. 9, pp. 8279-8289, 2013.

[205] Y. Wei, Y. Ji, L.-L. Xiao, Q.-k. Lin, J.-p. Xu, K.-f. Ren, *et al.*, "Surface engineering of cardiovascular stent with endothelial cell selectivity for in vivo re-endothelialisation," *Biomaterials,* vol. 34, pp. 2588-2599, 2013.

[206] H. Ceylan, A. B. Tekinay, and M. O. Guler, "Selective adhesion and growth of vascular endothelial cells on bioactive peptide nanofiber functionalized stainless steel surface," *Biomaterials,* vol. 32, pp. 8797-8805, 2011.

[207] K. Vallieres, P. Chevallier, C. Sarra-Bournet, S. Turgeon, and G. Laroche, "AFM imaging of immobilized fibronectin: Does the surface conjugation scheme affect the protein orientation/conformation?," *Langmuir,* vol. 23, pp. 9745-9751, 2007.

[208] M. Byad, K. Vallières, P. Chevallier, C. Hoesli, and G. Laroche, "Influence of chemical conjugation strategies on fibronectin's bioactivity," *Biophysical Journal,* vol. 108, p. 486a, 2015.

[209] N. Tajima, M. Takai, and K. Ishihara, "Significance of antibody orientation unraveled: Well-oriented antibodies recorded high binding affinity," *Analytical Chemistry,* vol. 83, pp. 1969-1976, 2011.

[210] S. Petersen, A. Strohbach, R. Busch, S. B. Felix, K. P. Schmitz, and K. Sternberg, "Site-selective immobilization of anti-CD34 antibodies to poly (l-lactide) for endovascular implant surfaces," *Journal of Biomedical Materials Research Part B: Applied Biomaterials,* vol. 102, pp. 345-355, 2014.

[211] Y. Yuan, M. Yin, J. Qian, and C. Liu, "Site-directed immobilization of antibodies onto blood contacting grafts for enhanced endothelial cell adhesion and proliferation," *Soft Matter,* vol. 7, pp. 7207-7216, 2011.

[212] Y. Assal, M. Mie, and E. Kobatake, "The promotion of angiogenesis by growth factors integrated with ECM proteins through coiled-coil structures," *Biomaterials,* vol. 34, pp. 3315-3323, 2013.

[213] B. Liberelle, C. Boucher, J. Chen, M. Jolicoeur, Y. Durocher, and G. De Crescenzo, "Impact of epidermal growth factor tethering strategy on cellular response," *Bioconjugate Chemistry,* vol. 21, pp. 2257-2266, 2010.

[214] C. Boucher, G. St-Laurent, M. Loignon, M. Jolicoeur, G. De Crescenzo, and Y. Durocher, "The bioactivity and receptor affinity of recombinant tagged EGF designed for tissue engineering applications is defined by the nature and position of the tags," *Tissue Engineering Part A,* vol. 14, pp. 2069-2077, 2008.

[215] C. Boucher, J.-C. Ruiz, M. Thibault, M. D. Buschmann, M. R. Wertheimer, M. Jolicoeur, *et al.*, "Human corneal epithelial cell response to epidermal growth factor tethered via coiled-coil interactions," *Biomaterials,* vol. 31, pp. 7021-7031, 2010.

[216] P. K. Thalla, A. Contreras-García, H. Fadlallah, J. Barrette, G. De Crescenzo, Y. Merhi, *et al.*, "A versatile star PEG grafting method for the generation of nonfouling and nonthrombogenic surfaces," *BioMed Research International,* vol. 2013, 2012.

[217] J. Chen, J. Cao, J. Wang, M. F. Maitz, L. Guo, Y. Zhao, *et al.*, "Biofunctionalization of titanium with PEG and anti-CD34 for hemocompatibility and stimulated endothelialization," *Journal of Colloid and Interface Science,* vol. 368, pp. 636-647, 2012.

[218] T. A. Gaziano, "Cardiovascular disease in the developing world and its cost-effective management," *Circulation,* vol. 112, pp. 3547-3553, 2005.

[219] R. Y. Kannan, H. J. Salacinski, P. E. Butler, G. Hamilton, and A. M. Seifalian, "Current status of prosthetic bypass grafts: A review," *Journal of Biomedical Materials Research Part B-Applied Biomaterials,* vol. 74B, pp. 570-581, 2005.

[220] S. Sarkar, T. Schmitz-Rixen, G. Hamilton, and A. M. Seifalian, "Achieving the ideal properties for vascular bypass grafts using a tissue engineered approach: A review," *Medical & Biological Engineering & Computing,* vol. 45, pp. 327-336, 2007.

[221] C. Y. Xu, R. Inai, M. Kotaki, and S. Ramakrishna, "Electrospun nanofiber fabrication as synthetic extracellular matrix and its potential for vascular tissue engineering," *Tissue Engineering,* vol. 10, pp. 1160-1168, 2004.

[222] W. He, Z. W. Ma, W. E. Teo, Y. X. Dong, P. A. Robless, T. C. Lim, *et al.*, "Tubular nanofiber scaffolds for tissue engineered small-diameter vascular grafts," *Journal of Biomedical Materials Research Part A,* vol. 90A, pp. 205-216, 2009.

[223] C. Grasl, H. Bergmeister, M. Stoiber, H. Schima, and G. Weigel, "Electrospun polyurethane vascular grafts: In vitro mechanical behavior and endothelial adhesion molecule expression," *Journal of Biomedical Materials Research Part A,* vol. 93A, pp. 716-723, 2010.

[224] M. Zhang, K. Wang, Z. X. Wang, B. Xing, Q. Zhao, and D. L. Kong, "Small-diameter tissue engineered vascular graft made of electrospun PCL/Lecithin blend," *Journal of Materials Science-Materials in Medicine,* vol. 23, pp. 2639-2648, 2012.

[225] N. Detta, C. Errico, D. Dinucci, D. Puppi, D. A. Clarke, G. C. Reilly, *et al.*, "Novel electrospun polyurethane/gelatin composite meshes for vascular grafts," *Journal of Materials Science-Materials in Medicine,* vol. 21, pp. 1761-1769, 2010.

[226] A. Andukuri, M. Kushwaha, A. Tambralli, J. M. Anderson, D. R. Dean, J. L. Berry, *et al.*, "A hybrid biomimetic nanomatrix composed of electrospun polycaprolactone and bioactive peptide amphiphiles for cardiovascular implants," *Acta Biomaterialia,* vol. 7, pp. 225-233, 2011.

[227] X. Zhang, V. Thomas, and Y. K. Vohra, "Two ply tubular scaffolds comprised of proteins/poliglecaprone/polycaprolactone fibers," *Journal of Materials Science-Materials in Medicine,* vol. 21, pp. 541-549, 2010.

[228] S. G. Wise, M. J. Byrom, A. Waterhouse, P. G. Bannon, M. K. C. Ng, and A. S. Weiss, "A multilayered synthetic human elastin/polycaprolactone hybrid vascular graft with tailored mechanical properties," *Acta Biomaterialia,* vol. 7, pp. 295-303, 2011.

[229] A. Hasan, A. Memic, N. Annabi, M. Hossain, A. Paul, M. R. Dokmeci, *et al.*, "Electrospun scaffolds for tissue engineering of vascular grafts," *Acta Biomaterialia,* vol. 10, pp. 11-25, 2014.

[230] D. Shum-Tim, U. Stock, J. Hrkach, T. Shinoka, J. Lien, M. A. Moses, *et al.*, "Tissue engineering of autologous aorta using a new biodegradable polymer," *Annals of Thoracic Surgery,* vol. 68, pp. 2298-2304, 1999.

[231] A. Hadjizadeh, A. Ajji, and M. N. Bureau, "Nano/micro electro-spun polyethylene terephthalate fibrous mat preparation and characterization," *Journal of the Mechanical Behavior of Biomedical Materials,* vol. 4, pp. 340-351, 2011.

[232] Z. W. Ma, M. Kotaki, T. Yong, W. He, and S. Ramakrishna, "Surface engineering of electrospun polyethylene terephthalate (PET) nanofibers towards development of a new material for blood vessel engineering," *Biomaterials,* vol. 26, pp. 2527-2536, 2005.

[233] M. Chun, C. S. Nabzdyk, J. D. Glaser, S. Pathan, M. Phaneuf, J.-O. You, *et al.*, "Composite electrospun polyethylene terephthalate: A method towards improving graft patency," *Journal of Vascular Surgery,* vol. 56, p. 1482, 2012.

[234] B. Veleirinho, M. F. Rei, and J. A. Lopes-da-Silva, "Solvent and concentration effects on the properties of electrospun poly(ethylene terephthalate) nanofiber mats," *Journal of Polymer Science Part B-Polymer Physics,* vol. 46, pp. 460-471, 2008.

[235] M. C. Burrows, V. M. Zamarion, F. B. Filippin-Monteiro, D. C. Schuck, H. E. Toma, A. Campa, *et al.*, "Hybrid scaffolds built from PET and collagen as a model for vascular graft architecture," *Macromolecular Bioscience,* vol. 12, pp. 1660-1670, 2012.

[236] A. Gigout, J. C. Ruiz, M. R. Wertheimer, M. Jolicoeur, and S. Lerouge, "Nitrogen-rich plasma-polymerized coatings on PET and PTFE surfaces improve endothelial cell attachment and resistance to shear flow," *Macromolecular Bioscience,* vol. 11, pp. 1110-1119, 2011.

[237] R. S. Benson, "Use of radiation in biomaterials science," *Nuclear Instruments & Methods in Physics Research Section B-Beam Interactions with Materials and Atoms,* vol. 191, pp. 752-757, 2002.

[238] F. Poncinepaillard, B. Chevet, and J. C. Brosse, "Modification of isotactic polypropylene by a cold-plasma or an electron-beam and grafting of the acrylic-acid onto these activated polymers," *Journal of Applied Polymer Science,* vol. 53, pp. 1291-1306, 1994.

[239] F. Abbasi, H. Mirzadeh, and A. A. Katbab, "Bulk and surface modification of silicone rubber for biomedical applications," *Polymer International,* vol. 51, pp. 882-888, 2002.

[240] Z. W. Ma, Z. W. Mao, and C. Y. Gao, "Surface modification and property analysis of biomedical polymers used for tissue engineering," *Colloids and Surfaces B-Biointerfaces,* vol. 60, pp. 137-157, 2007.

[241] P. K. Chu, J. Y. Chen, L. P. Wang, and N. Huang, "Plasma-surface modification of biomaterials," *Materials Science & Engineering R-Reports,* vol. 36, pp. 143-206, 2002.

[242] J. Marchandbrynaert, M. Deldime, I. Dupont, J. L. Dewez, and Y. J. Schneider, "Surface functionalization of poly(ethylene-terephthalate) film and membrane by controlled wet chemistry - chemical characterization of carboxylated surfaces," *Journal of Colloid and Interface Science,* vol. 173, pp. 236-244, 1995.

[243] C. Salvagnini, A. Roback, M. Momtaz, V. Pourcelle, and J. Marchand-Brynaert, "Surface functionalization of a poly(butylene terephthalate) (PBT) melt-blown filtration membrane by wet chemistry and photo-grafting," *Journal of Biomaterials Science-Polymer Edition,* vol. 18, pp. 1491-1516, 2007.

[244] M. Voue, E. Goormaghtigh, F. Homble, J. Marchand-Brynaert, J. Conti, S. Devouge, *et al.*, "Biochemical interaction analysis on ATR devices: A wet chemistry approach for surface functionalization," *Langmuir,* vol. 23, pp. 949-955, 2007.

[245] J. G. A. Terlingen, A. S. Hoffman, and J. Feijen, "Effect of glow-discharge treatment of poly(acrylic acid) pre-adsorbed onto poly(ethylene)," *Journal of Applied Polymer Science,* vol. 50, pp. 1529-1539, 1993.

[246] A. Gigout, J. C. Ruiz, M. R. Wertheimer, M. Jolicoeur, and S. Lerouge, "Nitrogen-rich plasma-polymerized coatings on PET and PTFE surfaces improve endothelial cell attachment and resistance to shear flow," *Macromolecular Bioscience,* vol. 11, pp. 1110-1119, 2011.

[247] J. C. Ruiz, A. St-Georges-Robillard, C. Thérésy, S. Lerouge, and M. R. Wertheimer, "Fabrication and characterisation of amine-rich organic thin films: Focus on stability," *Plasma Processes and Polymers,* vol. 7, pp. 737-753, 2010.

[248] A. St-Georges-Robillard, J. C. Ruiz, A. Petit, H. T. Wang, F. Mwale, B. Elkin, *et al.*, "Adhesion of U937 monocytes on different amine-functionalised polymer surfaces," *Plasma Processes and Polymers,* vol. 9, pp. 243-252, 2012.

[249] S. T. Ho and D. W. Hutmacher, "A comparison of micro CT with other techniques used in the characterization of scaffolds," *Biomaterials,* vol. 27, pp. 1362-1376, 2006.

[250] P. Favia, M. V. Stendardo, and R. d'Agostino, "Selective grafting of amine groups on polyethylene by means of NH_3–H_2 RF glow discharges," *Plasmas and Polymers,* vol. 1, pp. 91-112, 1996.

[251] A. M. Malek, S. L. Alper, and S. Izumo, "Hemodynamic shear stress and its role in atherosclerosis," *JAMA,* vol. 282, pp. 2035-2042, 1999.

[252] N. G. dela Paz and P. A. D'Amore, "Arterial versus venous endothelial cells," *Cell and Tissue Research,* vol. 335, pp. 5-16, 2009.

[253] H. Salacinski, A. Tiwari, G. Hamilton, and A. Seifalian, "Cellular engineering of vascular bypass grafts: Role of chemical coatings for enhancing endothelial cell attachment," *Medical and Biological Engineering and Computing,* vol. 39, pp. 609-618, 2001.

[254] C. Wang, L. Cen, S. Yin, Q. Liu, W. Liu, Y. Cao, *et al.*, "A small diameter elastic blood vessel wall prepared under pulsatile conditions from polyglycolic acid mesh and smooth muscle cells differentiated from adipose-derived stem cells," *Biomaterials,* vol. 31, pp. 621-630, 2010.

[255] S. Sell, M. J. McClure, C. P. Barnes, D. C. Knapp, B. H. Walpoth, D. G. Simpson, *et al.*, "Electrospun polydioxanone–elastin blends: Potential for bioresorbable vascular grafts," *Biomedical Materials,* vol. 1, p. 72, 2006.

[256] K. Schröder, A. Meyer-Plath, D. Keller, W. Besch, G. Babucke, and A. Ohl, "Plasma-induced surface functionalization of polymeric biomaterials in ammonia plasma," *Contributions to Plasma Physics,* vol. 41, pp. 562-572, 2001.

[257] A. Meyer-Plath, K. Schröder, B. Finke, and A. Ohl, "Current trends in biomaterial surface functionalization—nitrogen-containing plasma assisted processes with enhanced selectivity," *Vacuum,* vol. 71, pp. 391-406, 2003.

[258] C. Grasl, H. Bergmeister, M. Stoiber, H. Schima, and G. Weigel, "Electrospun polyurethane vascular grafts: In vitro mechanical behavior and endothelial adhesion molecule expression," *Journal of Biomedical Materials Research Part A,* vol. 93, pp. 716-723, 2010.

[259] W. He, Z. Ma, W. E. Teo, Y. X. Dong, P. A. Robless, T. C. Lim, *et al.*, "Tubular nanofiber scaffolds for tissue engineered small-diameter vascular grafts," *Journal of Biomedical Materials Research Part A,* vol. 90, pp. 205-216, 2009.

[260] B. C. Heng, P. P. Bezerra, P. R. Preiser, S. Alex Law, Y. Xia, F. Boey, *et al.*, "Effect of cell-seeding density on the proliferation and gene expression profile of human umbilical vein endothelial cells within ex vivo culture," *Cytotherapy,* vol. 13, pp. 606-617, 2011.

[261] E. Vinard, G. Lesèche, B. Andreassian, and D. Costagliola, "In vitro endothelialization of PTFE vascular grafts: A comparison of various substrates, cell densities, and incubation times," *Annals of Vascular Surgery*, vol. 13, pp. 141-150, 1999.

[262] S. Wang, X. M. Mo, B. J. Jiang, C. J. Gao, H. S. Wang, Y. G. Zhuang, *et al.*, "Fabrication of small-diameter vascular scaffolds by heparin-bonded P(LLA-CL) composite nanofibers to improve graft patency," *International Journal of Nanomedicine*, vol. 8, pp. 2131-2139, 2013.

[263] C. Bouten, P. Dankers, A. Driessen-Mol, S. Pedron, A. Brizard, and F. Baaijens, "Substrates for cardiovascular tissue engineering," *Advanced Drug Delivery Reviews*, vol. 63, pp. 221-241, 2011.

[264] M. Moreno, A. Ajji, D. Mohebbi-Kalhori, M. Rukhlova, A. Hadjizadeh, and M. Bureau, "Development of a compliant and cytocompatible micro-fibrous polyethylene terephthalate vascular scaffold," *Journal of Biomedical Materials Research Part B: Applied Biomaterials*, vol. 97, pp. 201-214, 2011.

[265] S. Ramakrishna, K. Fujihara, W.-E. Teo, T. Yong, Z. Ma, and R. Ramaseshan, "Electrospun nanofibers: Solving global issues," *Materials Today*, vol. 9, pp. 40-50, 2006.

[266] J.-C. Ruiz, P.-L. Girard-Lauriault, F. Truica-Marasescu, and M. R. Wertheimer, "Plasma- and vacuum-ultraviolet (VUV) photo-polymerisation of N-and O-rich thin films," *Radiation Physics and Chemistry*, vol. 79, pp. 310-314, 2010.

[267] W. He, T. Yong, Z. W. Ma, R. Inai, W. E. Teo, and S. Ramakrishna, "Biodegradable polymer nanofiber mesh to maintain functions of endothelial cells," *Tissue Engineering*, vol. 12, pp. 2457-2466, 2006.

[268] M. R. Wertheimer, A. St-Georges-Robillard, S. Lerouge, F. Mwale, B. Elkin, C. Oehr, *et al.*, "Amine-rich organic thin films for cell culture: Possible electrostatic effects in cell–surface interactions," *Japanese Journal of Applied Physics*, vol. 51, p. 11PJ04, 2012.

[269] J. Stitzel, J. Liu, S. J. Lee, M. Komura, J. Berry, S. Soker, *et al.*, "Controlled fabrication of a biological vascular substitute," *Biomaterials*, vol. 27, pp. 1088-1094, 2006.

[270] C. E. Ayres, B. S. Jha, H. Meredith, J. R. Bowman, G. L. Bowlin, S. C. Henderson, *et al.*, "Measuring fiber alignment in electrospun scaffolds: A user's guide to the 2D fast fourier transform approach," *Journal of Biomaterials Science, Polymer Edition*, vol. 19, pp. 603-621, 2008.

[271] F. Chen, Y. Su, X. Mo, C. He, H. Wang, and Y. Ikada, "Biocompatibility, alignment degree and mechanical properties of an electrospun chitosan–P(LLA-CL) fibrous scaffold," *Journal of Biomaterials Science, Polymer Edition*, vol. 20, pp. 2117-2128, 2009.

[272] A. Lynn, I. Yannas, and W. Bonfield, "Antigenicity and immunogenicity of collagen," *Journal of Biomedical Materials Research Part B: Applied Biomaterials*, vol. 71, pp. 343-354, 2004.

[273] N. L'Heureux, N. Dusserre, A. Marini, S. Garrido, L. de la Fuente, and T. McAllister, "Technology insight: The evolution of tissue-engineered vascular grafts-from research to clinical practice," *Nature Clinical Practice Cardiovascular Medicine*, vol. 4, pp. 389-395, 2007.

[274] B. C. Isenberg and J. Y. Wong, "Building structure into engineered tissues," *Materials Today*, vol. 9, pp. 54-60, 2006.

[275] A. Ratcliffe, "Tissue engineering of vascular grafts," *Matrix Biology*, vol. 19, pp. 353-357, 2000.

[276] M. K. O'Connell, S. Murthy, S. Phan, C. Xu, J. Buchanan, R. Spilker, *et al.*, "The three-dimensional micro- and nanostructure of the aortic medial lamellar unit measured using 3D confocal and electron microscopy imaging," *Matrix Biology*, vol. 27, pp. 171-181, 2008.

[277] N. L'Heureux, N. Dusserre, A. Marini, S. Garrido, L. de la Fuente, and T. McAllister, "Technology insight: The evolution of tissue-engineered vascular grafts - from research to clinical practice," *Nature Clinical Practice Cardiovascular Medicine*, vol. 4, pp. 389-395, 2007.

[278] T. J. Sill and H. A. von Recum, "Electro spinning: Applications in drug delivery and tissue engineering," *Biomaterials*, vol. 29, pp. 1989-2006, 2008.

[279] M. J. McClure, S. A. Sell, C. E. Ayres, D. G. Simpson, and G. L. Bowlin, "Electrospinning-aligned and random polydioxanone-polycaprolactone-silk fibroin-blended scaffolds: Geometry for a vascular matrix," *Biomedical Materials*, vol. 4, p. 13, 2009.

[280] H. J. Wu, J. T. Fan, C. C. Chu, and J. Wu, "Electrospinning of small diameter 3D nanofibrous tubular scaffolds with controllable nanofiber orientations for vascular grafts," *Journal of Materials Science-Materials in Medicine*, vol. 21, pp. 3207-3215, 2010.

[281] Y. B. Zhu, Y. Cao, J. Pan, and Y. X. Liu, "Macro-alignment of electrospun fibers for vascular tissue engineering," *Journal of Biomedical Materials Research Part B-Applied Biomaterials*, vol. 92B, pp. 508-516, 2010.

[282] C. Y. Xu, R. Inai, M. Kotaki, and S. Ramakrishna, "Aligned biodegradable nanotibrous structure: A potential scaffold for blood vessel engineering," *Biomaterials*, vol. 25, pp. 877-886, 2004.

[283] V. Thomas, M. V. Jose, S. Chowdhury, J. F. Sullivan, D. R. Dean, and Y. K. Vohra, "Mechano-morphological studies of aligned nanofibrous scaffolds of polycaprolactone fabricated by electrospinning," *Journal of Biomaterials Science-Polymer Edition*, vol. 17, pp. 969-984, 2006.

[284] L. Nivison-Smith and A. S. Weiss, "Alignment of human vascular smooth muscle cells on parallel electrospun synthetic elastin fibers," *Journal of Biomedical Materials Research Part A*, vol. 100A, pp. 155-161, 2012.

[285] M. J. Moreno, A. Ajji, D. Mohebbi-Kalhori, M. Rukhlova, A. Hadjizadeh, and M. N. Bureau, "Development of a compliant and cytocompatible micro-fibrous polyethylene terephthalate vascular scaffold," *Journal of Biomedical Materials Research Part B-Applied Biomaterials*, vol. 97B, pp. 201-214, 2011.

[286] W. He, T. Yong, W. E. Teo, Z. W. Ma, and S. Ramakrishna, "Fabrication and endothelialization of collagen-blended biodegradable polymer nanofibers: Potential vascular graft for blood vessel tissue engineering," *Tissue Engineering*, vol. 11, pp. 1574-1588, 2005.

[287] R. Ng, X. D. Zhang, N. Liu, and S. T. Yang, "Modifications of nonwoven polyethylene terephthalate fibrous matrices via NaOH hydrolysis: Effects on pore size, fiber diameter, cell seeding and proliferation," *Process Biochemistry*, vol. 44, pp. 992-998, 2009.

[288] J. H. Lee, S. H. Park, K. W. Oh, C. H. Lee, and S. H. Kim, "Effect of pretreatment conditions on the hydrolysis and water absorption behavior of poly(ethylene terephthalate) fibrous assembly," *Polymer International*, vol. 61, pp. 657-663, 2012.

[289] W. Kosorn, B. Thavornyutikarn, and W. Janvikul, "Effects of surface treatments of polycaprolactone scaffolds on their properties," in *Multi-functional Materials and*

Structures vol. 747, N. Sombatsompop, D. Bhattacharyya, and K. H. Y. Cheung, Eds., ed Stafa-Zurich: Trans Tech Publications Ltd, 2013, pp. 178-181.

[290] S. G. Jordan, G. R. Gray, and A. Malhotra, "Chemical-mechanical etch (CME) method for patterned etching of a substrate surface," ed: Google Patents, 2002.

[291] M. Rahman and G. C. East, "Titanium dioxide particle-induced alkaline degradation of poly(ethylene terephthalate): Application to medical textiles," *Textile Research Journal,* vol. 79, pp. 728-736, 2009.

[292] E. S. Kim, C. H. Lee, and S. H. Kim, "Effects of pretreatment reagents on the hydrolysis and physical properties of PET fabrics," *Journal of Applied Polymer Science,* vol. 112, pp. 3071-3078, 2009.

[293] R. Morent, N. De Geyter, J. Verschuren, K. De Clerck, P. Kiekens, and C. Leys, "Non-thermal plasma treatment of textiles," *Surface & Coatings Technology,* vol. 202, pp. 3427-3449, 2008.

[294] D. Hegemann, H. Brunner, and C. Oehr, "Plasma treatment of polymers for surface and adhesion improvement," *Nuclear Instruments and Methods in Physics Research Section B: Beam Interactions with Materials and Atoms,* vol. 208, pp. 281-286, 2003.

[295] X. Chen, L. Yao, J. Xue, D. Zhao, Y. Lan, X. Qian, *et al.*, "Plasma penetration depth and mechanical properties of atmospheric plasma-treated 3D aramid woven composites," *Applied Surface Science,* vol. 255, pp. 2864-2868, 2008.

[296] M. O. H. Cioffi, H. J. C. Voorwald, L. R. O. Hein, and L. Ambrosio, "Effect of cold plasma treatment on mechanical properties of PET/PMMA composites," *Composites Part A-Applied Science and Manufacturing,* vol. 36, pp. 615-623, 2005.

[297] C. Riccardi, R. Barni, E. Selli, G. Mazzone, M. R. Massafra, B. Marcandalli, *et al.*, "Surface modification of poly(ethylene terephthalate) fibers induced by radio frequency air plasma treatment," *Applied Surface Science,* vol. 211, pp. 386-397, 2003.

[298] M. Keller, A. Ritter, P. Reimann, V. Thommen, A. Fischer, and D. Hegemann, "Comparative study of plasma-induced and wet-chemical cleaning of synthetic fibers," *Surface & Coatings Technology,* vol. 200, pp. 1045-1050, 2005.

[299] P. Verdonck, P. B. Caliope, E. D. Hernandez, and A. N. R. da Silva, "Plasma etching of electrospun polymeric nanofibres," *Thin Solid Films,* vol. 515, pp. 831-834, 2006.

[300] C. Zanden, M. Voinova, J. Gold, D. Morsdorf, I. Bernhardt, and J. H. Liu, "Surface characterisation of oxygen plasma treated electrospun polyurethane fibres and their interaction with red blood cells," *European Polymer Journal,* vol. 48, pp. 472-482, 2012.

[301] H. J. Jeon, H. Lee, and G. H. Kim, "Nano-sized surface patterns on electrospun microfibers fabricated using a modified plasma process for enhancing initial cellular activities," *Plasma Processes and Polymers,* vol. 11, pp. 142-148, 2014.

[302] S. Guimond, I. Radu, G. Czeremuszkin, D. J. Carlsson, and M. R. Wertheimer, "Biaxially oriented polypropylene (BOPP) surface modification by nitrogen atmospheric pressure glow discharge (APGD) and by air corona," *Plasmas and Polymers,* vol. 7, pp. 71-88, 2002.

[303] S. Guimond and M. R. Wertheimer, "Surface degradation and hydrophobic recovery of polyolefins treated by air corona and nitrogen atmospheric pressure glow discharge," *Journal of Applied Polymer Science,* vol. 94, pp. 1291-1303, 2004.

[304] M. Moisan, C. Barbeau, R. Claude, C. M. Ferreira, J. Margot, J. Paraszczak, *et al.*, "Radio-frequency or microwave plasma reactors-factors determining the optimum frequency of operation," *Journal of Vacuum Science & Technology B,* vol. 9, pp. 8-25, 1991.

[305] B. Lamontagne, O. M. Küttel, and M. R. Wertheimer, "Etching of polymers in microwave/radio-frequency O_2–CF_4 plasma," *Canadian Journal of Physics*, vol. 69, pp. 202-206, 1991.

[306] C. Ayres, G. L. Bowlin, S. C. Henderson, L. Taylor, J. Shultz, J. Alexander, *et al.*, "Modulation of anisotropy in electrospun tissue-engineering scaffolds: Analysis of fiber alignment by the fast fourier transform," *Biomaterials*, vol. 27, pp. 5524-5534, 2006.

[307] B. H. Bimestre and C. Saron, "Chain extension of poly (ethylene terephthalate) by reactive extrusion with secondary stabilizer," *Materials Research*, vol. 15, pp. 467-472, 2012.

[308] N. B. Sanches, M. L. Dias, and E. B. A. V. Pacheco, "Comparative techniques for molecular weight evaluation of poly (ethylene terephthalate) (PET)," *Polymer Testing*, vol. 24, pp. 688-693, 2005.

[309] S. A. Sell, M. J. McClure, C. P. Barnes, D. C. Knapp, B. H. Walpoth, D. G. Simpson, *et al.*, "Electrospun polydioxanone–elastin blends: Potential for bioresorbable vascular grafts," *Biomedical Materials*, vol. 1, pp. 72-80, 2006.

[310] C. X. Wang, Y. Liu, H. L. Xu, Y. Ren, and Y. P. Qiu, "Influence of atmospheric pressure plasma treatment time on penetration depth of surface modification into fabric," *Applied Surface Science*, vol. 254, pp. 2499-2505, 2008.

[311] J. Johansson and T. Masuoka, "Penetration of pores in membranes by plasma polymer forming species," *Macromolecular Rapid Communications*, vol. 20, pp. 12-15, 1999.

[312] Y. Qiu, Y. Hwang, C. Zhang, B. Bures, and M. McCord, "Atmospheric pressure helium+ oxygen plasma treatment of ultrahigh modulus polyethylene fibers," *Journal of Adhesion Science and Technology*, vol. 16, pp. 449-457, 2002.

[313] A. Dekker, K. Reitsma, T. Beugeling, A. Bantjes, J. Feijen, and W. Van Aken, "Adhesion of endothelial cells and adsorption of serum proteins on gas plasma-treated polytetrafluoroethylene," *Biomaterials*, vol. 12, pp. 130-138, 1991.

[314] C. Y. Xu, R. Inai, M. Kotaki, and S. Ramakrishna, "Aligned biodegradable nanofibrous structure: A potential scaffold for blood vessel engineering," *Biomaterials*, vol. 25, pp. 877-886, 2004.

[315] Q. Cheng, B. L.-P. Lee, K. Komvopoulos, Z. Yan, and S. Li, "Plasma surface chemical treatment of electrospun poly (l-lactide) microfibrous scaffolds for enhanced cell adhesion, growth, and infiltration," *Tissue Engineering Part A*, vol. 19, pp. 1188-1198, 2013.

[316] B. De Schoenmaker, L. Van der Schueren, S. De Vrieze, P. Westbroek, and K. De Clerck, "Wicking properties of various polyamide nanofibrous structures with an optimized method," *Journal of Applied Polymer Science*, vol. 120, pp. 305-310, 2011.

[317] K. Wong, X. Tao, C. Yuen, and K. Yeung, "Wicking properties of linen treated with low temperature plasma," *Textile Research Journal*, vol. 71, pp. 49-56, 2001.

[318] D. Yan, J. Jones, X. Yuan, X. Xu, J. Sheng, J. M. Lee, *et al.*, "Plasma treatment of electrospun PCL random nanofiber meshes (NFMs) for biological property improvement," *Journal of Biomedical Materials Research Part A*, vol. 101, pp. 963-972, 2013.

[319] M. Yamaguchi, T. Shinbo, T. Kanamori, P.-C. Wang, M. Niwa, H. Kawakami, *et al.*, "Surface modification of poly (l-lactic acid) affects initial cell attachment, cell morphology, and cell growth," *Journal of Artificial Organs*, vol. 7, pp. 187-193, 2004.

[320] S. L. Dahl, A. P. Kypson, J. H. Lawson, J. L. Blum, J. T. Strader, Y. Li, *et al.*, "Readily available tissue-engineered vascular grafts," *Science Translational Medicine,* vol. 3, pp. 68ra9-68ra9, 2011.
[321] N. L'Heureux, N. Dusserre, G. Konig, B. Victor, P. Keire, T. N. Wight, *et al.*, "Human tissue-engineered blood vessels for adult arterial revascularization," *Nature Medicine,* vol. 12, pp. 361-365, 2006.
[322] D.-H. Kim, P. P. Provenzano, C. L. Smith, and A. Levchenko, "Matrix nanotopography as a regulator of cell function," *The Journal of Cell Biology,* vol. 197, pp. 351-360, 2012.
[323] M. W. Tibbitt and K. S. Anseth, "Dynamic microenvironments: The fourth dimension," *Science Translational Medicine,* vol. 4, pp. 160ps24-160ps24, 2012.
[324] S. Hom, J. O'Hara, W. Yin, and D. Rubenstein, "Effect of electrospun scaffold fiber alignment on endothelial cell growth," *The FASEB Journal,* vol. 29, p. 792.2, 2015.
[325] H. G. Sundararaghavan, R. L. Saunders, D. A. Hammer, and J. A. Burdick, "Fiber alignment directs cell motility over chemotactic gradients," *Biotechnology and Bioengineering,* vol. 110, pp. 1249-1254, 2013.
[326] R. A. Scott and A. Panitch, "Glycosaminoglycans in biomedicine," *Wiley Interdisciplinary Reviews: Nanomedicine and Nanobiotechnology,* vol. 5, pp. 388-398, 2013.
[327] M. K. O'Connell, S. Murthy, S. Phan, C. Xu, J. Buchanan, R. Spilker, *et al.*, "The three-dimensional micro-and nanostructure of the aortic medial lamellar unit measured using 3D confocal and electron microscopy imaging," *Matrix Biology,* vol. 27, pp. 171-181, 2008.
[328] P. Lacolley, V. Regnault, A. Nicoletti, Z. Li, and J.-B. Michel, "The vascular smooth muscle cell in arterial pathology: A cell that can take on multiple roles," *Cardiovascular Research,* vol. 95, pp. 194-204, 2012.
[329] F. Murschel, B. Liberelle, G. St-Laurent, M. Jolicoeur, Y. Durocher, and G. De Crescenzo, "Coiled-coil-mediated grafting of bioactive vascular endothelial growth factor," *Acta Biomaterialia,* vol. 9, pp. 6806-6813, 2013.
[330] T. Fujie, X. Shi, S. Ostrovidov, X. Liang, K. Nakajima, Y. Chen, *et al.*, "Spatial coordination of cell orientation directed by nanoribbon sheets," *Biomaterials,* vol. 53, pp. 86-94, 2015.
[331] J. L. Charest, A. J. García, and W. P. King, "Myoblast alignment and differentiation on cell culture substrates with microscale topography and model chemistries," *Biomaterials,* vol. 28, pp. 2202-2210, 2007.
[332] M. Nikkhah, N. Eshak, P. Zorlutuna, N. Annabi, M. Castello, K. Kim, *et al.*, "Directed endothelial cell morphogenesis in micropatterned gelatin methacrylate hydrogels," *Biomaterials,* vol. 33, pp. 9009-9018, 2012.
[333] J. C. Kohn, D. W. Zhou, F. Bordeleau, A. L. Zhou, B. N. Mason, M. J. Mitchell, *et al.*, "Cooperative effects of matrix stiffness and fluid shear stress on endothelial cell behavior," *Biophysical Journal,* vol. 108, pp. 471-478, 2015.
[334] S. Babaei and P.-L. Girard-Lauriault, "Tuning the surface properties of oxygen-rich and nitrogen-rich plasma polymers: Functional groups and surface charge," *Plasma Chemistry and Plasma Processing,* vol. 36, pp. 651-666, 2016.
[335] D. Gugutkov, J. Gustavsson, M. P. Ginebra, and G. Altankov, "Fibrinogen nanofibers for guiding endothelial cell behavior," *Biomaterials Science,* vol. 1, pp. 1065-1073, 2013.

[336] B. Bondar, S. Fuchs, A. Motta, C. Migliaresi, and C. J. Kirkpatrick, "Functionality of endothelial cells on silk fibroin nets: Comparative study of micro-and nanometric fibre size," *Biomaterials*, vol. 29, pp. 561-572, 2008.

[337] F. Guo, N. Wang, L. Wang, L. Hou, L. Ma, J. Liu, *et al.*, "An electrospun strong PCL/PU composite vascular graft with mechanical anisotropy and cyclic stability," *Journal of Materials Chemistry A*, vol. 3, pp. 4782-4787, 2015.

[338] C. Michiels, "Endothelial cell functions," *Journal of Cellular Physiology*, vol. 196, pp. 430-443, 2003.

[339] A. Karimi, M. Navidbakhsh, A. Shojaei, and S. Faghihi, "Measurement of the uniaxial mechanical properties of healthy and atherosclerotic human coronary arteries," *Materials Science and Engineering: C*, vol. 33, pp. 2550-2554, 2013.

[340] M. Gauthier, "Conception et optimisation d'une prothèse artérielle multicouche composée de tissu électrofilé," maîtrise génie concentration technologies de la santé, École de technologie supérieure 2016.

[341] M. Keller, A. Ritter, P. Reimann, V. Thommen, A. Fischer, and D. Hegemann, "Comparative study of plasma-induced and wet-chemical cleaning of synthetic fibers," *Surface and Coatings Technology*, vol. 200, pp. 1045-1050, 2005.

[342] R. Morent, N. De Geyter, J. Verschuren, K. De Clerck, P. Kiekens, and C. Leys, "Non-thermal plasma treatment of textiles," *Surface and Coatings Technology*, vol. 202, pp. 3427-3449, 2008.

[343] M. C. Tanzi, S. Farè, and P. Petrini, "In vitro stability of polyether and polycarbonate urethanes," *Journal of Biomaterials Applications*, vol. 14, pp. 325-348, 2000.

[344] M. Ferraresso, S. Bertoli, P. Nobili, and E. M. Bortolani, "Early experience with a newly developed electrospun polycarbonate-urethane vascular graft for hemodialysis access," *The Journal of Vascular Access*, vol. 14, pp. 252-256, 2012.

[345] P.-L. Girard-Lauriault, F. Truica-Marasescu, A. Petit, H. T. Wang, P. Desjardins, J. Antoniou, *et al.*, "Adhesion of human U937 monocytes to nitrogen-rich organic thin films: Novel insights into the mechanism of cellular adhesion," *Macromolecular Bioscience*, vol. 9, pp. 911-921, 2009.

[346] A. Manakhov, D. Nečas, J. Čechal, D. Pavliňák, M. Eliáš, and L. Zajíčková, "Deposition of stable amine coating onto polycaprolactone nanofibers by low pressure cyclopropylamine plasma polymerization," *Thin Solid Films*, vol. 581, pp. 7-13, 2015.

[347] X. Liu, Q. Feng, A. Bachhuka, and K. Vasilev, "Surface modification by allylamine plasma polymerization promotes osteogenic differentiation of human adipose-derived stem cells," *ACS Applied Materials & Interfaces*, vol. 6, pp. 9733-9741, 2014.

[348] M. Bauer, S. Schroeder, L. Tauhardt, K. Kempe, U. S. Schubert, and D. Fischer, "In vitro hemocompatibility and cytotoxicity study of poly (2-methyl-2-oxazoline) for biomedical applications," *Journal of Polymer Science Part A: Polymer Chemistry*, vol. 51, pp. 1816-1821, 2013.

[349] A. Contreras-García and M. R. Wertheimer, "Low-pressure plasma polymerization of acetylene–ammonia mixtures for biomedical applications," *Plasma Chemistry and Plasma Processing*, vol. 33, pp. 147-163, 2013.

[350] H. Testrich, H. Rebl, B. Finke, F. Hempel, B. Nebe, and J. Meichsner, "Aging effects of plasma polymerized ethylenediamine (PPEDA) thin films on cell-adhesive implant coatings," *Materials Science and Engineering: C*, vol. 33, pp. 3875-3880, 2013.

[351] M. Ramiasa, A. Cavallaro, A. Mierczynska, S. Christo, J. Gleadle, J. Hayball, *et al.*, "Plasma polymerised polyoxazoline thin films for biomedical applications," *Chemical Communications,* vol. 51, pp. 4279-4282, 2015.

[352] L. Bacakova, E. Filova, M. Parizek, T. Ruml, and V. Svorcik, "Modulation of cell adhesion, proliferation and differentiation on materials designed for body implants," *Biotechnology Advances,* vol. 29, pp. 739-767, 2011.

[353] P. R. Sreerekha and L. K. Krishnan, "Cultivation of endothelial progenitor cells on fibrin matrix and layering on Dacron/polytetrafluoroethylene vascular grafts," *Artificial Organs,* vol. 30, pp. 242-249, 2006.

[354] P. Feugier, R. Black, J. Hunt, and T. How, "Attachment, morphology and adherence of human endothelial cells to vascular prosthesis materials under the action of shear stress," *Biomaterials,* vol. 26, pp. 1457-1466, 2005.

[355] S. K. Williams, L. B. Kleinert, and V. Patula-Steinbrenner, "Accelerated neovascularization and endothelialization of vascular grafts promoted by covalently bound laminin type 1," *Journal of Biomedical Materials Research Part A,* vol. 99, pp. 67-73, 2011.

[356] J. Chlupác, E. Filová, T. Riedel, M. Houska, E. Brynda, M. Remy-Zolghadri, *et al.*, "Attachment of human endothelial cells to polyester vascular grafts: Pre-coating with adhesive protein assemblies and resistance to short-term shear stress," *Physiological Research,* vol. 63, p. 167, 2014.

[357] J.-p. J. De Sandro, K. L. House, J. Koh, and P. Mazumder, "Method and apparatus for providing a uniform coating thickness along an axial direction within a substrate tube," ed: Google Patents, 2005.

[358] N. Muller, "Method of coating internal surfaces of an object by plasma spraying," ed: Google Patents, 1990.

[359] H. N. Tuin, "Method and arrangement for internally coating a tube by reactive deposition from a gas mixture activated by a plasma," ed: Google Patents, 1983.

[360] A. Melchiorri, N. Hibino, T. Yi, Y. Lee, T. Sugiura, S. Tara, *et al.*, "Contrasting biofunctionalization strategies for the enhanced endothelialization of biodegradable vascular grafts," *Biomacromolecules,* vol. 16, pp. 437-446, 2015.

[361] J. M. Chupa, A. M. Foster, S. R. Sumner, S. V. Madihally, and H. W. T. Matthew, "Vascular cell responses to polysaccharide materials:: In vitro and in vivo evaluations," *Biomaterials,* vol. 21, pp. 2315-2322, 2000.

[362] A. G. Kidane, H. Salacinski, A. Tiwari, K. R. Bruckdorfer, and A. M. Seifalian, "Anticoagulant and antiplatelet agents: Their clinical and device application(s) together with usages to engineer surfaces," *Biomacromolecules,* vol. 5, pp. 798-813, 2004.

[363] K. S. Jee, H. D. Park, K. D. Park, Y. H. Kim, and J.-W. Shin, "Heparin conjugated polylactide as a blood compatible material," *Biomacromolecules,* vol. 5, pp. 1877-1881, 2004.

[364] M. C. Tanzi, "Bioactive technologies for hemocompatibility," *Expert Review of Medical Devices,* vol. 2, pp. 473-492, 2005.

[365] W. S. Choi, Y. K. Joung, Y. Lee, J. W. Bae, H. K. Park, Y. H. Park, *et al.*, "Enhanced patency and endothelialization of small-caliber vascular grafts fabricated by coimmobilization of heparin and cell-adhesive peptides," *ACS Applied Materials & Interfaces,* vol. 8, pp. 4336-4346, 2016.

[366] J. M. Heyligers, H. J. Verhagen, J. I. Rotmans, C. Weeterings, P. G. de Groot, F. L. Moll, *et al.*, "Heparin immobilization reduces thrombogenicity of small-caliber expanded polytetrafluoroethylene grafts," *Journal of Vascular Surgery*, vol. 43, pp. 587-591, 2006.
[367] S. Lu, P. Zhang, X. Sun, F. Gong, S. Yang, L. Shen, *et al.*, "Synthetic ePTFE grafts coated with an anti-CD133 antibody-functionalized heparin/collagen multilayer with rapid in vivo endothelialization properties," *ACS Applied Materials & Interfaces*, vol. 5, pp. 7360-7369, 2013.
[368] I. Capila and R. J. Linhardt, "Heparin–protein interactions," *Angewandte Chemie International Edition*, vol. 41, pp. 390-412, 2002.
[369] T. Huynh, G. Abraham, J. Murray, K. Brockbank, P.-O. Hagen, and S. Sullivan, "Remodeling of an acellular collagen graft into a physiologically responsive neovessel," *Nature Biotechnology*, vol. 17, pp. 1083-1086, 1999.
[370] E. F. Ritter, M. M. Fata, A. M. Rudner, and B. Klitzman, "Heparin bonding increases patency of long microvascular prostheses," *Plastic and Reconstructive Surgery*, vol. 101, pp. 142-146, 1998.
[371] B. H. Walpoth, R. Rogulenko, E. Tikhvinskaia, S. Gogolewski, T. Schaffner, O. M. Hess, *et al.*, "Improvement of patency rate in heparin-coated small synthetic vascular grafts," *Circulation*, vol. 98, pp. 319-324, 1998.
[372] S. Yakovlev, S. Gorlatov, K. Ingham, and L. Medved, "Interaction of fibrin (ogen) with heparin: Further characterization and localization of the heparin-binding site," *Biochemistry*, vol. 42, pp. 7709-7716, 2003.
[373] S. A. Irvine, X. Yun, and S. Venkatraman, "Anti-platelet and tissue engineering approaches to biomaterial blood compatibilization: How well have these been translated into the clinic?," *Drug Delivery and Translational Research*, vol. 2, pp. 384-397, 2012.
[374] R. Michel, S. Pasche, M. Textor, and D. G. Castner, "Influence of peg architecture on protein adsorption and conformation," *Langmuir*, vol. 21, pp. 12327-12332, 2005.
[375] P. C. Billings and M. Pacifici, "Interactions of signaling proteins, growth factors and other proteins with heparan sulfate: Mechanisms and mysteries," *Connective Tissue Research*, vol. 56, pp. 272-280, 2015.
[376] M. Rémy, R. Bareille, V. Rerat, C. Bourget, J. Marchand-Brynaert, and L. Bordenave, "Polyethylene terephthalate membrane grafted with peptidomimetics: Endothelial cell compatibility and retention under shear stress," *Journal of Biomaterials Science, Polymer Edition*, vol. 24, pp. 269-286, 2013.
[377] R. Steward, D. Tambe, C. C. Hardin, R. Krishnan, and J. J. Fredberg, "Fluid shear, intercellular stress, and endothelial cell alignment," *American Journal of Physiology-Cell Physiology*, vol. 308, pp. C657-C664, 2015.
[378] V. Shankarraman, G. Davis-Gorman, J. G. Copeland, M. R. Caplan, and P. F. McDonagh, "Standardized methods to quantify thrombogenicity of blood-contacting materials via thromboelastography," *Journal of Biomedical Materials Research Part B: Applied Biomaterials*, vol. 100, pp. 230-238, 2012.
[379] T. Asahara, A. Kawamoto, and H. Masuda, "Concise review: Circulating endothelial progenitor cells for vascular medicine," *Stem Cells*, vol. 29, pp. 1650-1655, 2011.
[380] M. Avci-Adali, G. Ziemer, and H. P. Wendel, "Induction of EPC homing on biofunctionalized vascular grafts for rapid in vivo self-endothelialization—a review of current strategies," *Biotechnology Advances*, vol. 28, pp. 119-129, 2010.
[381] N. Nagai, Y. Nakayama, S. Nishi, and M. Munekata, "Development of novel covered stents using salmon collagen," *Journal of Artificial Organs*, vol. 12, pp. 61-66, 2009.

[382] W. Zeng, C. Wen, Y. Wu, L. Li, Z. Zhou, J. Mi, *et al.*, "The use of BDNF to enhance the patency rate of small-diameter tissue-engineered blood vessels through stem cell homing mechanisms," *Biomaterials,* vol. 33, pp. 473-484, 2012.

[383] H. Ghanbari, D. Radenkovic, S. M. Marashi, S. Parsno, N. Roohpour, G. Burriesci, *et al.*, "Novel heart valve prosthesis with self-endothelialization potential made of modified polyhedral oligomeric silsesquioxane-nanocomposite material," *Biointerphases,* vol. 11, pp. 29-30, 2016.

[384] C.-K. Kang, W.-H. Lim, S. Kyeong, W.-S. Choe, H.-S. Kim, B.-H. Jun, *et al.*, "Fabrication of biofunctional stents with endothelial progenitor cell specificity for vascular re-endothelialization," *Colloids and Surfaces B: Biointerfaces,* vol. 102, pp. 744-751, 2013.

[385] B. A. Butruk-Raszeja, M. S. Dresler, A. Kuźmińska, and T. Ciach, "Endothelialization of polyurethanes: Surface silanization and immobilization of REDV peptide," *Colloids and Surfaces B: Biointerfaces,* vol. 144, pp. 335-343, 2016.

[386] Y. Lei, M. Rémy, C. Labrugère, and M.-C. Durrieu, "Peptide immobilization on polyethylene terephthalate surfaces to study specific endothelial cell adhesion, spreading and migration," *Journal of Materials Science: Materials in Medicine,* vol. 23, pp. 2761-2772, 2012.

[387] J. M. Bastijanic, R. E. Marchant, F. Kligman, M. T. Allemang, R. O. Lakin, D. Kendrick, *et al.*, "In vivo evaluation of biomimetic fluorosurfactant polymer-coated expanded polytetrafluoroethylene vascular grafts in a porcine carotid artery bypass model," *Journal of Vascular Surgery,* vol. 63, pp. 1620-1630.e4, 2016.

[388] P. Qi, W. Yan, Y. Yang, Y. Li, Y. Fan, J. Chen, *et al.*, "Immobilization of DNA aptamers via plasma polymerized allylamine film to construct an endothelial progenitor cell-capture surface," *Colloids and Surfaces B: Biointerfaces,* vol. 126, pp. 70-79, 2015.

[389] M. B. Chan-Park, J. Y. Shen, Y. Cao, Y. Xiong, Y. Liu, S. Rayatpisheh, *et al.*, "Biomimetic control of vascular smooth muscle cell morphology and phenotype for functional tissue-engineered small-diameter blood vessels," *Journal of Biomedical Materials Research Part A,* vol. 88, pp. 1104-1121, 2009.

[390] Q. L. Loh and C. Choong, "Three-dimensional scaffolds for tissue engineering applications: Role of porosity and pore size," *Tissue Engineering Part B: Reviews,* vol. 19, pp. 485-502, 2013.

[391] D. Poncelet, P. de Vos, N. Suter, and S. N. Jayasinghe, "Bio-electrospraying and cell electrospinning: Progress and opportunities for basic biology and clinical sciences," *Advanced Healthcare Materials,* vol. 1, pp. 27-34, 2012.

[392] S. L. Sampson, L. Saraiva, K. Gustafsson, S. N. Jayasinghe, and B. D. Robertson, "Cell electrospinning: An in vitro and in vivo study," *Small,* vol. 10, pp. 78-82, 2014.